



Modelling the stability of ternary solid dispersions

Title	Modelling the stability of ternary solid dispersions
Author(s)	Albaqami, Modhi
Publication Date	2025-03-29
Publisher	University Of Galway

Modelling the stability of ternary solid dispersions

PHD THESIS

by

Modhi Albaqami

Supervisor: Dr Martin Meere

SCHOOL OF MATHEMATICAL AND STATISTICAL SCIENCES

UNIVERSITY OF GALWAY, GALWAY



OLLSCOIL NA GAILLIMHE
UNIVERSITY OF GALWAY

August 2024

Abstract

This thesis provides a mathematical analysis of the stability of some ternary solid dispersions using thermodynamic theory. Solid dispersions have been developed to improve the solubility of poorly soluble drugs. Traditional solid dispersions typically consist of two components - a drug and a hydrophilic polymer, the purpose of the polymer being to improve the solubility of the drug when administered orally. More recently, ternary dispersions (that is, systems with three components) have been developed. Ternary dispersions provide an extra degree of freedom to enable system designers to optimize both the stability and solubility properties of the dispersion. Unstable dispersions may phase separate, thereby limiting their shelf life. In this thesis, I mathematically model ternary solid dispersions with a view to identifying parameter regimes that lead to favourable and unfavourable stability properties for the dispersion. A systematic study of this kind has hitherto been lacking in the literature.

The methodology used is as follows. The solid dispersions are modelled using Flory-Huggins solution theory, a well-established thermodynamic model in polymer science for polymer blends. The stability properties of the dispersions are determined by constructing phase diagrams using the Gibbs free energy of mixing. The phase diagrams determine whether a particular ternary composition is stable or unstable or metastable. The requisite numerical calculations to construct the diagrams are carried out by programs that I wrote using the mathematical packages Maple and MATLAB.

Thermodynamic theory determines the broad character of the ultimate state of the mixture, but yields no information on how the mixture evolves to that state, or what the detailed character of the final state is for unstable compositions. To address these issues, a partial differential equations model is developed to describe the dispersion mixture evolution, and some simulations of this model are also presented.

A few notable results are as follows. For polymer-polymer-drug ternary systems, it is found that for desirable stability properties to be possible, the two polymers need to be compatible (in a sense that has been described quantitatively). Also, the stability behaviour can be finely dependent on the asymmetry between how the two polymers interact with the drug. Closed loops of immiscibility are shown to be theoretically possible. For polymer-surfactant-drug ternary systems, it is shown that the stability behaviour can be sensitive to the character of the interaction between the polymer and the surfactant, and the molecular weight of the surfactant. Numerous other predictions are made.

Contents

Abstract	i
Declaration	vi
Acknowledgements	vii
1 Introduction	1
1.1 The Biopharmaceutical Classification System	1
1.2 Methods For Improving Drug Solubility	3
1.3 Solid Dispersions	5
1.3.1 First Generation Solid Dispersions	6
1.3.2 Second Generation Solid Dispersions	6
1.3.3 Third Generation Solid Dispersions	7
1.3.4 Fourth Generation Solid Dispersions	8
1.4 Ternary Solid Dispersions	8
1.5 Key Research Question And Methodology	8
1.6 Structure Of Remainder Of Thesis	9
2 General Stability Theory For Ternary Mixtures	10
2.1 Binary Mixtures	10
2.1.1 Stability Of A Binary Mixture	11
2.1.2 Unstable Binary Mixtures; Binodal Points	14
2.1.3 The Binary Phase Diagram	15
2.2 Ternary Phase Diagrams	16

2.3	The Gibbs Free Energy of A Mixture	18
2.4	Calculating The Phase Diagram For A Ternary System	19
2.4.1	Stable Regions	20
2.4.2	The Spinodal Curve	20
2.5	The Binodal Curve	21
2.6	Plait Point	22
3	The Ternary Flory-Huggins System	23
3.1	Derivation Of The Flory-Huggins Model	23
3.1.1	Regular Solution Theory	23
3.1.2	Flory-Huggins Theory	29
3.2	Flory-Huggins Chemical Potentials	34
3.3	The Spinodal Curve and Plait Points	35
3.3.1	The Intersection Of The Spinodal With The $\phi_3 = 0$ Binary	39
3.4	Numerical calculations	40
3.4.1	Binodal calculations	40
3.4.2	Optimization Approach	41
3.4.3	The Matlab Optimization Toolbox and <code>fmincon</code>	42
3.4.4	Using Maple to Calculate the Plait Points	44
3.4.5	Using Maple to Calculate the Spinodal Curves	44
3.4.6	Using MATLAB to Calculate the Binodal Curve	44
3.4.7	Testing The Accuracy Of The Numerical Procedures	45
4	Stability Analysis Of Polymer-Polymer-Drug Ternary Solid Dispersions	47
4.1	Interpretation Of The Flory-Huggins Interaction Parameters	48
4.2	P-P-D Systems In The Literature	49
4.3	Values For Flory-Huggins Interaction Parameters	50
4.3.1	Some General Remarks About Flory-Huggins Interaction Parameters	50

4.3.2	Values Of The Flory-Huggins Interaction Parameter For Drug-Polymer Systems	52
4.3.3	Values Of The Flory-Huggins Interaction Parameter For Polymer-Polymer Systems	54
4.4	Analysis And Results	56
4.4.1	Case I: $\chi_{12} > 0, \chi_{12} = O(1)$	57
4.4.2	Case II: $\chi_{12} = O(1/m_1), \chi_{12} > 0, \chi_{13} - \chi_{23} = O(1/m_1)$	59
4.4.3	Case III: $\chi_{12} = O(1/m_1), \chi_{12} > 0, \chi_{13} - \chi_{23} = O(1/\sqrt{m_1})$	65
4.5	Conclusions	70
5	Analyzing The Stability Of Polymer-Surfactant-Drug Ternary Solid Dispersions	71
5.1	Introduction	71
5.2	Drug-Surfactant-Drug Ternary Solid Dispersions	71
5.3	Analysis And Results	72
5.3.1	Asymptotic Analysis	73
5.3.2	Numerical Results	75
5.4	Conclusions	81
6	A Diffusion Model For A Ternary Solid Dispersion	83
6.1	Introduction	83
6.2	Model Formulation	83
6.2.1	Activity coefficients	85
6.2.2	Ternary Systems	86
6.2.3	Using Maple To Numerically Integrate The PDEs	89
6.2.4	Linearizing The Governing Equations	91
6.3	Numerical Results	93
6.3.1	Parameter Values	93
7	Conclusions	100
7.1	Key Findings	100

7.2	Limitations Of This Work And Some Proposals For Future Work . . .	101
7.2.1	Shortcomings Of Flory-Huggins Theory	101
7.2.2	Further Numerical Simulations Of The Diffusion Model	102
A	Maple and MATLAB Codes	103
A.1	Using Maple to Calculate the Plait Points	103
A.2	Using Maple to Calculate the Spinodal Curves	104
A.3	Using MATLAB to Calculate the Binodal Curve	105
A.4	Using Maple to Solve ternary system in Chapter 6	108
	Bibliography	110

Declaration

I, Modhi Albaqami, certify that the thesis is all my own work and that I have not obtained a degree in this University or elsewhere on the basis of any of this work.

Acknowledgements

All praises to Allah for giving me the strength and ability to finish this thesis

I would like to express my deepest gratitude to my supervisor Dr.Martin Meere, for his unwavering support, guidance, and encouragement in every aspect during the course of this thesis. I thank him for the opportunity to work under his mentorship.

I extend my gratitude to the Saudi Ministry of Education for their generous scholarship and support, which has enabled me to pursue my PhD. This achievement would not have been possible without their support.

Special thanks goes to the thesis committee: Prof.Michel Destrade, Dr.Giuseppe Zurlo and Dr.Emma Holian for their thoughtful feedback and suggestions throughout the research process.

I take this opportunity to thank and show my gratitude to my parents for their endless love and support in all aspects of my life. I would like to also thank my husband and my daughters for their love and encouragement, their belief in me and my abilities has been a constant source to pursue my dreams.

I'm also grateful to the staff of Mathematics department/ University of Galway for their support and assistance throughout this research.

List Of Symbols

X_i	Mole Fraction Of Species i
G_m	Gibbs Free Energy Of Mixing
n_i	The Number Of Moles Of Species i
T	Temperature
P	Pressure
μ	Chemical Potential
S	Entropy
H	Enthalpy
R	Gas Constant
N_{AV}	Avogadro's Number
V	Volume
F-H	Flory-Huggins
TSD	Ternary Solid Dispersions
w	Energy Of Interaction
χ	Flory-Huggins Interaction Parameter
ϕ	Volume Fraction
m	Molar Volume
λ	Positive Parameter
K	The Coulomb Constant

- x Spatial Variable
- k Boltzmann's Constant
- c Molar Concentration
- J Flux Of Species
- v Drift Velocity
- D Diffusion Coefficients
- t Time

Chapter 1

Introduction

This thesis is concerned with the mathematical modelling of *solid dispersions*, and in particular, *ternary* solid dispersions (that is, dispersions containing three distinct components). In this chapter, I will explain what solid dispersions are, what they are used for, how they are manufactured, and the advantages associated with ternary solid dispersions. The particular focus of this study will be on assessing the stability of solid dispersions in storage. I will also give an overview of the remainder of the thesis at the end of the chapter, and highlight the novel aspects of the work.

The principal application of solid dispersions is to improve the solubility of drugs, and so we begin our discussion here with the drug classification system for which solubility is a key feature.

1.1 The Biopharmaceutical Classification System

Drugs are frequently categorized using two key characteristics: their solubility in aqueous solution and their intestinal permeability. Poor water solubility is a major challenge in the development of novel drugs. At least 50% of drugs under development are inherently poorly water soluble. This is a major problem because poorly soluble drugs tend to pass through the patient without dissolving and thus have little therapeutic effect. Another key feature of drugs is their intestinal permeability - effective drugs clearly need to be capable of passing through the intestinal wall to be bioavailable. Before proceeding further, it is of value here to define the terms *drug solubility* and *intestinal permeability* more carefully.

Drug solubility. Drug solubility is the property of a drug (the solute) to dissolve in a solvent (usually a liquid) to form a homogeneous solution of the solute in the solvent. Quantitatively, it is the maximum concentration of drug the solvent can sustain so that if more drug is added to the solution, it will not increase its concentration in the solution. Drug solubility depends on temperature and pressure as well as on the character of the solute ([73],[54]).

Drug intestinal permeability. This quantity measures the ability of a drug to pass from inside the gastrointestinal tract through the cells lining the gut wall and into the rest of the body ([24],[54]). Quantitatively, it is given by the rate at which a substance moves through the gut wall, and it is encapsulated in a quantity called the permeability coefficient; see, for example, Chapter 3 of the book by Schreiber & Schönherr [77].

The Biopharmaceutics Classification System (BCS) uses these two features to classify drugs ([6],[10]). This is achieved by plotting compound solubility versus compound permeability on a single graph; see Figure 1.1.

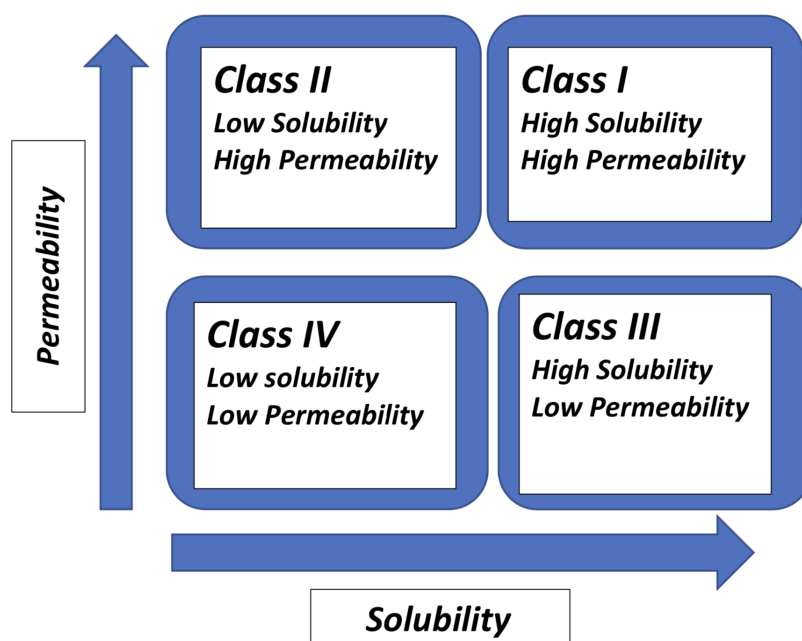


Figure 1.1: The biopharmaceutical classification system.

The BCS classifies drugs into four broad classes, as shown in Figure 1.1.

- **Class I - High permeability, high solubility.** Drugs in this class have high aqueous solubility and can easily pass through the intestinal wall. These drugs typically do not need special formulation techniques; examples of drugs in this class are Diazepam, Paracetamol, and Zidovudine.
- **Class II - High permeability, low solubility.** Drugs in this category have low solubility in water, but can easily pass through the intestinal wall. The solid dispersion technique (see below) is sometimes used to improve the solubility of drugs in this class. Drugs in this class include Felodipine, Ibuprofen, and Valsartan.
- **Class III - Low permeability, high solubility.** Drugs in this category have high solubility in water, and are poorly permeable to biological membranes. Permeability enhancers such as surfactants are sometimes used to improve the

behaviour of drugs in this class. Vibegron and Zinc Sulfate are examples of such drugs.

- **Class IV - Low permeability, low solubility.** Drugs in this class provide the biggest challenge to the pharmaceutical industry since they have both poor solubility and permeability. One technique for improving the delivery behaviour of these drugs is to formulate them in polymeric nanoparticles. Two examples of drugs in this class are ritonavir and paclitaxel.

1.2 Methods For Improving Drug Solubility

In this section, I briefly discuss some commonly used methods for improving drug solubility. A comprehensive review of these methods can be found in the paper by Williams *et al.* [97]; other relevant references are Kumar *et al.* [50], Savjani *et al.* [73], and Ainurofiq *et al.* [2]. Figure 1.2 illustrates some of the methods used to improve drug solubility, and I will briefly consider some of these techniques here. In the next section, I will then consider the method of solid dispersions in some detail since this forms the topic for the current study.

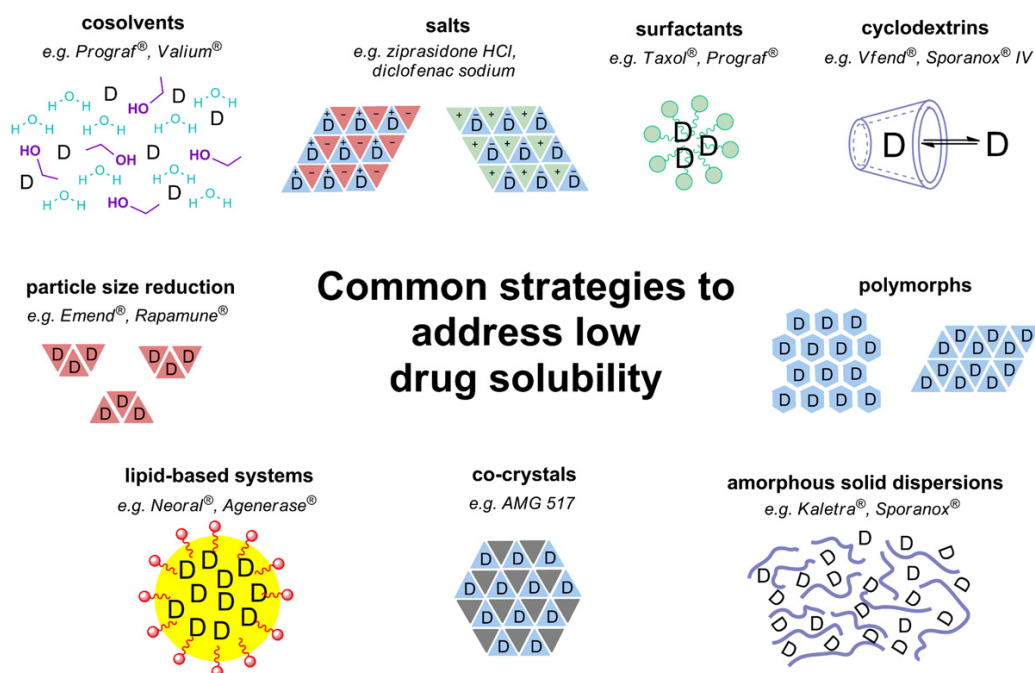


Figure 1.2: Some common methods used to improve solubility; adapted from [97]. In all of these diagrams, D refers to the drug.

Particle size reduction

Reducing the size of drug particles increases their surface area to volume ratio - for example, for spherical particles, the surface area to volume ratio is inversely proportional to the particle radius. Hence, smaller drug particles present a larger total surface area to the surrounding solvent than the same volume of larger particles,

and this increases the drug dissolution rate. Milling, also referred to as grinding or pulverization, and high pressure homogenization are two commonly used methods to reduce particle size [97].

Surfactants

Surfactants are organic compounds that contain both a hydrophobic (water hating) component and a hydrophilic (water loving) component. The addition of surfactants to solvents is one of the oldest methods for improving drug solubility. They are especially useful for improving the solubility of lipophilic drugs. In solution, and above a certain concentration, surfactants spontaneously self-assemble to form molecular structures called micelles; see Figure 1.3. These micelles are usually (though not always) spherical, and they can enclose the drug molecules thereby improving their solubility in solution. Surfactants also reduce surface tension and can improve the wettability of solids ([97], [50], [73]).

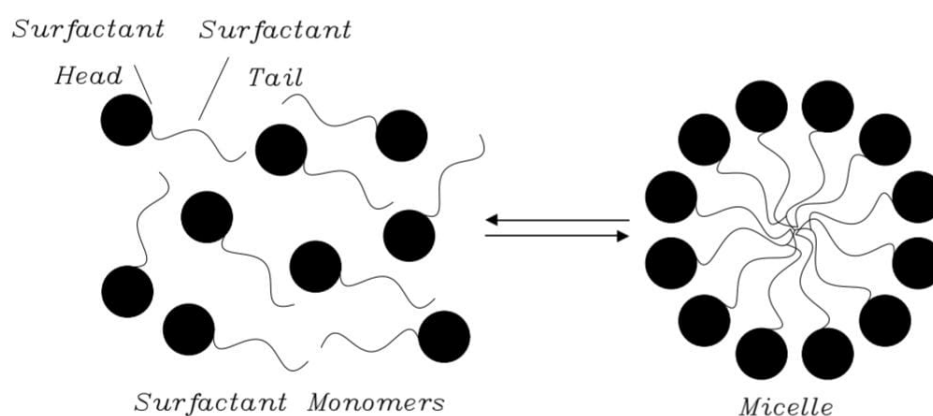


Figure 1.3: Surfactant molecules contain a hydrophilic head and a hydrophobic tail. Above a critical concentration, these molecules self-assemble to form micelles that can enclose drug molecules and improve their solubility. Adapted from [70].

Cosolvents

Cosolvents are organic solvents that are used to increase the solubility of many compounds, including drugs. Cosolvents have a lower polarity than water, and so when they are added to water in sufficient quantities, they reduce the overall polarity of the solvent. This lower polarity matches the polarity of the drug more closely, thereby improving its solubility [97]. Cosolvent formulations are frequently used for the parenteral delivery (that is, modes of delivery other than oral delivery) of drugs [15].

Cyclodextrins

Cyclodextrins (CDs) are naturally occurring ring-shaped sugar molecules that have found many uses in medicine and industry. CDs have a hydrophilic outer shell and a hydrophobic interior cavity - see Figure 1.4. Poorly soluble drug molecules can bind with the hydrophobic CD cavity to form CD-drug complexes that are more soluble

than the drug would be on its own due to their hydrophilic exterior.

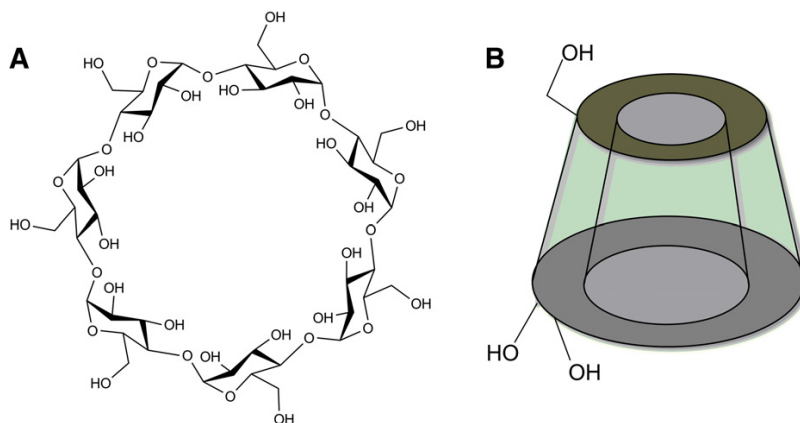


Figure 1.4: A β -cyclodextrin ring. Here (A) gives the chemical structure, while (B) schematically depicts the molecular geometry. Adapted from [91].

I next discuss the use of solid dispersions for improving drug solubility. This discussion will be more detailed than that for the other methods considered above since solid dispersions form the topic of the current study.

1.3 Solid Dispersions

A solid dispersion is broadly defined as the dispersion of one or more active ingredients in at least one inert carrier or matrix. In the modern context, the matrix is often an amorphous polymer. The drug is usually hydrophobic, and the matrix is typically hydrophilic, and the purpose of the matrix is to improve the solubility of the drug. The matrix frequently achieves this by maintaining the drug in a more soluble molecularly dispersed form.

Solid dispersions are sometimes categorized into four generations, and we adopt this approach here; see Figure 1.5 for a summary of the generations.

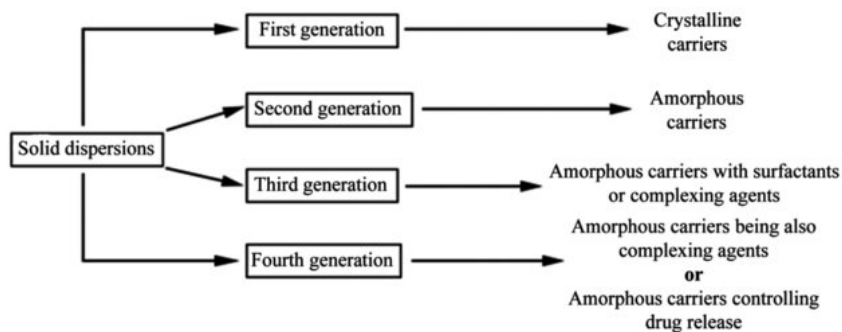


Figure 1.5: The four generations of solid dispersions. Adapted from [31].

1.3.1 First Generation Solid Dispersions

The first generation of solid dispersions had a crystalline character [94]. The earliest scientific study on solid dispersions appeared in 1961 and was due to Sekiguchi & Oni [79]. These authors found that a eutectic mixture of the active ingredient sulfathiazole with highly soluble urea led to improved drug absorption *in vivo* compared with sulfathiazole on its own. I will not discuss the technical details of eutectic mixtures here, other than to mention that the drug and carrier are both in crystalline form in these mixtures; the interested reader can find more information in the review by Vo *et al.* [94]. In 1966, Goldberg *et al.* [28] found that a eutectic mixture of the drug chloramphenicol with urea dissolved almost four times as rapidly as the drug on its own. Vippagunta *et al.* [93] took a more theoretical approach to assess the factors influencing the formation of eutectic solid dispersions and their subsequent dissolution behaviour.

However, one disadvantage of this approach is that the drug is largely present in crystalline form in a eutectic mixture, and the crystalline form dissolves more slowly than the amorphous form due to its lower free energy state [43]. This observation was one of the motivations that led to the development of second generation solid dispersions.

1.3.2 Second Generation Solid Dispersions

The second generation of solid dispersions use an amorphous (as opposed to a crystalline) carrier for the drug. The carrier is frequently a hydrophilic amorphous polymer matrix, where the matrix maintains the drug in a more soluble molecularly dispersed form - see panel (A) of Figure 1.6. The earliest studies to use amorphous polymer carriers in solid dispersions appeared in the late 1960's, two examples of such being Simonelli *et al.* [81] and Chiou & Riegelman [17]. In [17], Chiou & Riegelman observed a marked increase in the rate of dissolution of griseofulvin (an antifungal medicine) dispersed in a variety of polymers when compared with the dissolution of the drug on its own. In the modern context, povidone (PVP) [84], polyethylene glycol (PEG) [11], and hydroxypropylmethyl cellulose (HPMC) [55] are amongst the most popular choices for amorphous polymeric carriers in solid dispersion formulations.

However, there are disadvantages associated with the use of amorphous solid dispersions, particularly in relation to formulation stability. Vo *et al.* [94] and Huang & Dai [40] have pointed out that the drug can simultaneously exist in more than one state in the polymer carrier. In fact, the drug can simultaneously exist in three states in the polymer - the molecularly dispersed state, the amorphous state, and the crystalline state; see Figure 1.6. When the dispersion is first manufactured, the drug is ideally prepared in a high-energy, soluble, molecularly dispersed state. However, over time, the drug may seek to reduce its free energy by precipitating out of solution in less soluble amorphous or crystalline clumps ([40], [43]), and this negatively affects the dissolution rate. Hence, product stability can be a major issue for such formulations, and this is the principal focus of the current study.

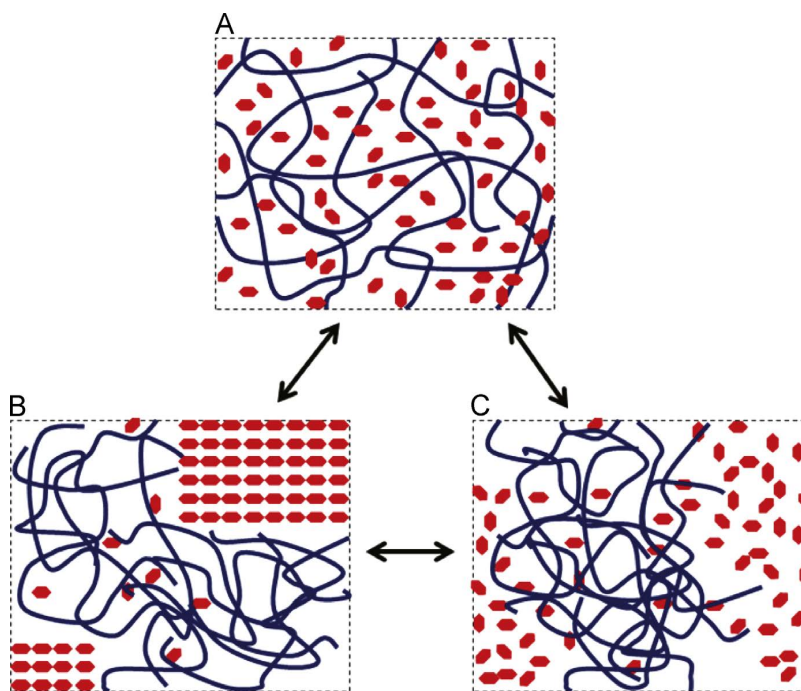


Figure 1.6: Three possible states for the drug in a drug/polymer solid dispersion. In these diagrams, the red hexagonal symbols represent drug molecules and the blue strings represent polymer molecules. Here (A) represents the most desirable scenario in which the drug is molecularly dispersed; (B) represents the least desirable scenario in which a significant fraction of the drug has crystallized out of solution; and (C) represents a dispersion containing amorphous drug-rich domains. Adapted from [58].

1.3.3 Third Generation Solid Dispersions

In third generation solid dispersions, surfactants or emulsifiers are added to the formulation to improve stability or dissolution behaviour (or both) [94]. As noted earlier in this chapter, surfactants have long been used to improve the solubility of lipophilic drugs. In a binary drug/polymer system, the polymer itself can be the surfactant [22], while in a ternary system, the surfactant can be one of the three constituent components, as in a drug/polymer/surfactant system [18].

Damian *et al.* [18] used the surfactant Gelucire 44/14 in a dispersion of the antiviral drug thiocarboxanilide and the polymer PEG 6000, and found that it significantly improved the dissolution properties of the drug when compared with the drug on its own. Van den Mooter *et al.* [22] used the polymeric surfactant Inutec SP1 to formulate a solid dispersion with the drug itraconazole (an antifungal) and observed significantly improved dissolution properties compared with the pure drug. I will return to third generation systems throughout this thesis in the context of ternary solid dispersions.

1.3.4 Fourth Generation Solid Dispersions

The fourth generation of solid dispersions are the so-called Controlled Release Solid Dispersions (CRSDs). These dispersions frequently serve a dual purpose - they improve the solubility of the drug as before, but they also control the rate at which the drug is released (they usually slow down the rate of release). A delayed drug release can reduce the dosing frequency and improve patient compliance. Technologists have long experience with using polymers to control the release rate of drugs ([83]). Two notable mechanisms for controlled release in polymers are diffusion, in which the drug molecules must diffuse through the polymer matrix before being released, or polymer erosion in which the drug must wait to be washed away as the polymer erodes.

1.4 Ternary Solid Dispersions

A ternary solid dispersion (TSD) is a dispersion consisting of *three* components. The three components are frequently a hydrophilic polymer, a poorly soluble drug, and one other component. The other component provides an extra system degree of freedom that opens up the intriguing possibility of optimising both the solubility *and* the stability properties of the formulation. In the current work, I will focus my attention on the stability properties of two different types of ternary solid dispersions. In Chapter 4, I consider polymer-polymer-drug dispersions, and in Chapter 5, I consider polymer-surfactant-drug dispersions. Other types of solid dispersions are reviewed in the relatively recent article by Borde *et al.* [13]. Some of the manufacturing methods for these dispersions are also discussed in this reference.

1.5 Key Research Question And Methodology

The key research question addressed by this thesis is the investigation of the stability of ternary solid dispersions, with a particular emphasis on polymer-polymer-drug and polymer-surfactant-drug systems. By stable, I mean here that the solid dispersion retains its initial uniformly mixed homogeneous formulation. By unstable, I mean that the mixture phase separates, with a resultant loss of the favourable properties of the formulation (notably enhanced dissolution). This clearly has implications for the shelf life of the product. In particular, this study aims to identify parameter regimes that lead to favourable stability behaviour, as well as identifying parameter regimes that should be avoided. Such results are clearly of value for system design.

The methodology used is as follows. The solid dispersions are modelled using Flory-Huggins solution theory, a well-established thermodynamic model in polymer science for polymer blends. The stability properties of the dispersions are determined by constructing phase diagrams using the Gibbs free energy of mixing. The phase diagrams determine whether a particular ternary composition is stable or unstable

or metastable. The requisite numerical calculations to construct the diagrams are carried out by programs that I wrote using the mathematical packages Maple and MATLAB.

Thermodynamic theory determines the broad character of the ultimate state of the mixture, but yields no information on how the mixture evolves to that state, or what the detailed character of the final state is for unstable compositions. To address these issues, a partial differential equations model is developed to describe the dispersion mixture evolution, and some simulations of this model are also presented.

1.6 Structure Of Remainder Of Thesis

I now briefly describe how the remainder of this thesis is organized, chapter by chapter.

- Chapter 2. In this chapter, I briefly revise the thermodynamics of mixture stability at constant temperature and pressure. I begin with a binary mixture, and review the criterion for stability using the Gibbs free energy of mixing. I introduce the concept of a phase diagram and its various components. I then give the corresponding discussion for a ternary system, which is the focus of the current study.
- Chapter 3. This chapter begins by recalling the derivation of the Flory-Huggins model for polymer blends from first principles. As a point of novelty, the equations are derived for a ternary system, as opposed to the standard binary calculations presented in text books. Using the Gibbs free energy of mixing, expressions for the spinodal, the binodal, and the plait points are presented. The Maple (2022) and MATLAB (R2024a) programs used to calculate these quantities are described, and some illustrative test calculations presented.
- Chapter 4. In this chapter, I present a stability analysis for polymer-polymer-drug solid dispersions. The chapter begins with a brief review of the literature for these systems, with a particular emphasis on Flory-Huggins interaction parameter values. I then calculate phase diagrams using asymptotic and numerical methods, and identify parameter regimes with desirable/undesirable stability properties.
- Chapter 5. In this chapter, I present a stability analysis of polymer-surfactant-drug systems. The analysis mirrors that of Chapter 4, beginning with a literature review, followed by the numerical and analytical calculation of phase diagrams and a discussion of results.
- Chapter 6. In this chapter, the partial differential equations model describing the evolution of a ternary solid dispersion is formulated. Effective diffusion coefficients in terms of composition volume fractions are derived. Some illustrative model simulations are presented.
- Chapter 7. This chapter gives a brief discussion of conclusions and some suggestions for future work.

Chapter 2

General Stability Theory For Ternary Mixtures

A ternary mixture is a mixture that contains three distinct components. In the current chapter, I will give a general discussion of the stability properties of ternary systems without specifying any particular thermodynamic model for the mixture. Then in the next chapter, Chapter 3, I will specialize to the particular case of the Flory-Huggins thermodynamic model. Flory-Huggins theory is commonly used in applications to describe polymer solutions, It should be noted that all of the calculations displayed in this chapter come from well established theory, and have appeared in the literature before. Nevertheless, I think it is important to review this material here to properly set the stage for the novel calculations to come. A particularly useful reference for this chapter is the book by Tompa [90].

2.1 Binary Mixtures

Although the current thesis is primarily concerned with ternary mixtures, I will begin the discussion here with binary mixtures because they are easier to describe mathematically. The extension to the ternary discussion will be relatively straightforward once the binary discussion has been completed. I shall confine the discussion here to mixtures that are at constant temperature and pressure because these are usually the relevant conditions in applications. Specifically, in applications, the temperature is frequently close to room temperature and the pressure is often close to one atmosphere. However, the analysis we present here remains valid for any system in which the temperature and pressure remain constant. At constant temperature and pressure, standard thermodynamic theory [8] gives that the Gibbs free energy of the mixture is minimized at equilibrium. Since the Gibbs free energies for the pure components are constant, we can conclude that the Gibbs free energy of mixing, which we denote here by ΔG_m , is minimized at equilibrium. For systems in the which the temperature and volume are held constant, the Gibbs free energy needs to be replaced by the Helmholtz free energy [8]. For systems in which the temperature and pressure can vary, the techniques of non-equilibrium thermodynamics [21] need

to be employed.

Denoting by X_1 , X_2 the mole fractions of the two species in the mixture, it is clear that

$$X_1 + X_2 = 1,$$

so that we can write $X_1 = 1 - X_2$. Since $\Delta G_m = \Delta G_m(X_1, X_2)$, it is now clear that we can write ΔG_m as a function of X_2 only, so that we can write

$$\Delta G_m = \Delta G_m(X_2).$$

2.1.1 Stability Of A Binary Mixture

In Figure 2.1, we plot an illustrative graph for the Gibbs free energy of mixing $\Delta G_m = \Delta G_m(X_2)$. The curve shown here is concave up [86] (or convex).

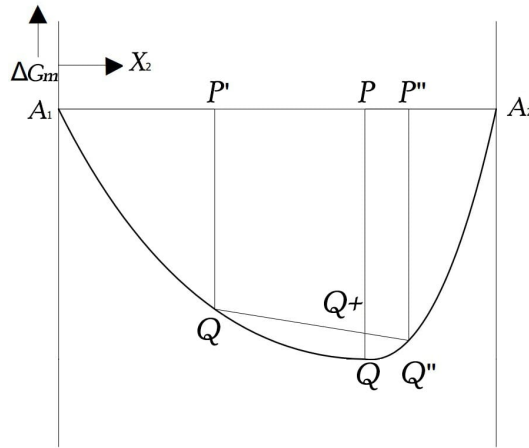


Figure 2.1: An illustrative curve for the Gibbs free energy of mixing $\Delta G_m = \Delta G_m(X_2)$. The curve shown here is concave up.

In Figure 2.1, we suppose that the point P corresponds to a binary mixture consisting of n_1 moles of species 1 and n_2 moles of species 2. We denote by P' and P'' two phases into which the mixture $P(n_1, n_2)$ might phase separate. We denote by (n'_1, n'_2) and (n''_1, n''_2) the moles corresponding to the points P' and P'' , respectively. From mass conservation, it is clear that

$$n_1 = n'_1 + n''_1, \quad n_2 = n'_2 + n''_2.$$

Also

$$A_1 P' = \frac{n'_2}{n'_1 + n'_2}, \quad A_1 P = \frac{n_2}{n_1 + n_2},$$

and

$$A_1 P'' = \frac{n''_2}{n''_1 + n''_2} = \frac{n_2 - n'_2}{n_1 + n_2 - n'_1 - n'_2},$$

so that

$$PP' = A_1P - A_1P' = \frac{n_2}{n_1 + n_2} - \frac{n_2'}{n_1' + n_2'}, \quad (2.1)$$

$$PP'' = A_1P'' - A_1P = \frac{n_2 - n_2'}{n_1 + n_2 - n_1' - n_2'} - \frac{n_2}{n_1 + n_2}.$$

From (2.1), it follows in a straightforward manner that

$$\frac{PP''}{PP'} = \frac{n_1' + n_2'}{n_1'' + n_2''} \quad (2.2)$$

so that $PP'' : PP'$ gives the ratio of the two phases into which the mixture $P(n_1, n_2)$ separates. From Figure 2.1, it is clear that

$$\frac{PQ^+ - P'Q'}{PP'} = \frac{P''Q'' - PQ^+}{PP''}$$

so that

$$PQ^+(PP'' + PP') = (PP'')(P'Q') + (PP')(P''Q'')$$

and using (2.1),(2.2), this leads to

$$(n_1 + n_2)PQ^+ = (n_1' + n_2')P'Q' + (n_1'' + n_2'')P''Q''. \quad (2.3)$$

Now if the curve $\Delta G_m(X_2)$ is strictly convex (concave up [86]), then

$$PQ^+ > PQ$$

and (2.3) then gives

$$(n_1' + n_2')P'Q' + (n_1'' + n_2'')P''Q'' > (n_1 + n_2)PQ. \quad (2.4)$$

Equation (2.4) is readily interpreted. It states that the free energy of phase P' plus the free energy of the phase P'' exceeds the free energy of the original mixture P . Hence the decomposition of P into P' and P'' is energetically unfavoured. This means that the decomposition of P into P' and P'' will not occur, and this provides us with a sufficient condition for a binary mixture to be stable. If $\Delta G_m(X_2)$ is strictly convex for all $0 \leq X_2 \leq 1$, then the binary mixture is miscible (stable) for all compositions. A smooth function $\Delta G_m(X_2)$ is strictly convex on an interval if and only if (see [86])

$$\frac{\partial^2 \Delta G_m(X_2)}{\partial X_2^2} > 0. \quad (2.5)$$

Hence a binary mixture is miscible and stable for all compositions if (2.5) holds for all $0 \leq X_2 \leq 1$.

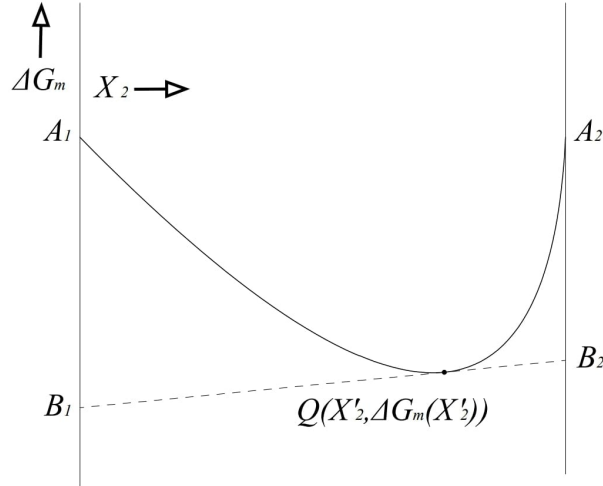


Figure 2.2: Plot of a typical free energy of mixing $\Delta G_m(X_2)$ for a binary mixture.

The Gibbs free energy of mixing can be written as (see, for example, [90])

$$\Delta G_m = X_1 \Delta \mu_1 + X_2 \Delta \mu_2 = \Delta \mu_1 + X_2 (\Delta \mu_2 - \Delta \mu_1), \quad (2.6)$$

where μ_1, μ_2 give the chemical potentials of species 1 and 2, respectively. Now consider Figure 2.2 which depicts a typical free energy of mixing $\Delta G_m(X_2)$ for a binary mixture. Consider a typical point Q on the curve with coordinates $(X'_2, \Delta G_m(X'_2))$. Setting $X_2 = X'_2$ in (2.6) gives

$$\Delta G_m(X'_2) = \Delta \mu_1(X'_2) + X'_2 (\Delta \mu_2(X'_2) - \Delta \mu_1(X'_2)). \quad (2.7)$$

Now consider the tangent to the curve at the point Q . It takes the general form (linear in X_2)

$$\Delta G_m(X_2) = K(X'_2)X_2 + b(X'_2)$$

so that

$$\Delta G_m(X'_2) = K(X'_2)X'_2 + b(X'_2). \quad (2.8)$$

Comparing (2.7) and (2.8) and noting that the equality must hold for all X'_2 , it follows that

$$K(X'_2) = \Delta \mu_2(X'_2) - \Delta \mu_1(X'_2), \quad b(X'_2) = \Delta \mu_1(X'_2).$$

Hence the tangent to ΔG_m at Q takes the form

$$\Delta G_m(X_2) = (\Delta \mu_2(X'_2) - \Delta \mu_1(X'_2))X_2 + \Delta \mu_1(X'_2). \quad (2.9)$$

It follows immediately that

$$\Delta G_m(X_2 = 0) = \Delta \mu_1(X'_2), \quad \Delta G_m(X_2 = 1) = \Delta \mu_2(X'_2), \quad (2.10)$$

so that the tangent to Q intercepts $X_2 = 0$ at $\Delta \mu_1(X'_2)$ and intercepts $X_2 = 1$ at $\Delta \mu_2(X'_2)$.

2.1.2 Unstable Binary Mixtures; Binodal Points

In this subsection, I will give a similar discussion to that given for Figure 2.2, but now for a different type of curve for ΔG_m ; see Figure 2.3.

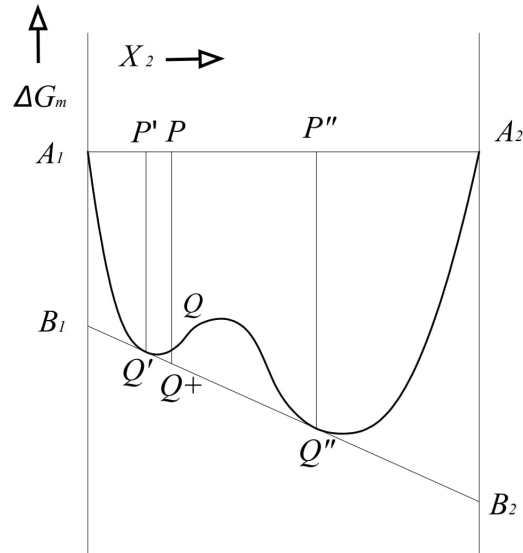


Figure 2.3: A Gibbs free energy diagram for which phase separation can occur.

It is clear here that the curve $\Delta G_m(X_2)$ in Figure 2.3 has a region that is concave down. We now argue that the composition Q shown in Figure 2.3 will decompose into compositions Q' and Q'' where Q', Q'' are the intercepts with the common tangent B_1B_2 . There are two parts to the argument. Firstly, following the arguments given in Section 2.1.1, it is now clear that

$$(n'_1 + n'_2)P'Q' + (n''_1 + n''_2)P''Q'' < (n_1 + n_2)PQ, \quad (2.11)$$

so that the total free energy of compositions Q' and Q'' is less than the free energy of Q so that the decomposition is energetically favored. The second part of the argument concerns the common tangent construction, originally due to Maxwell ([90]). From Section 2.1.1, we know that point B_1 corresponds to

$$\Delta\mu_1(Q') = \Delta\mu_1(Q'') \quad (2.12)$$

and the point B_2 corresponds to

$$\Delta\mu_2(Q') = \Delta\mu_2(Q'') \quad (2.13)$$

Equations (2.12) and (2.13) are precisely the conditions for coexisting phases Q' and Q'' to be in equilibrium ([8]). Hence the common tangent construction selected the correct compositions into which Q decomposes. The points Q' and Q'' are referred to as *binodal points*.

2.1.3 The Binary Phase Diagram

Calculating pairs of binodal points Q' and Q'' for various temperatures T defines a curve in composition (X_2) - temperature (T) space known as the *binodal curve*; see Figure 2.4.

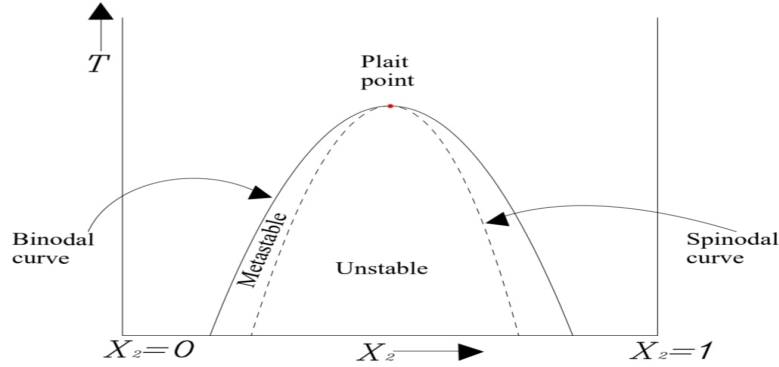


Figure 2.4: Representative phase diagram for a binary mixture. The diagram is defined by the binodal curve, the spinodal curve, and the plait point. These quantities are explained in the main text.

As previously discussed, unstable regions correspond to points X_2 for which

$$\frac{\partial^2 \Delta G_m}{\partial X_2^2}(X_2, T) < 0$$

and stable regions correspond to

$$\frac{\partial^2 \Delta G_m}{\partial X_2^2}(X_2, T) > 0.$$

The boundary between these two regions is defined by the equation

$$\frac{\partial^2 \Delta G_m}{\partial X_2^2}(X_2, T) = 0, \quad (2.14)$$

and solving (2.14) for X_2 gives the *spinodal points*. Plotting the spinodal points for various different temperatures T gives a *spinodal curve* in composition (X_2) - temperature (T) space. An illustrative binodal curve is shown in Figure 2.4.

The final feature of Figure 2.4 that we describe is the critical point, or the *plait point*. This is the point (X_c, T_c) in the (X_2, T) diagram for which the binary mixture is unconditionally stable for $T > T_c$, and in Figure 2.4, it corresponds to the intersection of the spinodal and binodal curves ([90]). We know that the critical point (X_c, T_c) lies on the spinodal curve, so that

$$\frac{\partial^2 \Delta G_m}{\partial X_2^2}(X_c, T_c) = 0, \quad (2.15)$$

but this is insufficient to determine (X_c, T_c) since there are two unknowns. A second

equation is provided by realizing that at the plait point, the two spinodal solutions (that is the solutions to (2.14)) coincide and at this point we have

$$\frac{\partial^3 \Delta G_m}{\partial X_2^3}(X_c, T_c) = 0. \quad (2.16)$$

Solving (2.15) and (2.16) simultaneously uniquely determines the plait point (X_c, T_c) .

The binodal curve, spinodal curve, and plait point define the phase diagram for the binary mixture. An illustrative phase diagram is shown in Figure 2.4. The phase diagram summarises the stability behavior of the binary mixture for all compositions and temperatures. In the diagram, points underneath the spinodal curve correspond to unstable mixtures since the curvature of ΔG_m is negative there. Points outside the spinodal region are stable, although we distinguish between points outside the binodal curve and points between the binodal curve and spinodal curve. The latter region is referred to as metastable ([33]), and corresponds to a region where the mixture is stable to small perturbations but unstable to sufficiently large perturbations.

2.2 Ternary Phase Diagrams

I now turn my attention to ternary systems, which are the main focus of the current study. I begin by showing that a ternary mixture can be represented by a point in an equilateral triangle. As a preliminary, I recall Viviani's theorem for equilateral triangles ([1]); see Figures 2.5. Viviani's theorem states that the altitude of an equilateral triangle (see h in Figure 2.5 (a)) is the sum of the three perpendicular distances defined by any interior point of the triangle (see s, t, u in Figure 2.5 (b)).

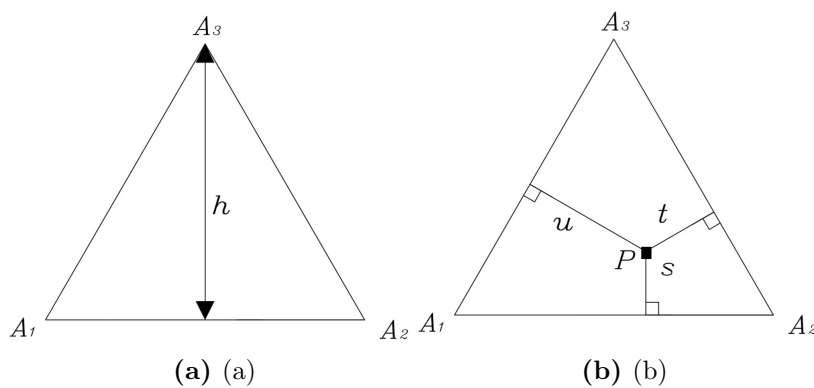


Figure 2.5: (a) An equilateral triangle with altitude h . (b) Any interior point P of the triangle defines three perpendicular distances s, t, u as shown, and Viviani's theorem states that $h = s + t + u$. [36]

Using the notation of Figure 2.5, this gives that

$$h = s + t + u. \quad (2.17)$$

The proof of equation (2.17) is elementary, and is given by considering the triangles PA_1A_2 , PA_1A_3 and PA_2A_3 in Figure 2.5 (b). From Figure 2.5 (b), it is clear that

$$\text{area}(A_1A_2A_3) = \text{area}(PA_1A_2) + \text{area}(PA_2A_3) + \text{area}(PA_1A_3),$$

so that

$$\frac{1}{2}|A_1A_2|h = \frac{1}{2}|A_1A_2|s + \frac{1}{2}|A_2A_3|t + \frac{1}{3}|A_1A_3|u$$

and since $|A_1A_2| = |A_2A_3| = |A_1A_3|$ for an equilateral triangle, the result (2.17) follows.

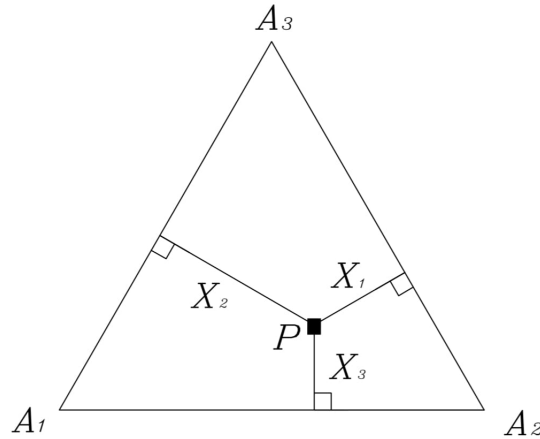


Figure 2.6: In this equilateral triangle, A_1 , A_2 and A_3 represent the three components of a ternary mixture. The point P represents a ternary mixture where species A_1 has mole fraction X_1 , species A_2 has mole fraction X_2 , and species A_3 has mole fraction X_3 .

I now describe how an equilateral triangle can be used to represent a ternary mixture; see Figure 2.6. The use of triangular ternary phase diagrams is well-established in materials science, with excellent discussions on their application available in the books by [65] and [96]. In Figure 2.6, the altitude of the equilateral triangle is taken to be 1, and the mole fractions of A_1 , A_2 , A_3 in the mixture are given by X_1 , X_2 , X_3 as shown, respectively. This representation is possible since from Viviani's theorem, we have that

$$\sum_{i=1}^3 X_i = 1,$$

so that the constraint of the mole fractions summing to unity is automatically satisfied. With this representation, it is clear that point A_1 corresponds to a mixture consisting of 100% species one, 0% species two, and 0% species three. The edge A_1A_2 corresponds to a binary mixture of species one and two, with 0% of species three. Moving along the edge A_1A_2 from left to right, the binary mixture switches from 100% species one to 100% species two. The other two edges have similar interpretations. Figure 2.7 shows how an interior point P of the equilateral triangle may be interpreted. In this figure, the edges of the equilateral triangle are taken to be of unit length, so that the height of the equilateral triangle is $\sqrt{3}/2$. If from an interior point P , we then run lines parallel to the edges of the triangle, an elemen-

tary geometrical argument shows that the molar fractions of the three species can be read off the intersection of the lines with the edges as shown in Figure 2.7.

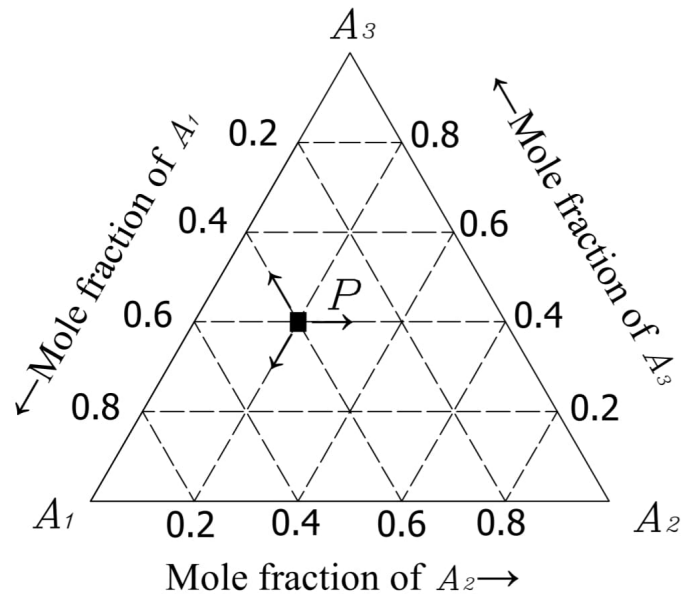


Figure 2.7: In this ternary plot, the point P corresponds to a ternary mixture consisting of 40% of species A_1 , 20% of species A_2 , and 40% of species A_3 .

2.3 The Gibbs Free Energy of A Mixture

I now consider a ternary mixture with mole fractions X_1 , X_2 , X_3 for species one, two, and three, respectively. Since $X_1 + X_2 + X_3 = 1$, it follows that

$$X_1 = 1 - X_2 - X_3, \quad (2.18)$$

and in this way the X_1 dependence can be removed from the discussion. We are usually interested in systems at constant temperature and pressure since in applications the temperature is frequently close to room temperature and the pressure is close to one atmosphere. Hence, the focus of the attention here is usually on the Gibbs free energy G ([8]). In particular, I am interested here in the Gibbs free energy of mixing of a ternary mixture at constant pressure and temperature. I denote this quantity by ΔG_m , and in view of (2.18), write

$$\Delta G_m = \Delta G_m(X_2, X_3), \quad (2.19)$$

which represents a surface in $(X_2, X_3, \Delta G_m)$ space. In Figure 2.8, we plot a representative free surface for a ternary system (adapted from Tompa [90], page 44).

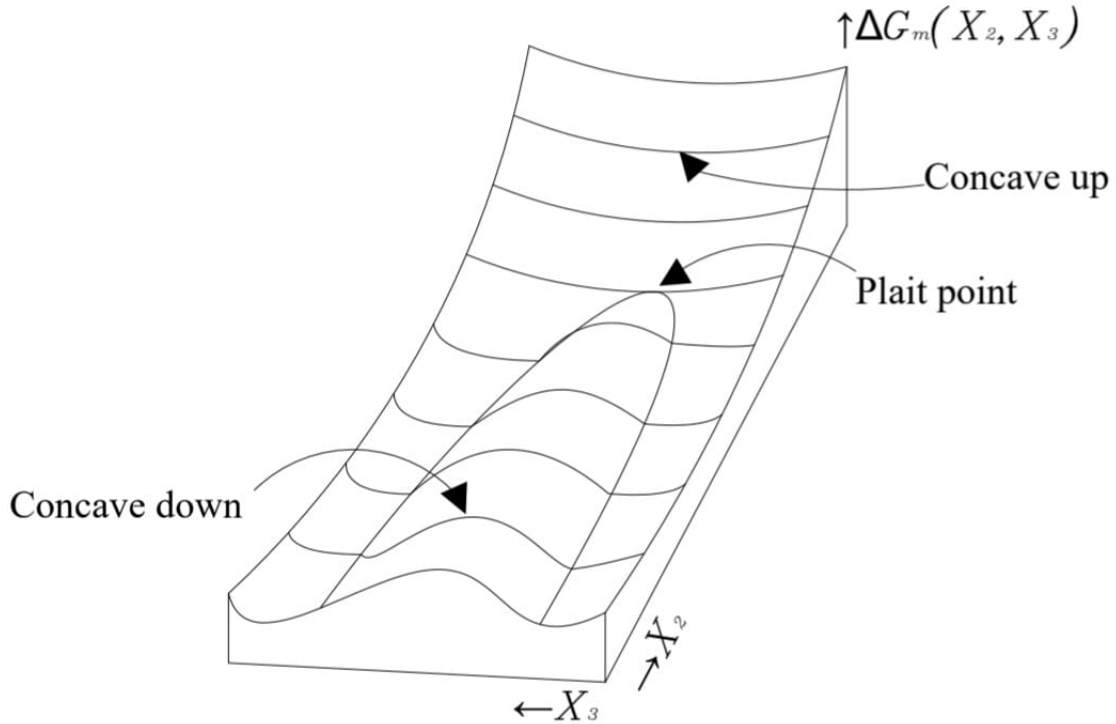


Figure 2.8: Illustration of a free energy surface $\Delta G_m(X_2, X_3)$ of a ternary system at constant temperature and pressure (adapted from [90]).

2.4 Calculating The Phase Diagram For A Ternary System

The discussion given here mirrors that given in Section 2.1 for a binary system, and so the descriptions given here will be briefer. The aim here is to show how to calculate the phase diagram for a ternary system at constant temperature and pressure using the Gibbs free energy of mixing $\Delta G_m(X_2, X_3)$; that is, we identify the regions of (X_1, X_2, X_3) space where the mixture is stable, metastable, and unstable. Like for the binary system, this will involve the definition of a spinodal curve, a binodal curve, and critical points. However, unlike for binary systems, these entities will be plotted in the ternary equilateral triangle for a *fixed* temperature. For binary systems, these quantities are plotted on a temperature and composition diagram. For ternary systems, the quantities are calculated for a given fixed temperature, and need to be recalculated for another temperature.

We begin by introducing some convenient notation. We write

$$G_2 = \frac{\partial \Delta G_m(X_2, X_3)}{\partial X_2},$$

where the derivative is taken with respect to X_2 holding X_3 fixed, and recalling that X_1 has been replaced by $1 - X_2 - X_3$. We can also define second derivatives, for

example

$$G_{23} = \frac{\partial^2 \Delta G_m(X_2, X_3)}{\partial X_2 \partial X_3}$$

and similarly for G_{32} , G_{22} , and G_{33} etc. Higher order derivatives are also similarly defined, for example

$$G_{223} = \frac{\partial^3 \Delta G_m(X_2, X_3)}{\partial X_2^2 \partial X_3},$$

and so on.

2.4.1 Stable Regions

Like for the binary composition case, compositions (X_1, X_2, X_3) are stable homogeneous mixtures if the function $\Delta G_m(X_2, X_3)$ is concave above (or convex), and the calculus of several variables ensures this is the case if (see Appendix A of [71])

$$\det \begin{pmatrix} G_{22} & G_{23} \\ G_{23} & G_{33} \end{pmatrix} > 0 \quad \text{and} \quad G_{22} > 0,$$

or equivalently,

$$G_{22}G_{33} - G_{23}^2 > 0 \quad \text{and} \quad G_{22} > 0. \quad (2.20)$$

Notice the equation (2.20) also implies that $G_{33} > 0$.

2.4.2 The Spinodal Curve

The boundary of the region defined by (2.20) is defined by

$$G_{22}G_{33} - G_{23}^2 = 0,$$

or

$$G_{22}(X_2, X_3)G_{33}(X_2, X_3) = G_{23}^2(X_2, X_3), \quad (2.21)$$

and this defines a curve in (X_2, X_3) space called the spinodal curve; see Figure 2.9.

2.5 The Binodal Curve

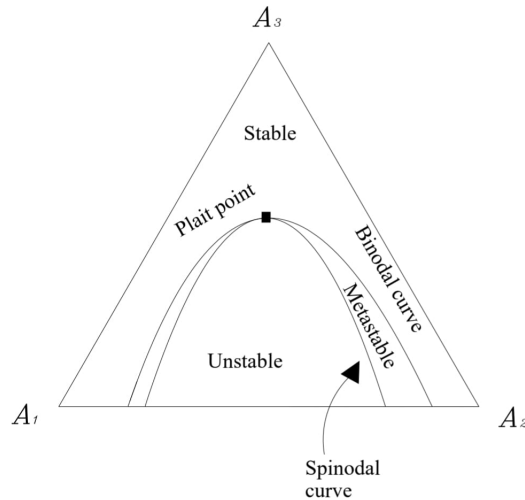


Figure 2.9: An equilateral triangle ternary diagram representation. Here we show representative plots for the spinodal curve, the binodal curve, and a plait point for a fixed temperature and pressure.

In regions where the free energy surface $\Delta G_m(X_2, X_3)$ is not concave above, the ternary mixture may be unstable and phase separation can occur. As for unstable binary mixtures, the question then arises as to how the system will eventually phase separate. To answer this question, we refer to Figure 2.8 and recall the corresponding discussion for binary mixtures. We note that for some vertical cross sections of the surface, the surface has regions which are concave above and concave below. The compositions of coexisting phases are determined by constructing tangent planes to the surface that touch the surface at two distinct points. If we denote these points by P and P' , respectively, then from Maxwell construction, we have that

$$\Delta\mu_1(P) = \Delta\mu_1(P'), \quad \Delta\mu_2(P) = \Delta\mu_2(P'), \quad \Delta\mu_3(P) = \Delta\mu_3(P'), \quad (2.22)$$

and these are just the conditions for coexisting phases P and P' . Hence the solution to equations (2.22) will determine the two coexisting phases that the unstable ternary mixtures will split into for fixed temperature and pressure. The collection of pairs of such points determine the binodal curve; see Figure 2.10. In Figure 2.10, the line joining P to P' is referred to as a tie line.

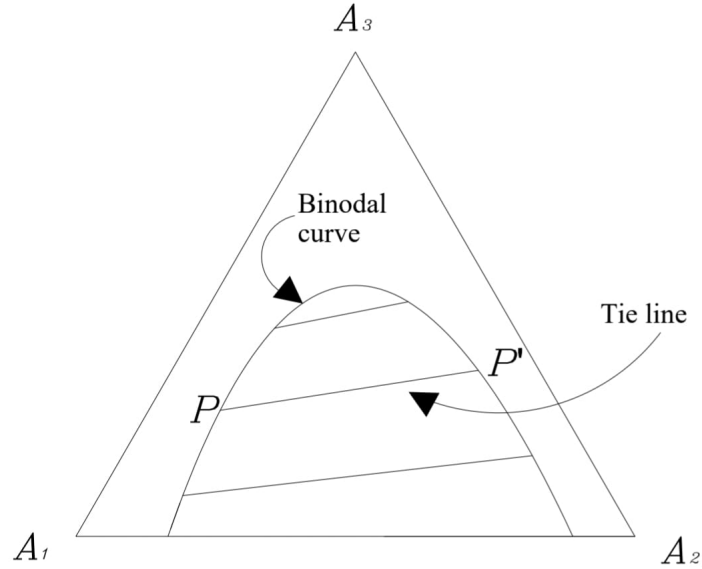


Figure 2.10: A representative ternary diagram showing the binodal curve and a tie line PP' .

The calculation of the binodal curve cannot usually be carried out analytically, and numerical methods typically need to be used. In Chapter 3, we discuss the numerical calculation of binodal curves, and calculate some examples using the mathematical package MATLAB.

2.6 Plait Point

As for binary systems, plait points for ternary systems occur at the intersection of the binodal and spinodal curves; see Figure 2.9. From equation (2.21), we have that along the spinodal

$$\frac{G_{22}}{G_{23}} = \frac{G_{23}}{G_{33}} = g.$$

In Tompa [90], it is shown that at a plait point we have

$$G_{222} - 3gG_{223} + 3g^2G_{233} - g^3G_{333} = 0. \quad (2.23)$$

Chapter 3

The Ternary Flory-Huggins System

In the previous chapter, I discussed general thermodynamic principles for ternary systems. In particular, I discussed the construction of ternary phase diagrams - these diagrams identify the mixture compositions for which the system is stable, unstable, and metastable. In the current chapter, I carry out these calculations for the particular case of a ternary Flory-Huggins system for various temperatures. The Flory-Huggins formulation is the principal model used in this thesis for solid dispersions. Some illustrative numerical calculations are also presented. The accuracy of these calculations is tested by comparing with results in the existing literature.

I begin the discussion with a first principles derivation of the Flory-Huggins model for polymer solutions.

3.1 Derivation Of The Flory-Huggins Model

Although Flory-Huggins theory here has been well-described elsewhere (see, for example, Chapter 7 of the book by Hiemenz [33] or Chapter 21 of the book by Hill [35]), I will review it here because its results will form a key part of the subsequent analysis. Also, deriving the formulae from first principles will yield physical insight into the meaning of the parameters arising, and these intuitions will be of value in the analysis to come. Flory-Huggins theory is really nothing more than an extension of regular solution theory, and so I begin my discussion here with regular solution theory. As a point of novelty and because it is the relevant case for this thesis, I will give the derivation for a ternary system here.

3.1.1 Regular Solution Theory

I use a lattice-based approach ([33]). I consider a ternary mixture, and I suppose that the three species composing the mixture live on a two-dimensional lattice, as

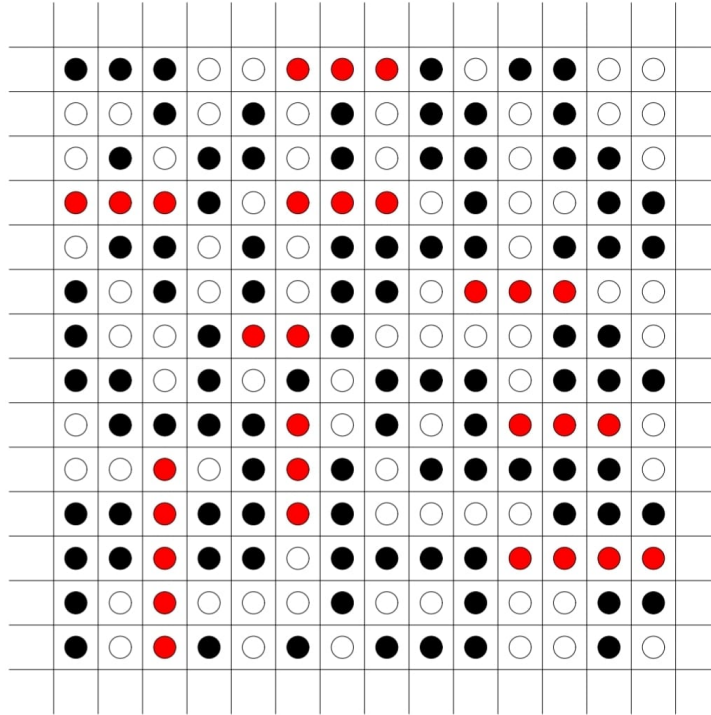


Figure 3.1: Portion of a two-dimensional square lattice containing three species. A molecule of each of the three species is represented by either a red, white, or black circle.

depicted in Figure 3.1. However, the modelling I shall present will also be applicable to a lattice of any dimension. I will label the three components of the mixture by Species i for $i = 1, 2, 3$. In Figure 3.1, a molecule of Species 1 is denoted by a white circle, a molecule of Species 2 by a black circle, and a molecule of Species 3 by a red circle. The size of each square in the lattice is the same, and this reflects the assumption here that a molecule of each species occupies the same volume.

Entropy Of Mixing Of A Regular Solution

In the lattice, I suppose that a lattice site is occupied by either a molecule of Species 1 or Species 2 or Species 3, so that there are no vacant sites. I denote by N_i the number of molecules of Species i for $i = 1, 2, 3$ so that

$$N = N_1 + N_2 + N_3$$

is the total number of lattice sites.

The total entropy of the mixture, $S_{\text{mix}}^{\text{tot}}$, is given by Boltzmann's formula as ([12])

$$S_{\text{mix}}^{\text{tot}} = k \ln(\Omega), \quad (3.1)$$

where k is Boltzmann's constant and Ω is the total number of configurations the mixture can adopt. From the theory of combinatorics (see, for example, [14, Chapter

2], the total number of possible configurations for the system is given by

$$\Omega = \frac{N!}{N_1!N_2!N_3!}. \quad (3.2)$$

It is useful here to use Stirling's approximation for factorials, which states that

$$q! \approx q \ln(q) - q,$$

for large integers q . Since in applications the N_i ($i = 1, 2, 3$) and N are all large integers, we can write

$$\begin{aligned} \ln(\Omega) &\approx N \ln(N) - \cancel{N} - N_1 \ln(N_1) + \cancel{N_1} - N_2 \ln(N_2) + \cancel{N_2} - N_3 \ln(N_3) + \cancel{N_3} \\ &= (N_1 + N_2 + N_3) \ln(N) - N_1 \ln(N_1) - N_2 \ln(N_2) - N_3 \ln(N_3) \\ &= -N_1 \ln\left(\frac{N_1}{N}\right) - N_2 \ln\left(\frac{N_2}{N}\right) - N_3 \ln\left(\frac{N_3}{N}\right). \end{aligned} \quad (3.3)$$

Denoting the mole fraction of Species i by X_i we have that

$$X_i = \frac{N_i}{N_1 + N_2 + N_3} = \frac{N_i}{N}, \quad i = 1, 2, 3, \quad (3.4)$$

and (3.3) then gives

$$\ln(\Omega) \approx -N_1 \ln(X_1) - N_2 \ln(X_2) - N_3 \ln(X_3).$$

Using Boltzmann's formula (3.1), we then have that

$$S_{\text{mix}}^{\text{tot}} \approx -k (N_1 \ln(X_1) + N_2 \ln(X_2) + N_3 \ln(X_3)).$$

I am interested here in the total entropy of mixing (as distinct from the entropy of the mixture) given by

$$\Delta S_{\text{mix}}^{\text{tot}} = S_{\text{mix}}^{\text{tot}} - S_1^{\text{tot}} - S_2^{\text{tot}} - S_3^{\text{tot}},$$

where S_i^{tot} denotes the total entropy of the pure Species i for $i = 1, 2, 3$. Using (3.1), gives

$$S_i^{\text{tot}} = k \ln\left(\frac{N_i!}{N_i!}\right) = 0, \quad i = 1, 2, 3,$$

so that

$$\Delta S_{\text{mix}}^{\text{tot}} = -k (N_1 \ln(X_1) + N_2 \ln(X_2) + N_3 \ln(X_3)), \quad (3.5)$$

where I have now dropped the approximation notation. The entropy of mixing per lattice site is given

$$\Delta S_{\text{mix}}^{\text{latt}} = \frac{\Delta S_{\text{mix}}^{\text{tot}}}{N} = -k (X_1 \ln(X_1) + X_2 \ln(X_2) + X_3 \ln(X_3)), \quad (3.6)$$

and the entropy of mixing per mole of lattice sites is given by

$$\Delta S_{\text{mix}} = N_{Av} \Delta S_{\text{mix}}^{\text{latt}} = -k N_{Av} (X_1 \ln(X_1) + X_2 \ln(X_2) + X_3 \ln(X_3)), \quad (3.7)$$

where N_{Av} is Avogadro's number. Recalling that

$$R = N_{Av}k \quad (3.8)$$

where R is the gas constant, we can rewrite (3.7) as

$$\Delta S_{\text{mix}} = -R(X_1 \ln(X_1) + X_2 \ln(X_2) + X_3 \ln(X_3)). \quad (3.9)$$

Enthalpy Of Mixing For A Regular Solution

I now calculate the enthalpy of mixing of the system. The enthalpy H is given by ([8])

$$H = U + pV,$$

where U is the internal energy of the system, p is the pressure, and V is the volume of the system. Throughout this thesis, I am assuming that the temperature T and the pressure p is constant (T being close to room temperature and p being close to one atmosphere). Also, it is implicitly assumed in the lattice-based picture here that the volume of the system remains constant. Hence, we shall see that the $p - V$ terms will ultimately not contribute to the enthalpy of mixing.

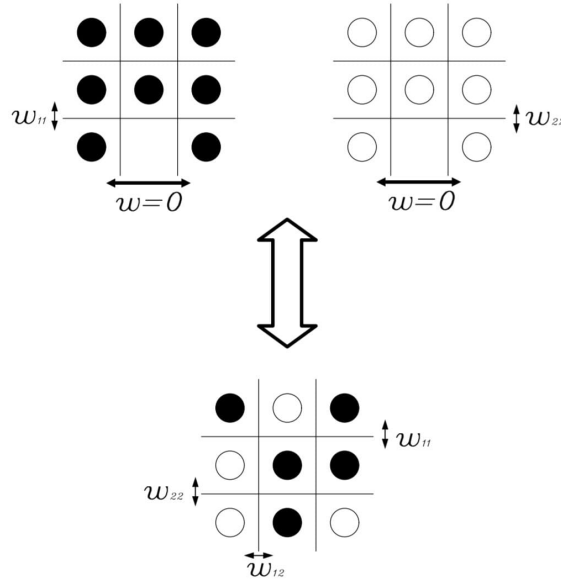


Figure 3.2: Energies of interaction between nearest neighbours of Species 1 and 2 in the lattice. The top two panels illustrate the pure components and the bottom panel illustrates the mixture.

The total enthalpy of the mixture is given by

$$H_{\text{mix}}^{\text{tot}} = U_{\text{mix}}^{\text{tot}} + pV_{\text{mix}}^{\text{tot}},$$

where $U_{\text{mix}}^{\text{tot}}$, $V_{\text{mix}}^{\text{tot}}$ give the total internal energy and volume, respectively, of the mixture. I calculate the total internal energy of the mixture $U_{\text{mix}}^{\text{tot}}$ by consider-

ing energies of interaction between neighbouring atoms. I introduce the following notation; see Figure 3.2.

w_{ii} - the energy of interaction between a molecule of Species i and a neighbouring molecule of Species i for $i = 1, 2, 3$.

w_{ij} - the energy of interaction between a molecule of Species i and a neighbouring molecule of Species j for $i \neq j$ and $i, j = 1, 2, 3$. Here we take $w_{ij} = w_{ji}$ since from Newton's third law, the force that molecule i exerts on molecule j is equal and opposite to the force molecule j exerts on molecule i .

I begin by calculating the expected internal energy associated with a single lattice site, U_s . We denote by z the number of closest neighbours of a lattice site. It is clear that

$$\begin{aligned} U_s &= \sum_{i=1}^3 (\text{probability site is occupied by a molecule of Species } i) \\ &\quad \times (\text{expected energy of interaction given that site is occupied by Species } i) \\ &= X_1 \times (w_{11}(zX_1) + w_{12}(zX_2) + w_{13}(zX_3)) \\ &\quad + X_2 \times (w_{12}(zX_1) + w_{22}(zX_2) + w_{23}(zX_3)), \\ &\quad + X_3 \times (w_{13}(zX_1) + w_{23}(zX_2) + w_{33}(zX_3)) \end{aligned}$$

so that

$$U_s = z (w_{11}X_1^2 + w_{22}X_2^2 + w_{33}X_3^2 + 2w_{12}X_1X_2 + 2w_{13}X_1X_3 + 2w_{23}X_2X_3).$$

Hence the total internal energy of the lattice is given by

$$U_{mix}^{tot} = \frac{1}{2}NU_s = \frac{1}{2}Nz (w_{11}X_1^2 + w_{22}X_2^2 + w_{33}X_3^2 + 2w_{12}X_1X_2 + 2w_{13}X_1X_3 + 2w_{23}X_2X_3),$$

where the 1/2 term has been included here to remove double counting of the energy of interaction between two neighbouring sites. Hence

$$H_{mix}^{tot} = \frac{1}{2}Nz (w_{11}X_1^2 + w_{22}X_2^2 + w_{33}X_3^2 + 2w_{12}X_1X_2 + 2w_{13}X_1X_3 + 2w_{23}X_2X_3) + pV_{tot}. \quad (3.10)$$

For the pure Species i , the enthalpy is given by

$$H_i^{tot} = \frac{1}{2}N_i z w_{ii} + pV_i = \frac{1}{2}N z w_{ii} X_i + pV_i, \quad (3.11)$$

where V_i is the volume of pure Species i for $i = 1, 2, 3$.

Using (3.10) and (3.11), the enthalpy of mixing ΔH_{mix} can now be calculated as

$$\begin{aligned}
\Delta H_{mix}^{tot} &= H_{mix}^{tot} - H_1^{tot} - H_2^{tot} - H_3^{tot} \\
&= \frac{1}{2}Nz (w_{11}X_1^2 + w_{22}X_2^2 + w_{33}X_3^2 + 2w_{12}X_1X_2 + 2w_{13}X_1X_3 + 2w_{23}X_2X_3) \\
&\quad + \cancel{pV_{tot}} - \frac{1}{2}Nzw_{11}X_1 - \cancel{pV_1} - \frac{1}{2}Nzw_{22}X_2 - \cancel{pV_2} - \frac{1}{2}Nzw_{33}X_3 - \cancel{pV_3} \\
&= \frac{1}{2}Nz (w_{11}(X_1^2 - X_1) + w_{22}(X_2^2 - X_2) + w_{33}(X_3^2 - X_3) \\
&\quad + 2w_{12}X_1X_2 + 2w_{13}X_1X_3 + 2w_{23}X_2X_3),
\end{aligned}$$

since I am assuming here that $V_{tot} = V_1 + V_2 + V_3$ - that is, it is assumed here that there is no change in volume in the mixing process. As an aside, Rubinstein & Colby [72] (Chapter 4 of their book) have pointed out that assuming that there is no volume change on mixing is often incorrect, and that polymer blends, for example, will usually undergo a change in volume when mixed. They further point out that the inclusion of volume changes in the modelling will result in the inclusion of non-temperature dependent terms in the interaction parameters χ . In practice, deviations from the standard lattice model are usually lumped into the interaction parameters; see Chapter 4 of this thesis for some further discussion of this topic.

Returning to the calculation, we now have that

$$\begin{aligned}
\Delta H_{mix}^{tot} &= \frac{1}{2}Nz (-w_{11}X_1(X_2 + X_3) - w_{22}X_2(X_1 + X_3) - w_{33}X_3(X_1 + X_2) \\
&\quad + 2w_{12}X_1X_2 + 2w_{13}X_1X_3 + 2w_{23}X_2X_3)
\end{aligned}$$

or

$$\begin{aligned}
\Delta H_{mix}^{tot} &= \frac{1}{2}Nz(2w_{12} - w_{11} - w_{22})X_1X_2 + \frac{1}{2}Nz(2w_{13} - w_{11} - w_{33})X_1X_3 \\
&\quad + \frac{1}{2}Nz(2w_{23} - w_{22} - w_{33})X_2X_3,
\end{aligned}$$

or

$$\Delta H_{mix}^{tot} = Nz\Delta w_{12}X_1X_2 + Nz\Delta w_{13}X_1X_3 + Nz\Delta w_{23}X_2X_3,$$

where

$$\Delta w_{12} = w_{12} - \frac{w_{11} + w_{22}}{2}, \quad \Delta w_{13} = w_{13} - \frac{w_{11} + w_{33}}{2}, \quad \Delta w_{23} = w_{23} - \frac{w_{22} + w_{33}}{2}. \quad (3.12)$$

Here the Δw 's are referred to as *exchange energies*; I will return to the physical interpretation of these parameters later. At this juncture, it is also usual to introduce *interaction parameters* defined by

$$\chi_{12} = \frac{z\Delta w_{12}}{kT}, \quad \chi_{13} = \frac{z\Delta w_{13}}{kT}, \quad \chi_{23} = \frac{z\Delta w_{23}}{kT}, \quad (3.13)$$

so that

$$\begin{aligned}
\Delta H_{mix}^{tot} &= NkT \{ \chi_{12}X_1X_2 + \chi_{13}X_1X_3 + \chi_{23}X_2X_3 \} \\
&= kT \{ N_1X_2\chi_{12} + N_1X_3\chi_{13} + N_2X_3\chi_{23} \}. \quad (3.14)
\end{aligned}$$

The Gibbs free energy of mixing is now given by

$$\Delta G_{mix}^{tot} = \Delta H_{mix}^{tot} - T\Delta S_{mix}^{tot}$$

and using (3.5) and (3.14), this gives

$$\Delta G_{mix}^{tot} = kT \{N_1 \ln(X_1) + N_2 \ln(X_2) + N_3 \ln(X_3) + \chi_{12}N_1X_2 + \chi_{13}N_1X_3 + \chi_{23}N_2X_3\}. \quad (3.15)$$

The Gibbs free energy of mixing per lattice site is

$$\begin{aligned} \Delta G_{mix}^{latt} &= \frac{\Delta G_{mix}^{tot}}{N} \\ &= kT \{X_1 \ln(X_1) + X_2 \ln(X_2) + X_3 \ln(X_3) + \chi_{12}X_1X_2 + \chi_{13}X_1X_3 + \chi_{23}X_2X_3\}, \end{aligned} \quad (3.16)$$

and the Gibbs free energy of mixing per mole of lattice sites is

$$\begin{aligned} \Delta G_{mix} &= N_{Av} \Delta G_{mix}^{latt} \\ &= RT \{X_1 \ln(X_1) + X_2 \ln(X_2) + X_3 \ln(X_3) + \chi_{12}X_1X_2 + \chi_{13}X_1X_3 + \chi_{23}X_2X_3\}. \end{aligned} \quad (3.17)$$

3.1.2 Flory-Huggins Theory

Flory-Huggins theory can be thought of as an extension of regular solution theory in which the molecules of the three species are no longer confined to occupying just one lattice site. The molecules of each species can now occupy a fixed number of contiguous lattice sites. In particular, we suppose here that a molecule of Species i can occupy m_i (≥ 1) contiguous lattice sites for $i = 1, 2, 3$; see Figure 3.3. As an illustrative example, taking $m_1, m_2 \gg 1$ and $m_3 = 1$ could model a ternary system in which Species 1 and Species 2 are both polymers and Species 3 is a drug. I suppose that there are N_i molecules of Species i so that the total number of lattice sites is given by

$$N = m_1N_1 + m_2N_2 + m_3N_3. \quad (3.18)$$

In Flory-Huggins theory, it is convenient to work with volume fractions, and I denote here by ϕ_i the volume fraction of Species i . Clearly, these quantities are given here by

$$\phi_i = \frac{m_iN_i}{m_1N_1 + m_2N_2 + m_3N_3}, \quad (3.19)$$

for $i = 1, 2, 3$.

Entropy Of Mixing For Flory-Huggins Theory

I begin by calculating Ω_1 , the total number of ways in which the N_1 molecules of Species 1 can be arranged on the initially empty lattice. I suppose that i such molecules have already been placed on the lattice, and then consider the number of ways the $(i + 1)$ st polymer chain can be arranged on the lattice. The probability p_i that any given lattice site is now *not* occupied by a polymer monomer is clearly

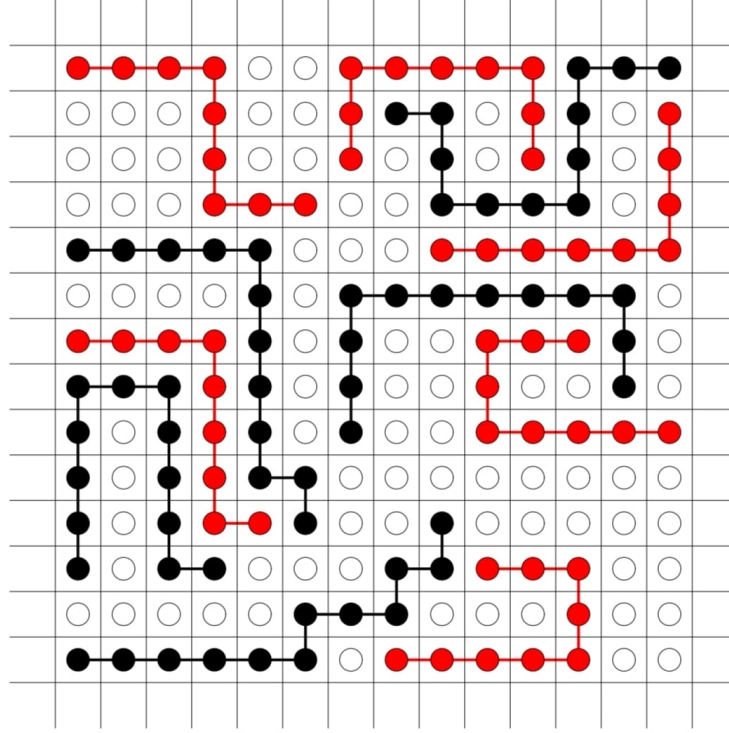


Figure 3.3: Portion of a two-dimensional square lattice containing three species. A molecule of each of the three species is represented by a chain of either red ($m_1 = 9$), black ($m_2 = 12$), or white circles ($m_3 = 1$).

given by

$$p_i = 1 - \frac{m_1 i}{N}.$$

The number of places available for the first bead of the next polymer is given by $N - m_1 i$. The second bead of the polymer has approximately an expected number of available places given by $z p_i$ (more accurately, p_i should be replaced here by $p_i - 1/N$ - but recall that N is typically enormous since macroscopic amounts of material frequently contain between $N = O(10^{21})$ and $N = O(10^{25})$ molecules). The third and subsequent beads of the $(i + 1)$ st polymer all have approximately an expected number of places $(z - 1)p_i$ available to them. Denoting by $\Omega_{1,i+1}$ the number of configurations for the $(i + 1)$ st molecule, I then have

$$\begin{aligned} \Omega_{1,i+1} &\approx (N - m_1 i)(z p_i)((z - 1)p_i)^{m_1 - 2} \approx (N - m_1 i)(z - 1)^{m_1 - 1} \left(\frac{N - m_1 i}{N}\right)^{m_1 - 1} \\ &= \left(\frac{z - 1}{N}\right)^{m_1 - 1} (N - m_1 i)^{m_1}, \end{aligned} \quad (3.20)$$

where I have replaced z by $z - 1$ in one term to simplify the algebra [33]. The total number of possible configurations for placing N_1 polymer molecules on the lattice is given by

$$\Omega_1 = \frac{1}{N_1!} \prod_{i=1}^{N_1} \Omega_{1,i},$$

where the factor $1/N_1!$ has been included to take account of the fact that the N_1 polymer molecules are indistinguishable (for example, for any given configuration, interchanging any two polymer molecules does not change the configuration). Then

$$\Omega_1 = \frac{1}{N_1!} \prod_{i=1}^{N_1} \Omega_{1,i} = \frac{1}{N_1!} \prod_{i=0}^{N_1-1} \Omega_{1,i+1} \approx \frac{1}{N_1!} \left(\frac{z-1}{N} \right)^{N_1(m_1-1)} \prod_{i=0}^{N_1-1} (N - m_1 i)^{m_1}, \quad (3.21)$$

where I have used the approximation (3.20). I now note that

$$\begin{aligned} \frac{(N - im_1)!}{(N - (i+1)m_1)!} &= \frac{(N - im_1)(N - im_1 - 1) \dots (N - (i+1)m_1 + 1)(N - (i+1)m_1)!}{(N - (i+1)m_1)!} \\ &= (N - im_1)(N - im_1 - 1) \dots (N - (i+1)m_1 + 1) \\ &\approx (N - im_1)(N - im_1) \dots (N - im_1) = (N - im_1)^{m_1}, \end{aligned} \quad (3.22)$$

where here we have assumed that $N \gg im_1$ and $im_1 \gg m_1$ for all but a few values of i . The assumption that $N \gg im_1$ is clearly valid in view of (3.18). The assumption that $im_1 \gg m_1$ will not be true for $i = O(1)$ but this will be the case for only a relatively small number of values since i ranges from 1 to $N_1 \gg 1$. Substituting (3.22) in (3.21) yields

$$\begin{aligned} \Omega_1 &\approx \frac{1}{N_1!} \left(\frac{z-1}{N} \right)^{N_1(m_1-1)} \prod_{i=0}^{N_1-1} \frac{(N - im_1)!}{(N - (i+1)m_1)!} \\ &= \frac{1}{N_1!} \left(\frac{z-1}{N} \right)^{N_1(m_1-1)} \left\{ \frac{N!}{(N - m_1)!} \frac{(N - m_1)!}{(N - 2m_1)!} \frac{(N - 2m_1)!}{(N - 3m_1)!} \dots \frac{(N - (N_1 - 1)m_1)!}{(N - N_1 m_1)!} \right\} \\ &= \frac{1}{N_1!} \left(\frac{z-1}{N} \right)^{N_1(m_1-1)} \frac{N!}{(N - N_1 m_1)!}, \end{aligned}$$

so that

$$\Omega_1 = \left(\frac{z-1}{N} \right)^{N_1(m_1-1)} \frac{N!}{N_1!(N - N_1 m_1)!}. \quad (3.23)$$

I now calculate the number of configurations for placing the N_2 molecules of Species 2 on the lattice given that the N_1 molecules of Species 1 have already been placed. The calculation proceeds in a manner very similar to that for Species 1, so I omit most of the details here. I suppose that i molecules of Species 2 have already been arranged on the lattice, and calculate the number of configurations for placing the $(i+1)$ st molecule, $\Omega_{2,i+1}$. I find that (see the derivation of (3.20))

$$\Omega_{2,i+1} = \left(\frac{z-1}{N} \right)^{m_2-1} (N - (m_1 N_1 + m_2 i))^{m_2}.$$

The total number of configurations for placing all N_2 molecules of Species 2 is now given by

$$\Omega_2 = \frac{1}{N_2!} \prod_{i=1}^{N_2} \Omega_{2,i},$$

and this leads to (see the derivation of (3.23))

$$\Omega_2 = \left(\frac{z-1}{N} \right)^{N_2(m_2-1)} \frac{(N - m_1 N_1)!}{N_2!(m_3 N_3)!}. \quad (3.24)$$

The total number of configurations for placing both the Species 1 and Species 2 molecules is now given by

$$\Omega = \Omega_1 \Omega_2 = \left(\frac{z-1}{N} \right)^{N_1(m_1-1)+N_2(m_2-1)} \frac{(N)!}{N_1! N_2! (m_3 N_3)!}.$$

Then (and using Stirling's approximation)

$$\begin{aligned} \ln(\Omega) &= \ln(N!) - \ln(N_1!) - \ln(N_2!) - \ln((m_3 N_3)!) \\ &\quad + (N_1(m_1-1) + N_2(m_2-1)) \ln(z-1) - (N_1(m_1-1) + N_2(m_2-1)) \ln(N) \\ &\approx N \ln(N) - N - N_1 \ln(N_1) + N_1 - N_2 \ln(N_2) + N_2 - m_3 N_3 \ln(m_3 N_3) + m_3 N_3 \\ &\quad + (N_1(m_1-1) + N_2(m_2-1)) \ln(z-1) - (N_1(m_1-1) + N_2(m_2-1)) \ln(N) \\ &= (m_1 N_1 + m_2 N_2 + m_3 N_3) \ln(N) - m_1 N_1 - m_2 N_2 - m_3 N_3 \\ &\quad - N_1 \ln(N_1) + N_1 - N_2 \ln(N_2) + N_2 - m_3 N_3 \ln(m_3 N_3) + m_3 N_3 \\ &\quad + (N_1(m_1-1) + N_2(m_2-1)) \ln(z-1) - (N_1(m_1-1) + N_2(m_2-1)) \ln(N) \\ &= (\text{after some algebra}) \\ &\quad (N_1 + N_2 + N_3) \ln(N) - N_1 \ln(N_1) - N_2 \ln(N_2) - m_3 N_3 \ln(m_3 N_3), \\ &\quad + (N_1(m_1-1) + N_2(m_2-1)) (\ln(z-1) - 1), \end{aligned}$$

so that the total entropy of the system, S_{mix}^{tot} , is given by

$$\begin{aligned} S_{mix}^{tot} &= k[(N_1 + N_2 + N_3) \ln(N) - N_1 \ln(N_1) - N_2 \ln(N_2) - m_3 N_3 \ln(m_3 N_3) \\ &\quad + (N_1(m_1-1) + N_2(m_2-1)) (\ln(z-1) - 1)]. \end{aligned} \quad (3.26)$$

I now calculate the total entropy of the unmixed pure species. These are given by

$$\begin{aligned} S_1^{tot} &= S_{mix}^{tot}(N_2 = 0, N_3 = 0) \\ &= k \{ N_1 \ln(m_1 N_1) - N_1 \ln(N_1) + N_1(m_1-1) (\ln(z-1) - 1) \}, \end{aligned}$$

and

$$\begin{aligned} S_2^{tot} &= S_{mix}^{tot}(N_1 = 0, N_3 = 0) \\ &= k \{ N_2 \ln(m_2 N_2) - N_2 \ln(N_2) + N_2(m_2-1) (\ln(z-1) - 1) \}, \end{aligned}$$

and

$$S_3^{tot} = S_{mix}^{tot}(N_1 = 0, N_2 = 0) = k \{ N_3 \ln(m_3 N_3) - m_3 N_3 \ln(m_3 N_3) \}.$$

The total entropy of mixing is now given by

$$\begin{aligned}\Delta S_{mix}^{tot} &= S_{mix}^{tot} - S_1^{tot} - S_2^{tot} - S_3^{tot} \\ &= k \{ (N_1 + N_2 + N_3) \ln(N) - N_1 \ln(m_1 N_1) - N_2 \ln(m_2 N_2) - N_3 \ln(m_3 N_3) \} \\ &= -k \left\{ N_1 \ln \left(\frac{m_1 N_1}{N} \right) + N_2 \ln \left(\frac{m_2 N_2}{N} \right) + N_3 \ln \left(\frac{m_3 N_3}{N} \right) \right\},\end{aligned}$$

and using (3.19), I now have

$$\Delta S_{mix}^{tot} = -k \{ N_1 \ln(\phi_1) + N_2 \ln(\phi_2) + N_3 \ln(\phi_3) \}. \quad (3.27)$$

Enthalpy Of Mixing For Flory-Huggins Theory

The derivation of the enthalpy of mixing for Flory-Huggins theory is very similar to that for regular solution theory (see [33]). From regular solution theory, we recall from (3.14) that

$$\Delta H_{mix}^{tot} = kT \{ N_1 X_2 \chi_{12} + N_1 X_3 \chi_{13} + N_2 X_3 \chi_{23} \}.$$

In this expression X_i refers to the probability that a given lattice site is occupied by a molecule of Species i . To obtain the corresponding formula for Flory-Huggins theory, we replace X_i by ϕ_i , since ϕ_i is now the probability that a monomer of Species i occupies a lattice site, and we replace N_i by $N_i m_i$. It should be noted that I am suppressing some technical details here for the sake of brevity, and I refer the interested reader to the standard textbooks (for example [35]) for more information. For Flory-Huggins theory, the appropriate form of the total enthalpy is thus given by

$$\Delta H_{mix}^{tot} = kT \{ \chi_{12} m_1 N_1 \phi_2 + \chi_{13} m_1 N_1 \phi_3 + \chi_{23} m_2 N_2 \phi_3 \}.$$

The Gibbs free energy of mixing for Flory-Huggins theory is now given by

$$\Delta G_{mix}^{tot} = \Delta H_{mix}^{tot} - T \Delta S_{mix}^{tot},$$

so that

$$\begin{aligned}\Delta G_{mix}^{tot} &= kT \{ N_1 \ln(\phi_1) + N_2 \ln(\phi_2) + N_3 \ln(\phi_3) \\ &\quad + \chi_{12} m_1 N_1 \phi_2 + \chi_{13} m_1 N_1 \phi_3 + \chi_{23} m_2 N_2 \phi_3 \}.\end{aligned} \quad (3.28)$$

The total number of moles in the mixture is given by

$$N_m = \frac{N_1 + N_2 + N_3}{N_{Av}},$$

and so the Gibbs free energy of mixing per mole is given by

$$\Delta G_{mix} = \frac{\Delta G_{mix}^{tot}}{N_m},$$

which gives

$$\begin{aligned} \Delta G_{mix} = RT \{ & X_1 \ln(\phi_1) + X_2 \ln(\phi_2) + X_3 \ln(\phi_3) \\ & + \chi_{12} m_1 X_1 \phi_2 + \chi_{13} m_1 X_1 \phi_3 + \chi_{23} m_2 X_2 \phi_3 \}. \end{aligned} \quad (3.29)$$

3.2 Flory-Huggins Chemical Potentials

From (3.29), it is clear that

$$\begin{aligned} \frac{\Delta G_{mix}}{RT} = & X_1 \ln(\phi_1) + X_2 \ln(\phi_2) + X_3 \ln(\phi_3) \\ & + (m_1 X_1 + m_2 X_2 + m_3 X_3) (\chi_{12} \phi_1 \phi_2 + \chi_{13} \phi_1 \phi_3 + \chi_{23} \phi_2 \phi_3). \end{aligned} \quad (3.30)$$

It is also worth remarking here that the m_i 's may be written as

$$m_1 = \frac{V_1}{V^*}, \quad m_2 = \frac{V_2}{V^*}, \quad m_3 = \frac{V_3}{V^*}, \quad (3.31)$$

where V_i is the volume of a molecule of species i , and V^* is the volume of a monomer unit.

Before calculating the chemical potentials, it is first worth doing a few preliminary calculations. Using

$$\phi_1 = \frac{m_1 X_1}{m_1 X_1 + m_2 X_2 + m_3 X_3},$$

it follows from straightforward differentiation that

$$\frac{\partial \phi_1}{\partial X_1} = \frac{\phi_1}{X_1} (\phi_2 + \phi_3), \quad (3.32)$$

where here X_2, X_3 are held fixed. Similar calculations give that

$$\frac{\partial \phi_2}{\partial X_2} = \frac{\phi_2}{X_2} (\phi_1 + \phi_3), \quad \frac{\partial \phi_3}{\partial X_3} = \frac{\phi_3}{X_3} (\phi_1 + \phi_2), \quad (3.33)$$

and also

$$\frac{\partial \phi_i}{\partial X_j} = -\frac{\phi_i \phi_j}{X_j} \quad \text{for } i \neq j, \quad i, j = 1, 2, 3. \quad (3.34)$$

Hence, for example,

$$\frac{\partial \phi_1}{\partial X_2} = -\frac{\phi_1 \phi_2}{X_2}, \quad \frac{\partial \phi_2}{\partial X_3} = -\frac{\phi_2 \phi_3}{X_3}.$$

I now calculate the chemical potentials. From [90], we have that

$$\frac{\Delta \mu_1}{RT} = \frac{\partial}{\partial X_1} \left(\frac{\Delta G_{mix}}{RT} \right)$$

and using (3.30), this leads to

$$\begin{aligned} \frac{\Delta\mu_1}{RT} &= \ln(\phi_1) + \frac{X_1}{\phi_1} \frac{\partial\phi_1}{\partial X_1} + \frac{X_2}{\phi_2} \frac{\partial\phi_2}{\partial X_1} + \frac{X_3}{\phi_3} \frac{\partial\phi_3}{\partial X_1} + m_1 (\chi_{12}\phi_1\phi_2 + \chi_{13}\phi_1\phi_3 + \chi_{23}\phi_2\phi_3) \\ &+ (m_1X_1 + m_2X_2 + m_3x_3) \left(\chi_{12} \left[\phi_1 \frac{\partial\phi_2}{\partial X_1} + \phi_2 \frac{\partial\phi_1}{\partial X_1} \right] + \chi_{13} \left[\phi_1 \frac{\partial\phi_3}{\partial X_1} + \phi_3 \frac{\partial\phi_1}{\partial X_1} \right] + \right. \\ &\left. \chi_{23} \left[\phi_2 \frac{\partial\phi_3}{\partial X_1} + \phi_3 \frac{\partial\phi_2}{\partial X_1} \right] \right). \end{aligned}$$

Substituting the expressions (3.32), (3.33) and (3.34) into this last expression, and simplifying the subsequent algebra gives,

$$\begin{aligned} \frac{\Delta\mu_1}{RT} &= \ln(\phi_1) + \left(1 - \frac{m_1}{m_2}\right)\phi_2 + \left(1 - \frac{m_1}{m_3}\right)\phi_3 \\ &+ m_1 (-\chi_{23}\phi_2\phi_3 + \chi_{12}\phi_2(\phi_2 + \phi_3) + \chi_{13}\phi_3(\phi_2 + \phi_3)). \end{aligned} \quad (3.35)$$

The expressions for the chemical potentials can be written in a somewhat simpler form if we introduce three new constants χ_1, χ_2, χ_3 as follows:

$$\begin{aligned} 2\chi_1 &= \chi_{12} + \chi_{13} - \chi_{23}, \\ 2\chi_2 &= \chi_{12} + \chi_{23} - \chi_{13}, \\ 2\chi_3 &= \chi_{13} + \chi_{23} - \chi_{12}. \end{aligned} \quad (3.36)$$

Using (3.36), equation (3.35) can be rewritten as

$$\frac{\Delta\mu_1}{RT} = \ln(\phi_1) + \left(1 - \frac{m_1}{m_2}\right)\phi_2 + \left(1 - \frac{m_1}{m_3}\right)\phi_3 + m_1 (\chi_1(\phi_2 + \phi_3)^2 + \chi_2\phi_2^2 + \chi_3\phi_3^2). \quad (3.37)$$

It follows from symmetry that

$$\begin{aligned} \frac{\Delta\mu_2}{RT} &= \ln(\phi_2) + \left(1 - \frac{m_2}{m_1}\right)\phi_1 + \left(1 - \frac{m_2}{m_3}\right)\phi_3 + m_2 (\chi_2(\phi_1 + \phi_3)^2 + \chi_1\phi_1^2 + \chi_3\phi_3^2), \\ \frac{\Delta\mu_3}{RT} &= \ln(\phi_3) + \left(1 - \frac{m_3}{m_2}\right)\phi_2 + \left(1 - \frac{m_3}{m_1}\right)\phi_1 + m_3 (\chi_3(\phi_1 + \phi_2)^2 + \chi_1\phi_1^2 + \chi_2\phi_2^2). \end{aligned} \quad (3.38)$$

3.3 The Spinodal Curve and Plait Points

I begin by calculating the spinodal curve for the ternary Flory-Huggins model using the theory developed in Chapter 2. The Gibbs free energy per unit volume, ΔG_V is given by

$$\frac{\Delta G_V}{RT} = \frac{\Delta G_{mix}}{RT(m_1X_1 + m_2X_2 + m_3X_3)},$$

and using (3.30), this gives

$$\begin{aligned} \frac{\Delta G_V}{RT} &= \frac{\phi_1}{m_1} \ln(\phi_1) + \frac{\phi_2}{m_2} \ln(\phi_2) + \frac{\phi_3}{m_3} \ln(\phi_3) \\ &\quad + \chi_{12}\phi_1\phi_2 + \chi_{13}\phi_1\phi_3 + \chi_{23}\phi_2\phi_3. \end{aligned} \quad (3.39)$$

For the subsequent calculations, I set $\phi_1 = 1 - \phi_2 - \phi_3$, so that (3.39) becomes

$$\begin{aligned} \frac{\Delta G_V}{RT} &= \frac{1 - \phi_2 - \phi_3}{m_1} \ln(1 - \phi_2 - \phi_3) + \frac{\phi_2}{m_2} \ln(\phi_2) + \frac{\phi_3}{m_3} \ln(\phi_3) \\ &\quad + \chi_{12}(1 - \phi_2 - \phi_3)\phi_2 + \chi_{13}(1 - \phi_2 - \phi_3)\phi_3 + \chi_{23}\phi_2\phi_3. \end{aligned} \quad (3.40)$$

I then define G_i , G_{ij} , G_{ijk} to be

$$\begin{aligned} G_i &= \frac{\partial}{\partial \phi_i} \left(\frac{\Delta G_V}{RT} \right) \quad \text{for } i = 2, 3, \\ G_{ij} &= \frac{\partial^2}{\partial \phi_i \partial \phi_j} \left(\frac{\Delta G_V}{RT} \right) \quad \text{for } i, j = 2, 3, \\ G_{ijk} &= \frac{\partial^3}{\partial \phi_i \partial \phi_j \partial \phi_k} \left(\frac{\Delta G_V}{RT} \right) \quad \text{for } i, j, k = 2, 3. \end{aligned} \quad (3.41)$$

Using (3.40) and (3.41), I obtain

$$\begin{aligned} \frac{G_{22}}{RT} &= \frac{1}{m_1} \frac{1}{\phi_1} + \frac{1}{m_2} \frac{1}{\phi_2} - 2\chi_1 - 2\chi_2, \\ \frac{G_{33}}{RT} &= \frac{1}{m_1} \frac{1}{\phi_1} + \frac{1}{m_3} \frac{1}{\phi_3} - 2\chi_1 - 2\chi_3, \\ \frac{G_{23}}{RT} &= \frac{1}{m_1} \frac{1}{\phi_1} - 2\chi_1. \end{aligned} \quad (3.42)$$

For convenience, I introduce quantities ψ_1, ψ_2, ψ_3 via

$$\frac{1}{\psi_1} = \frac{1}{m_1\phi_1} - 2\chi_1, \quad \frac{1}{\psi_2} = \frac{1}{m_2\phi_2} - 2\chi_2, \quad \frac{1}{\psi_3} = \frac{1}{m_3\phi_3} - 2\chi_3, \quad (3.43)$$

and then

$$\begin{aligned} \frac{G_{23}}{RT} &= \frac{1}{\psi_1}, \\ \frac{G_{22}}{RT} &= \frac{1}{\psi_1} + \frac{1}{\psi_2}, \\ \frac{G_{33}}{RT} &= \frac{1}{\psi_1} + \frac{1}{\psi_3}. \end{aligned} \quad (3.44)$$

The spinodal is determined from the equation (see (2.21) in Chapter 2)

$$G_{22}G_{33} = G_{23}^2,$$

and using (3.44), this gives

$$\left(\frac{1}{\psi_1} + \frac{1}{\psi_2}\right)\left(\frac{1}{\psi_1} + \frac{1}{\psi_3}\right) = \frac{1}{\psi_1^2},$$

and this can be simplified to give

$$\psi_1 + \psi_2 + \psi_3 = 0. \quad (3.45)$$

It is also useful to derive an equation for the spinodal in terms of the volume fractions ϕ_i . From (3.43) and (3.45), it is clear that

$$\frac{m_1\phi_1}{1 - 2\chi_1 m_1\phi_1} + \frac{m_2\phi_2}{1 - 2\chi_2 m_2\phi_2} + \frac{m_3\phi_3}{1 - 2\chi_3 m_3\phi_3} = 0, \quad (3.46)$$

and this can be rewritten in the form

$$\begin{aligned} m_1\phi_1 + m_2\phi_2 + m_3\phi_3 - 2([\chi_1 + \chi_2]m_1m_2\phi_1\phi_2 + [\chi_1 + \chi_3]m_1m_3\phi_1\phi_3 \\ + [\chi_2 + \chi_3]m_2m_3\phi_2\phi_3) + 4(\chi_2\chi_3 + \chi_1\chi_3 + \chi_1\chi_2)m_1m_2m_3\phi_1\phi_2\phi_3 = 0, \end{aligned} \quad (3.47)$$

or

$$\sum_{i=1}^3 m_i\phi_i - 2 \sum_{\substack{i < j \\ i,j=1,3}} (\chi_i + \chi_j)m_im_j\phi_i\phi_j + Qm_1m_2m_3\phi_1\phi_2\phi_3 = 0, \quad (3.48)$$

where

$$Q = 4(\chi_2\chi_3 + \chi_1\chi_3 + \chi_1\chi_2). \quad (3.49)$$

I now turn my attention to the calculation of the plait points. At the plait points, equation (3.45) must be satisfied as well as the equation (see (2.23) in Chapter 2)

$$G_{222} - 3gG_{223} + 3g^2G_{233} - g^3G_{333} = 0, \quad (3.50)$$

where

$$g = \frac{G_{22}}{G_{23}} = \frac{G_{23}}{G_{33}}.$$

Using (3.44) gives

$$g = \frac{G_{22}}{G_{23}} = \frac{\frac{1}{\psi_1} + \frac{1}{\psi_2}}{\frac{1}{\psi_1}} = \frac{\psi_1 + \psi_2}{\psi_2} = -\frac{\psi_3}{\psi_2}. \quad (3.51)$$

Using (3.42), straightforward differentiation gives

$$\begin{aligned} \frac{G_{222}}{RT} &= \frac{1}{m_1\phi_1^2} - \frac{1}{m_2\phi_2^2}, & \frac{G_{223}}{RT} &= \frac{1}{m_1\phi_1^2}, \\ \frac{G_{233}}{RT} &= \frac{1}{m_1\phi_1^2}, & \frac{G_{333}}{RT} &= \frac{1}{m_1\phi_1^2} - \frac{1}{m_3\phi_3^2}. \end{aligned} \quad (3.52)$$

Using (3.43), these expressions may be rewritten as:

$$\begin{aligned}\frac{G_{222}}{RT} &= \frac{m_1(1 + 2\chi_1\psi_1)^2}{\psi_1^2} - \frac{m_2(1 + 2\chi_2\psi_2)^2}{\psi_2^2}, \\ \frac{G_{223}}{RT} &= \frac{m_1(1 + 2\chi_1\psi_1)^2}{\psi_1^2}, \\ \frac{G_{233}}{RT} &= \frac{m_1(1 + 2\chi_1\psi_1)^2}{\psi_1^2}, \\ \frac{G_{333}}{RT} &= \frac{m_1(1 + 2\chi_1\psi_1)^2}{\psi_1^2} - \frac{m_3(1 + 2\chi_3\psi_3)^2}{\psi_3^2}.\end{aligned}\tag{3.53}$$

Substituting (3.53) and (3.51) into (3.50) gives (after some algebra)

$$m_1\psi_1(1 + 2\chi_1\psi_1)^2 + m_2\psi_2(1 + 2\chi_2\psi_2)^2 + m_3\psi_3(1 + 2\chi_3\psi_3)^2 = 0,$$

or

$$\sum_{i=1}^3 m_i\psi_i(1 + 2\chi_i\psi_i)^2 = 0\tag{3.54}$$

Finally, using

$$\phi_1 + \phi_2 + \phi_3 = 1,$$

and (3.43) gives

$$\sum_{i=1}^3 \frac{\psi_i}{m_i(1 + 2\chi_i\psi_i)} = 1.\tag{3.55}$$

To summarise, the plait points are determined by simultaneously solving the three equations (3.45), (3.54), (3.55) for the three unknowns ψ_i . For convenience, I gather these equations together here:

$$\begin{aligned}\sum_{i=1}^3 \psi_i &= 0, \\ \sum_{i=1}^3 m_i\psi_i(1 + 2\chi_i\psi_i)^2 &= 0, \\ \sum_{i=1}^3 \frac{\psi_i}{m_i(1 + 2\chi_i\psi_i)} &= 1.\end{aligned}\tag{3.56}$$

I will return to the numerical solution of these equations using Maple later in this chapter 3.4.4

3.3.1 The Intersection Of The Spinodal With The $\phi_3 = 0$ Binary

The location of the points where the spinodal intersects the $\phi_3 = 0$ binary will feature in the coming chapters, and so I briefly address this issue here. In terms of volume fractions, the spinodal curve is determined by the following pair of equations

$$\begin{aligned}\phi_1 + \phi_2 + \phi_3 &= 1, \\ \frac{m_1\phi_1}{1 - 2\chi_1 m_1\phi_1} + \frac{m_2\phi_2}{1 - 2\chi_2 m_2\phi_2} + \frac{m_3\phi_3}{1 - 2\chi_3 m_3\phi_3} &= 0.\end{aligned}$$

The equations determining the intersection of the spinodal with the binary $\phi_3 = 0$ are thus

$$\begin{aligned}\phi_1 + \phi_2 &= 1, \\ \frac{m_1\phi_1}{1 - 2\chi_1 m_1\phi_1} + \frac{m_2\phi_2}{1 - 2\chi_2 m_2\phi_2} &= 0,\end{aligned}$$

and these equations imply that $\phi_1 = 1 - \phi_2$ where ϕ_2 is determined by solving the following quadratic equation for ϕ_2 :

$$(2\chi_{12}m_1m_2)\phi_2^2 - (m_1 - m_2 + 2\chi_{12}m_1m_2)\phi_2 + m_1 = 0.$$

Denoting the left and right points of intersection of the spinodal curve with the binary $\phi_3 = 0$ by $(\phi_{1L}^s, \phi_{2L}^s, 0)$ and $(\phi_{1R}^s, \phi_{2R}^s, 0)$, respectively, I now have that

$$\begin{aligned}\phi_{1L}^s &= \frac{m_2 - m_1 + 2\chi_{12}m_1m_2 + \sqrt{\text{discr}}}{4\chi_{12}m_1m_2}, & \phi_{2L}^s &= \frac{m_1 - m_2 + 2\chi_{12}m_1m_2 - \sqrt{\text{discr}}}{4\chi_{12}m_1m_2}, \\ \phi_{1R}^s &= \frac{m_2 - m_1 + 2\chi_{12}m_1m_2 - \sqrt{\text{discr}}}{4\chi_{12}m_1m_2}, & \phi_{2R}^s &= \frac{m_1 - m_2 + 2\chi_{12}m_1m_2 + \sqrt{\text{discr}}}{4\chi_{12}m_1m_2},\end{aligned}\tag{3.57}$$

where

$$\text{discr} = (m_1 - m_2 + 2\chi_{12}m_1m_2)^2 - 8\chi_{12}m_1m_2^2.\tag{3.58}$$

Clearly for both of these points to exist, we require that the volume fractions (ϕ) involved be real and that $0 \leq \phi \leq 1$, and this imposes restrictions on the values for m_1 , m_2 and χ_{12} . I will not pursue this issue in detail here except to make one comment about the value of χ_{12} since it will arise in the coming analysis. A necessary condition for the spinodal to intersect the binary $\phi_3^s = 0$ at two distinct points is that $\text{discr} > 0$, so that (using (3.58))

$$\chi_{12}^2 - \frac{m_1 + m_2}{m_1m_2}\chi_{12} + \frac{(m_1 - m_2)^2}{4m_1^2m_2^2} > 0.\tag{3.59}$$

It is easy to show that condition (3.59) is satisfied if

$$\chi_{12} > \chi_{12}^c$$

where the critical value χ_{12}^c is given by

$$\chi_{12}^c = \frac{1}{2} \left(\frac{1}{\sqrt{m_1}} + \frac{1}{\sqrt{m_2}} \right)^2. \quad (3.60)$$

The corresponding formulae for the intersects of the spinodal with the $\phi_1^s = 0$ and $\phi_2^s = 0$ binaries follow easily by symmetry.

3.4 Numerical calculations

I now give the details of how the numerical calculations for the ternary phase diagrams were carried out. The procedures were implemented using the mathematical packages MATLAB and Maple. I will give relevant snippets of the MATLAB and Maple codes here, and then list the complete code in the appendices. I will test the accuracy of the codes by reproducing some results that already exist in the literature. Then in Chapter 4, I present some new results for solid dispersions. I begin with the calculation of the binodal curve.

3.4.1 Binodal calculations

I now refer back to Section 2.5, and in particular Figure 2.10. For a given temperature, the binodal curve consists of a collection of pair of points P and P' (joined by a tie line) determined by solving equations (2.22) in a manner I now describe. It should be emphasized that the curve obtained is only valid for a given temperature value. For another temperature value, the curve needs to be re-calculated.

It is more convenient here to work in volume fraction space. I suppose that the left tie point P corresponds to volume fractions $(\phi_{1L}, \phi_{2L}, \phi_{3L})$ and that the right tie point corresponds to the volume fractions $(\phi_{1R}, \phi_{2R}, \phi_{3R})$. Since $\phi_{1L} = 1 - \phi_{2L} - \phi_{3L}$ and $\phi_{1R} = 1 - \phi_{2R} - \phi_{3R}$, it is clear that equations (2.22) can be rewritten as

$$\begin{aligned} \Delta\mu_1(1 - \phi_{2L} - \phi_{3L}, \phi_{2L}, \phi_{3L}) &= \Delta\mu_1(1 - \phi_{2R} - \phi_{3R}, \phi_{2R}, \phi_{3R}), \\ \Delta\mu_2(1 - \phi_{2L} - \phi_{3L}, \phi_{2L}, \phi_{3L}) &= \Delta\mu_2(1 - \phi_{2R} - \phi_{3R}, \phi_{2R}, \phi_{3R}), \\ \Delta\mu_3(1 - \phi_{2L} - \phi_{3L}, \phi_{2L}, \phi_{3L}) &= \Delta\mu_3(1 - \phi_{2R} - \phi_{3R}, \phi_{2R}, \phi_{3R}). \end{aligned} \quad (3.61)$$

Equations (3.61) constitute a set of three equations in the four unknowns $\phi_{2L}, \phi_{3L}, \phi_{2R}, \phi_{3R}$. Hence, the problem is clearly not well-posed. To pose the problem, I fixed the value of one of the unknowns. In the calculations presented here, I fixed the value of ϕ_{3L} , so that

$$\phi_{3L} = K, \quad (3.62)$$

where K is a fixed chosen constant. Equations (3.61) now become

$$\begin{aligned}\Delta\mu_1(1 - \phi_{2L} - K, \phi_{2L}, K) &= \Delta\mu_1(1 - \phi_{2R} - \phi_{3R}, \phi_{2R}, \phi_{3R}), \\ \Delta\mu_2(1 - \phi_{2L} - K, \phi_{2L}, K) &= \Delta\mu_2(1 - \phi_{2R} - \phi_{3R}, \phi_{2R}, \phi_{3R}), \\ \Delta\mu_3(1 - \phi_{2L} - K, \phi_{2L}, K) &= \Delta\mu_3(1 - \phi_{2R} - \phi_{3R}, \phi_{2R}, \phi_{3R}),\end{aligned}\tag{3.63}$$

which is a set of three equations for the three unknowns ϕ_{2L} , ϕ_{2R} and ϕ_{3R} . This well-posed problem can in principle be solved numerically to give one pair of points (P, P') on the binodal curve. The value for K can then be changed, and the process repeated to yield another pair of points (P, P') on the binodal curve.

This approach was attempted in the current thesis using the nonlinear solvers provided by the mathematical packages Maple [57] and MATLAB [41] - for example, the `fsolve` command of Maple. However, the results were unsatisfactory. For many parameter values, the solvers simply failed to find the relevant roots. The `fsolve` command of Maple [57] uses various methods for finding the roots depending on what type of equations it is trying to solve. In the current context, there are three nonlinear equations to be solved for three unknowns. Unfortunately, Maple's `fsolve` command does not allow the algorithm for finding the solutions to be explicitly specified, although providing hints giving approximate values for the solutions is permitted. Nevertheless, even when given good estimates for the solutions, the command frequently failed to find the relevant roots. MATLAB [41] also has a command called `fsolve` for root-finding, but this does allow for the method to be specified by using the `Algorithm` option in `optimoptions`. However, I found that this command also failed to reliably find the relevant roots even when given reasonable initial guesses. This approach was eventually abandoned in favor of an optimization procedure.

3.4.2 Optimization Approach

In this approach, an *objective function* is minimized. The objective function chosen here is (see [39],[89])

$$OBJ(P, P') = \frac{1}{(R^2T^2)} \sum_{i=1}^3 (\Delta\mu_i(P) - \Delta\mu_i(P'))^2,\tag{3.64}$$

since the absolute minimum of this objective function (zero) corresponds to the solution of (2.22). It is convenient to introduce the factor $1/(R^2T^2)$ in (3.64) to remove the dimensions from the objective function - recall that the temperature T is being held fixed here for a given binodal. However, there is one significant complication. The trivial solution $P = P'$ also minimizes (3.64), and this solution must be avoided; recall that we are searching for two distinct phases with $P \neq P'$. There are a number of approaches to avoiding the trivial solution - see, for example [39], where a scaling approach is used. However, we favor the approach taken in [89] here, where a nonlinear constraint is imposed. Specifically, I imposed

$$\| P - P' \| \geq \lambda > 0,\tag{3.65}$$

where

$$\| P - P' \| = \sqrt{(\phi_{1R} - \phi_{1L})^2 + (\phi_{2R} - \phi_{2L})^2 + (\phi_{3R} - \phi_{3L})^2}, \quad (3.66)$$

recalling that P has composition $(\phi_{1L}, \phi_{2L}, \phi_{3L})$ and P' has composition $(\phi_{1R}, \phi_{2R}, \phi_{3R})$. Also, λ is a chosen positive parameter which needed to be adjusted for different values of K and was selected by a process of trial and error. Recalling equations (3.63), equation (3.64) can be rewritten as

$$\begin{aligned} OBJ(\phi_{2L}, \phi_{2R}, \phi_{3R}; K) = & \quad (3.67) \\ & \frac{1}{(R^2T^2)} \sum_{i=1}^3 (\Delta\mu_i(1 - \phi_{2L} - K, \phi_{2L}, K) - \Delta\mu_i(1 - \phi_{2R} - \phi_{3R}, \phi_{2R}, \phi_{3R}))^2, \end{aligned}$$

and (3.65) as

$$\sqrt{(\phi_{2R} + \phi_{3R} - K - \phi_{2L})^2 + (\phi_{2R} - \phi_{2L})^2 + (\phi_{3R} - K)^2} \geq \lambda(K) > 0. \quad (3.68)$$

Since the ϕ 's are volume fractions, it is clear that we also have the constraints

$$0 \leq \phi_{2L} \leq 1, \quad 0 \leq \phi_{2R} \leq 1, \quad 0 \leq \phi_{3R} \leq 1. \quad (3.69)$$

To summarise: for a fixed value of K , the optimization problem consists of searching the three dimensional space $(\phi_{2L}, \phi_{2R}, \phi_{3R})$ to minimize the objective function (3.67) subject to the constraints (3.68) and (3.69). Notice that in (3.68) we have written $\lambda = \lambda(K)$ to emphasize the fact that in practice we needed to adjust the value of λ depending on the value of K . Each performance of the optimization process yields a pair of points (P, P') on the binodal curve. Other points on the binodal are calculated by varying the value of K .

I next needed a mathematical tool to solve the optimization problem defined by (3.68), (3.68) and (3.69), and this was provided by the mathematical package MATLAB.

3.4.3 The Matlab Optimization Toolbox and fmincon

MATLAB's Optimization Toolbox [42] provides a suite of tools for minimizing/-maximizing objective functions subject to constraints. In particular, I used the routine `fmincon` of the toolbox to solve our nonlinear optimization problem defined by (3.67), (3.68) and (3.69).

I have housed the code in three separate MATLAB programs as follows (the full programs are listed in the appendix for this chapter):

- `nonlcon.m` - this program contains the nonlinear constraint;
- `objective.m` - this program contains the objective function to be minimized;
- `minit.m` - this programs calls the `fmincon` routine that solves the minimization problem.

In `minit.m`, the `fmincon` routine is called as follows

$$\text{fmincon}(@(\mathbf{X})\text{objective}(\mathbf{X}), \mathbf{X0}, \mathbf{A}, \mathbf{b}, \mathbf{Aeq}, \mathbf{beq}, \mathbf{lb}, \mathbf{ub}, @(\mathbf{X})\text{nonlcon3}(\mathbf{X}), \text{options}); \quad (3.70)$$

We first note that \mathbf{X} is the vector $\mathbf{X} = [\mathbf{X}[1], \mathbf{X}[2], \mathbf{X}[3]]$ where

$$\mathbf{X}[1] = \phi_{2L}, \quad \mathbf{X}[2] = \phi_{2R}, \quad \mathbf{X}[3] = \phi_{3R}.$$

In this notation, the objective function can now be written in the form

$$\text{OBJ}(\mathbf{X}[1], \mathbf{X}[2], \mathbf{X}[3]) = \frac{1}{R^2 T^2} \sum_{i=1}^3 (\Delta\mu_i (1 - \mathbf{X}[1] - K, \mathbf{X}[1], K) - \Delta\mu_i (1 - \mathbf{X}[2] - \mathbf{X}[3], \mathbf{X}[2], \mathbf{X}[3]))^2.$$

We now explain each argument in the call to `fmincom` given in (3.70).

- `@(X)objective(X)` - here `objective(X)` defines the function to be minimized.
- `X0` - this contains the initial guess given to `fmincon` for the solution $\mathbf{X} = [\mathbf{X}[1], \mathbf{X}[2], \mathbf{X}[3]] = [\phi_{2L}, \phi_{2R}, \phi_{3R}]$. These values can be adjusted as `fmincon` closes in on the solution.
- `A, b` - here `A` is a 3×3 matrix and `b` is a 1×3 vector that defines linear inequalities of the form $\mathbf{AX} \leq \mathbf{b}$. In our problem, there are no linear inequalities and so we set `A = []`; `b = []`; - see `minit.m` in the appendices.
- `Aeq, beq` - here `Aeq` is a 3×3 matrix and `beq` is a 1×3 vector that defines linear equalities of the form $\mathbf{AeqX} = \mathbf{beq}$. In our problem, there are no linear equality constraints and so we set `A = []`; `b = []`; - see `minit.m` in the appendices.
- `lb, ub` - here `lb` and `ub` refer to lower bounds and upper bounds, respectively, for $\mathbf{X} = [\mathbf{X}[1], \mathbf{X}[2], \mathbf{X}[3]]$. Recalling that the \mathbf{X} 's here are volume fractions, we have that $0 \leq \mathbf{X}[i] \leq 1$ for $i = 1, 2, 3$. Hence, in the program `minit.m`, we set `lb = [0.0, 0.0, 0.0]`; `ub = [1.0, 1.0, 1.0]`;
- `@(X)nonlcon(X)` - this function defines the nonlinear constraints on the unknowns \mathbf{X} . The nonlinear constraints can take the form of an equality `ceq(X) = 0` or an inequality `c(X) ≤ 0`. In the problem solved here, there are no equality constraints, so we set `ceq = []`. For the problem I solve, the function `c(X)` is given by (see equation (3.68) above)

$$c(\mathbf{X}) = \text{lambda}^2 - (\mathbf{X}(3) - K)^2 - (\mathbf{X}(2) - \mathbf{X}(1))^2 - (\mathbf{X}(2) + \mathbf{X}(3) - K - \mathbf{X}(1))^2.$$

- `options` - creates options for the optimization procedure `fmincon`. Specifically, the `options` are set using `optimoptions`. I now display a typical set of `options`, and explain their meaning.

```
options = optimoptions ('fmincon', 'Algorithm', 'sqp', ...
'OptimalityTolerance', 1.0e-9, 'ConstraintTolerance', 1.0e-8, ...,
'MaxFunctionEvaluation', 300000, 'StepTolerarne', 1.0e-8, ...
```

```
'Display', 'iter', 'MaxIterations', 6000, ...
'FunctionTolerance', 1.0e-11);
```

The general structure for optimoptions is

```
options = optimoptions (Solver Name, Name, Value, ...
Name, Value, Name, Value, ....)
```

If we were to just specify

```
options = optimoptions('fmincom')
```

then all of the default values for the parameters of the solver `fmincon` are used. Specifying

```
options = optimoptions ('fmincon', 'Algorithm', 'sqp')
```

changes the default value for `Algorithm` to `sqp`, and so on. `sqp` here stands for sequential quadratic programming. The meaning of the other values can be found in the MATLAB documentation [41].

In the numerical results calculated here, I usually did not accept a solution unless

$$\text{OBJ}(X[1], X[2], X[3], K) \leq 10^{-13}.$$

The value 10^{-13} produced results that were acceptable from visual inspection of the binodals, and is three orders of magnitudes smaller than the value used by Hsu & Prausnitz [39].

3.4.4 Using Maple to Calculate the Plait Points

The Maple program used to calculate the Plait points can be found in Appendix A.1. This Maple program calculates the plait points by solving equations (3.56).

3.4.5 Using Maple to Calculate the Spinodal Curves

The Maple program used to calculate the spinodal curves in this thesis can be found in Appendix A.2. This Maple program calculated the spinodal curves using equation (3.46).

3.4.6 Using MATLAB to Calculate the Binodal Curve

The MATLAB program used to calculate the binodal curves in this thesis can be found in Appendix A.3.

3.4.7 Testing The Accuracy Of The Numerical Procedures

The first task is to test the accuracy of our numerical methods by comparing our results to results already existing in literature. Once good agreement has been found with existing results, I can then proceed with more confidence to calculate phase diagrams for the parameter regimes I am interested in studying for the current work. For these purposes, we chose the paper by Hsu & Prausnitz [39]. In this paper, they plot binodal curves for ternary Flory-Huggins systems for various sets of parameter values. Throughout their calculations, they use the values

$$m_1 = 1000, \quad m_2 = 1000, \quad m_3 = 1,$$

corresponding to a polymer-polymer-solvent system. In Figure 3.4, we plot the results of our calculations for ternary phase diagrams and note that these results are in good agreement with the binodals displayed in [39] as evaluated by visual inspection.

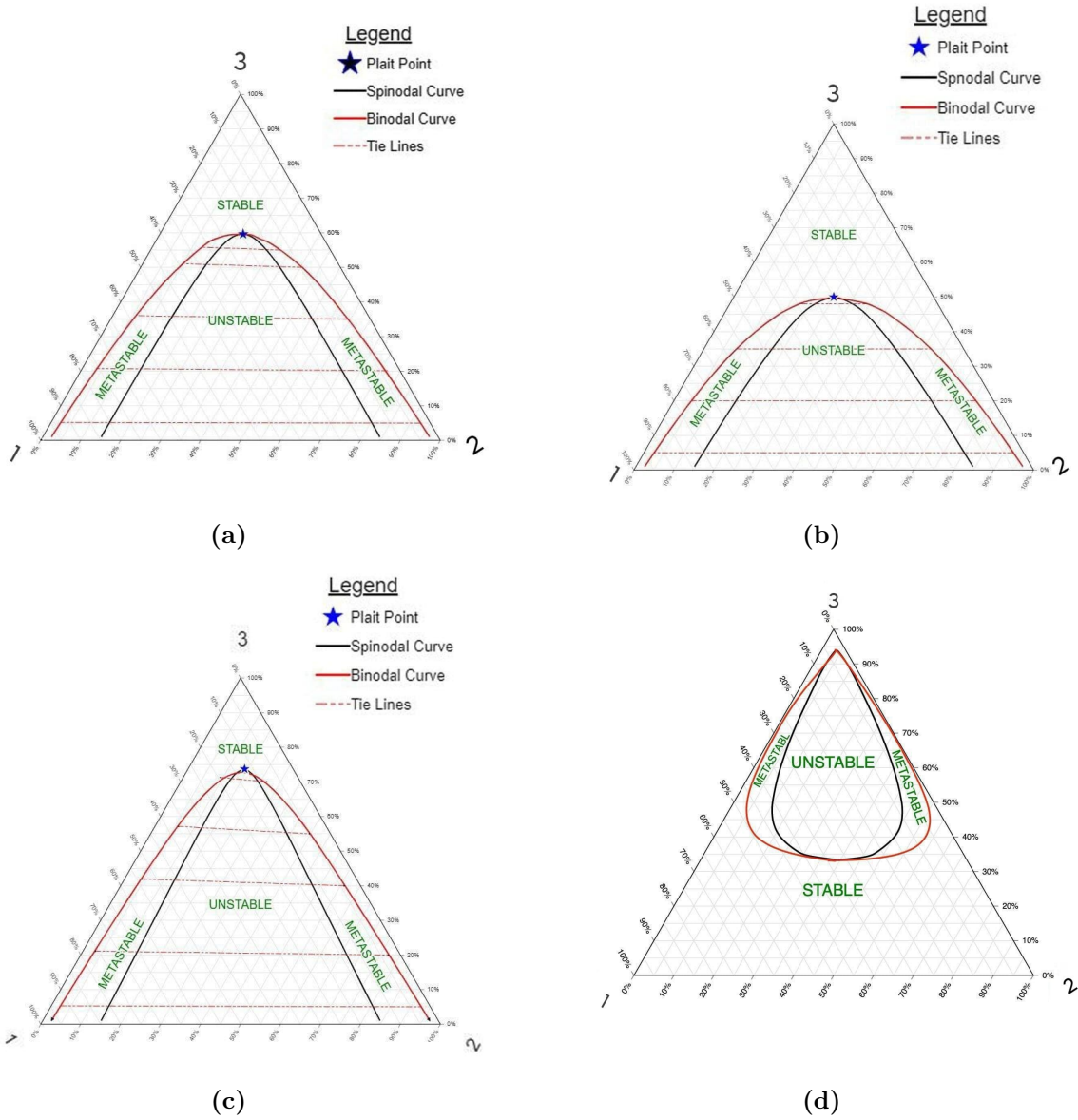


Figure 3.4: Numerically calculated phase diagrams for ternary systems with molar volume fractions $m_1 = 1000$, $m_2 = 1000$, and $m_3 = 1$. The Flory-Huggins interaction parameters are (a) $\chi_{12} = 0.004$, $\chi_{13} = 0.4$, $\chi_{23} = 0.44$; (b) $\chi_{12} = 0.004$, $\chi_{13} = 0.4$, $\chi_{23} = 0.4$; (c) $\chi_{12} = 0.004$, $\chi_{13} = 0.4$, $\chi_{23} = 0.46$; (d) $\chi_{12} = -0.002$, $\chi_{13} = 0.3$, $\chi_{23} = 0.45$.

Chapter 4

Stability Analysis Of Polymer-Polymer-Drug Ternary Solid Dispersions

In this chapter, I analyze the stability of Polymer-Polymer-Drug (P-P-D) solid dispersions within the framework of Flory-Huggins solution theory. Although the appropriateness of Flory-Huggins theory will vary from system to system ([7], [63]), this approach is a worthwhile first step for many systems. Nevertheless, Flory-Huggins theory does have its limitations when it comes to modelling amorphous solid dispersions. For example, hydrogen bonds are directional and relatively strong when compared to other non-covalent interactions, and it is well known that Flory-Huggins theory cannot adequately describe such specific interactions [63]. However, many amorphous solid dispersions do involve significant hydrogen-bonding, and more sophisticated models have been developed to describe such systems. A particularly noteworthy off-lattice model known as PC-SAFT was developed by Gross & Sadowski [30].

For solid dispersions, the polymers are frequently hydrophilic and are chosen to improve the solubility of the drug. However, the presence of the polymers can also affect the stability of the formulation, and in this chapter, I evaluate this effect. In particular, I identify parameter regimes that lead to desirable and undesirable stability properties. The ultimate goal is to identify a pair of polymers that optimise both the solubility and the stability properties of the dispersion.

I begin by physically interpreting the Flory-Huggins interaction parameters as this will help inform the coming analysis.

4.1 Interpretation Of The Flory-Huggins Interaction Parameters

Recall from Chapter 3 that the Flory-Huggins interaction parameters are given by (see equation (3.13))

$$\chi_{ij} = \frac{z\Delta w_{ij}}{kT},$$

for $i < j$ and $i, j = 1, 2, 3$, where $z > 0$ is the coordination number of the lattice (recall that this is the number of nearest-neighbouring lattice sites to a given lattice site), and where (see equation (3.12))

$$\Delta w_{ij} = w_{ij} - \frac{w_{ii} + w_{jj}}{2},$$

are the exchange energies. Here w_{ij} denotes the energy of interaction between a molecule of species i and a neighbouring molecule of species j .

I begin by considering a simple example to help develop an intuition for the interaction energy. Two point charges q and Q are separated by a distance $r > 0$. From the theory of electrodynamics ([29]), the energy of interaction between these two charges is given by

$$w_{qQ} = k\frac{qQ}{r},$$

where $k > 0$ is the Coulomb constant, and where it is assumed here that the interaction energy is zero at infinite separation. Typical intermolecular potentials are of course more complex than this (see, for example, [27]), but the intuition obtained from this simple example is nevertheless correct. If the two charges are of the same sign, then $qQ > 0$ and $w_{qQ} > 0$, so that

$$w_{qQ} > 0 \text{ corresponds to a repulsive force of interaction.}$$

If the two charges are of opposite sign, then $qQ < 0$ and $w_{qQ} < 0$, so that

$$w_{qQ} < 0 \text{ corresponds to an attractive force of interaction.}$$

Pure substances are clearly held together by attractive forces, so it can be immediately deduced that $w_{11} < 0$, $w_{22} < 0$, and $w_{33} < 0$. However, molecules of two different substances may attract or repel each other, so that w_{12} , w_{13} and w_{23} can be either positive or negative.

With this information, I can now interpret the Flory-Huggins interaction parameters; similar discussions to what follows can be found in [23] or [33].

$\chi_{ij} > 0$

Since $w_{ij} < 0$ corresponds to an attractive force of interaction, $-w_{ij} > 0$ may be used as a measure of intermolecular attraction. Consider, for example, χ_{12} . If $\chi_{12} > 0$, then

$$w_{12} > \frac{w_{11} + w_{22}}{2},$$

so that

$$-w_{12} < -\frac{w_{11} + w_{22}}{2}, \quad (4.1)$$

indicating that like molecules prefer to associate with other like molecules rather than with unlike molecules. The use of the word *indicating* is noteworthy here - equation (4.1) is in fact stating that, on average, like-like interactions are more attractive than like-unlike interactions. This is usually the case in practice so that $\chi_{ij} > 0$ normally.

If species 1 is a solute and species 2 a solvent, then a good solvent will have a relatively small value of χ_{12} , and a poor solvent will have a relatively large value of χ_{12} .

$$\boxed{\chi_{ij} < 0}$$

If $\chi_{12} < 0$, then

$$-w_{12} > -\frac{w_{11} + w_{22}}{2},$$

and this indicates that like molecules prefer to associate with unlike molecules rather than with other like molecules. However, it should be noted that this is far less common than the $\chi_{ij} > 0$ case.

4.2 P-P-D Systems In The Literature

The analysis presented here is not tied to any particular P-P-D system. As noted above, one of the objectives of the current chapter is to identify parameter regimes that lead to stable dispersions at typical storage temperatures, and thereby aid system design. Nevertheless, it is worth recalling here some P-P-D systems that have previously appeared in the literature to help identify the most relevant parameter regimes in applications, and to help evaluate the effect of polymers on the stability of previously developed systems.

Recall from Chapter 3 that

$$m_1 = \frac{V_1}{V^*}, \quad m_2 = \frac{V_2}{V^*}, \quad m_3 = \frac{V_3}{V^*},$$

where V_i is the molar volume of species i ($i = 1, 2, 3$) and V^* is some reference molar volume. In this chapter, I adopt the following notation -

$$1 = \text{first polymer}, \quad 2 = \text{second polymer}, \quad 3 = \text{drug},$$

and I make the choice

$$V^* = V_3,$$

so that

$$m_1 = \frac{V_1}{V_3}, \quad m_2 = \frac{V_2}{V_3}, \quad m_3 = 1.$$

Polymer molecules are typically much larger than drug molecules, so that $m_1 \gg 1$,

$m_2 \gg 1$ usually. Values for the molecular weights of polymers frequently used in solid dispersions can be found in the paper [61]. Some typical values for drug molecular weights can be found in [66].

Table 4.1 lists some P-P-D studies that have previously appeared in the literature. The list is far from comprehensive and emphasizes studies that used ternary dispersions to improve storage stability. Other studies considered P-P-D systems that were designed to improve drug solubility ([13]), but solubility is not the topic of the current study, and so these have been not been exhaustively listed here. The values for m_1 and m_2 listed in Table 4.1 should be treated as estimates. The calculation of the molar volume fractions m_1 , m_2 given in the table required the calculation of the molar volumes of the polymers and drugs listed there. The molar volume V of a species is calculated using the formula

$$V = \frac{M}{\rho}$$

where M is its molar mass and ρ is its mass density. The values required for the table were obtained from either the papers cited in the table or by searching the internet.

It should be noted that in reality polymer molecular weights typically fall within a distribution of values ([23], [33]), and that assigning a single value to their molecular weight is an approximation. However, removing this simplification would require a fundamental reassessment of the underlying thermodynamic calculations in the derivation of Flory-Huggins theory (see Chapter 3 of this thesis) and would complicate the analysis considerably.

4.3 Values For Flory-Huggins Interaction Parameters

It is also instructive to display some values for the Flory-Huggins interaction parameters that have appeared in earlier studies. Again, the objective here is to help identify the most relevant parameter values in practice. The purpose of this study is to analyze the stability of solid dispersions in storage, and so the temperatures of interest are usually in the range of 0 to 40 degrees Celsius.

4.3.1 Some General Remarks About Flory-Huggins Interaction Parameters

I begin by making some general remarks about Flory-Huggins interaction parameters. I first recall from my earlier discussion that $\chi > 0$ usually. In fact, using an approach developed by Scott and Hildebrand [34], it can be shown that ([33],[72])

$$\chi_{AB} = \frac{\alpha}{RT} (\delta_A - \delta_B)^2, \quad (4.2)$$

Drug	Polymer	Polymer	Purpose	Volume Fractions	References
Nilvadipine	Methylcellulose	Crospovidone	Stability ↑	$m_1 \approx 400, m_2 \approx 100$	[37]
Griseofulvin	HPMCAS	PHPMA	Stability ↑	$m_1 \approx 60, m_2 \approx 200$	[3]
Itraconazole	HPMC 2910 ES	PEG	Stability ↑	$m_1 \approx 40, m_2 \approx 10$	[44]
Itraconazole	HPMCP	Soluplus	Stability ↑	$m_1 \approx 100, m_2 \approx 150$	[19], [20], [5]
Nilvadipine	CI-PVP	MC	Stability ↑	$m_1 \approx 6736, m_2 \approx 112$	[37]
TEL	PVP K30	Solplus	Stability ↑	$m_1 \approx 77, m_2 \approx 687$	[80]
Ezetimibe	Simvastatin	Kollidon VA64	Stability ↑	$m_1 \approx 0.9, m_2 \approx 305$	[47]
HIV inhibitor	PVP K30	PLGA	Stability ↑ Control release	$m_1 \approx 70, m_2 \approx 60$	[59]
Itraconazole	HPMCP	Soluplus	Stability ↑ Solubility ↑	$m_1 \approx 100, m_2 \approx 150$	[19], [20], [5]
Griseofulvin	PVP	PHPMA	Stability ↑ Solubility ↑	$m_1 = 180, m_2 = 65$	[4]
Cinnarizine	Soluplus	HPMC	Stability ↑ Solubility ↑	$m_1 \approx 300, m_2 \approx 250$	[87]

Table 4.1: Polymer-Polymer-Drug ternary systems that have previously appeared in the literature. The list is not exhaustive and emphasizes stability studies.

where $\alpha > 0$ is a positive parameter related to molar volumes and δ_A, δ_B are the solubilities of species A and B , respectively. Hence, within the context of the Scott and Hildebrand approach, $\chi_{AB} > 0$ is automatic. This formula indicates that substances of similar solubility readily undergo mutual mixing, whereas substances of significantly different solubility are less likely to mix ([85]). Equation (4.2) makes reasonably accurate χ predictions for systems where van der Waals forces between the species dominate. However, mixtures where polar interactions (for example, hydrogen bonding) are significant are not well-modelled by equation (4.2).

Recall from Chapter 3 that the χ_{ij} arose from calculating the enthalpy of mixing on a lattice, and that they contain a $1/T$ dependence. However, the lattice-based approach did contain some significant simplifying assumptions. One particularly noteworthy assumption was that the volume of the mixture was simply the sum of the volumes of the two pure components. Rubinstein & Colby [72] have noted that this is frequently not the case for polymer blends, and that the lattice-based approach also contains quite a number of other questionable assumptions. These model shortcomings are frequently lumped into an empirical expression of the form

$$\chi(T) = A + \frac{B}{T}, \quad (4.3)$$

where here A and B here are often treated as experimental fitting parameters for a given system. In (4.3), the B/T term is sometimes referred to as the *enthalpic* part (consistent with the lattice-based derivation given in Chapter 3), and the A term is referred to as the *entropic* part.

For some systems, the interaction parameter is found to depend on mixture composi-

tion as well as temperature, and this dependence is sometimes incorporated into the A, B parameters in (4.3). Tian *et al.* [89] took a different approach, and proposed the following form for a drug-polymer dispersion system

$$\chi(\phi_d, T) = A + \frac{B}{T} + C_1\phi_d + C_2\phi_d^2, \quad (4.4)$$

where here ϕ_d is the volume fraction of the drug, and A, B, C_1, C_2 are constants; I will return to this study in Section 4.3.2.

4.3.2 Values Of The Flory-Huggins Interaction Parameter For Drug-Polymer Systems

I now display some Flory-Huggins interaction parameter values that have previously appeared in the literature for Drug-Polymer systems.

Indomethacin and PVP-VA [98]

Zhao *et al.* [98] studied the binary solid dispersion composed of the drug indomethacin (IND) and the copolymer polyvinylpyrrolidone–vinyl acetate (PVP-VA). Indomethacin is a drug used to relieve moderate to severe pain and to reduce swelling. These authors proposed the following temperature dependent form for the FH interaction parameter for this system

$$\chi_{\text{IND-PVP}}(T) = -5.2 + \frac{1998.63 \text{ K}}{T}, \quad (4.5)$$

where here T is measured in degrees Kelvin (K). Nevertheless, I will quote specific values here for degrees Celsius $^{\circ}\text{C}$ since these are more intuitive than degrees Kelvin for most people. Using the above expression gives

$$\begin{aligned} \chi_{\text{IND-PVP}}(T = 10^{\circ}\text{C}) &= 1.858, \quad \chi_{\text{IND-PVP}}(T = 30^{\circ}\text{C}) = 1.393, \\ \chi_{\text{IND-PVP}}(T = 100^{\circ}\text{C}) &= 0.156. \end{aligned}$$

Equation (4.5) predicts that drug miscibility with the polymer improves with increasing temperature, as might be expected.

Various Drugs And Polyethylene Glycol [85]

A large number of χ values for binary drug-polymer systems are listed in Table 1 of the paper by Thakral & Thakral [85]. The polymer was fixed to be polyethylene glycol (PEG) and the drug was allowed to vary. χ values for 83 different PEG-drug pairings are listed, and the relevant temperature was close to 25°C . Their results may be summarized as follows:

- 61% of the values are in the range $0 \leq \chi \leq 1$
- 28% of the values are in the range $1 < \chi \leq 5$
- 11% of the values are in the range $\chi > 5$

Norfloracin And Various Polymers [56]

Norfloracin (NFX) is an antibiotic used to treat bacterial infections, particularly urinary tract infections. Liu *et al.* [56] developed binary amorphous solid dispersion composed of norfloracin (in all cases) and one of the polymers polyvinylpyrrolidone (PVP), or hydroxypropylmethylcellulose (HPMC), or hydroxypropyl methylcellulose phthalate (HPMCP). These authors gave the following values for the FH interaction parameters

$$\chi_{\text{NFX-PVP}} = 2.89, \quad \chi_{\text{NFX-HPMC}} = 0.48, \quad \chi_{\text{NFX-HPMCP}} = 0.0023$$

Felodipine And HPMCAS / Felodipine And Soluplus [88]

Felodipine (FD) is a calcium channel blocker used to treat high blood pressure. Tian *et al.* [88] studied two FD solid dispersions, one composed of FD and hydroxypropyl methylcellulose acetate succinate (HPMCAS), and the other composed of FD and Soluplus. They proposed the following temperature-dependent forms for the FH interaction parameters

$$\chi_{\text{FD-HPMCAS}}(T) = -18.767 + \frac{7830.4 \text{ K}}{T},$$

and

$$\chi_{\text{FD-Soluplus}}(T) = -14.419 + \frac{5744.7 \text{ K}}{T}.$$

Since the principal purpose of this section is to get a feel for typical χ values at storage temperatures, it is worth displaying some specific values predicted by these expressions:

$$\begin{aligned} \chi_{\text{FD-HPMCAS}}(T = 10^\circ\text{C}) &= 8.887, & \chi_{\text{FD-HPMCAS}}(T = 30^\circ\text{C}) &= 7.063, \\ \chi_{\text{FD-HPMCAS}}(T = 100^\circ\text{C}) &= 2.218, & \chi_{\text{FD-Soluplus}}(T = 10^\circ\text{C}) &= 5.870, \\ \chi_{\text{FD-Soluplus}}(T = 30^\circ\text{C}) &= 4.531, & \chi_{\text{FD-Soluplus}}(T = 100^\circ\text{C}) &= 0.976. \end{aligned}$$

Felodipine And PVPK15 [89]

Tian *et al.* [89] studied a binary solid dispersion composed of FD and the polymer PVPK15. For this system, they proposed the following expression for χ that depends on both temperature and composition -

$$\chi_{\text{FD-PVPK15}}(\phi_d, T) = 1.72 - \frac{852 \text{ K}}{T} + 5.17\phi_d - 7.85\phi_d^2,$$

where here ϕ_d is the volume fraction of the drug. They argued that this expression remains valid across a broad range of temperatures and compositions. Illustrative values predicted by this formula are

$$\begin{aligned} \chi_{\text{FD-PVPK15}}(\phi_d = 0.5, T = 10^\circ\text{C}) &= -0.67, & \chi_{\text{FD-PVPK15}}(\phi_d = 0.5, T = 30^\circ\text{C}) &= -0.47, \\ \chi_{\text{FD-PVPK15}}(\phi_d = 0.5, T = 100^\circ\text{C}) &= 0.06. \end{aligned}$$

Aceclofenac And Soluplus [9]

Aceclofenac (AF) is an anti-inflammatory drug used to treat arthritis and related ailments. Bansal *et al.* [9] proposed the following formula for a AF-Soluplus dispersion

$$\chi_{\text{AF-Soluplus}}(T) = -3.386 + \frac{1709 \text{ K}}{T}.$$

This predicts that

$$\begin{aligned} \chi_{\text{AF-Soluplus}}(T = 10 \text{ }^\circ\text{C}) &= 2.650, & \chi_{\text{AF-Soluplus}}(T = 30 \text{ }^\circ\text{C}) &= 2.251, \\ \chi_{\text{AF-Soluplus}}(T = 100 \text{ }^\circ\text{C}) &= 1.194, & \chi_{\text{AF-Soluplus}}(T = 140 \text{ }^\circ\text{C}) &= 0.751. \end{aligned}$$

4.3.3 Values Of The Flory-Huggins Interaction Parameter For Polymer-Polymer Systems

Flory-Huggins theory was developed with polymer solutions in mind, and Flory-Huggins interaction parameters have been tabulated for many polymer-polymer systems. One particularly useful source of information for polymer systems is the *Polymer Blends Handbook* [92] - see, in particular, Section 2.5 of Chapter 2 where a large number of χ values for polymer pairs are listed. Table 2.8 of this book lists values for $\chi_{\text{poly-poly}}$ in the format

$$\chi_{\text{poly-poly}}(T) = A + \frac{B}{T} + \frac{C}{T^2},$$

where here the temperature T is measured in Kelvin (K) and A , B (K), C (K²) are constants. I now list some values of χ for particular pairs of polymers based on this table.

Unfortunately, I was unable to find interaction parameter values for the polymer pairings that have been used in ternary solid dispersions to date. It would be of particular value to experimentally investigate the interaction of hydrophilic polymer blends. Nevertheless, it is worthwhile displaying here some results for polymer blends that have been investigated.

It is also worth remarking that the values I will display here are frequently at least two orders of magnitude smaller than one.

Polystyrene - Poly(methyl methacrylate)

Polystyrene (PS) is a synthetic polymer made up of repeating units of the styrene molecule. Poly(methyl methacrylate) (PMMA) is a synthetic resin that is frequently used as a glass substitute. In [92], the following formula is given

$$\chi_{\text{PS-PMMA}}(T) = 0.0129 + \frac{1.96 \text{ K}}{T}.$$

This predicts that

$$\begin{aligned}\chi_{\text{PS-PMMA}}(T = 10\text{ }^\circ\text{C}) &= 0.01982, & \chi_{\text{PS-PMMA}}(T = 25\text{ }^\circ\text{C}) &= 0.01947, \\ \chi_{\text{PS-PMMA}}(T = 100\text{ }^\circ\text{C}) &= 0.01815.\end{aligned}$$

Polystyrene - Poly(vinyl methyl ether)

Poly(vinyl methyl ether) (PVME) is a polymer that is commonly used in industry for the manufacture of adhesives. For the PS - PVME polymer blend, the following form has been proposed ([92])

$$\chi_{\text{PS-PVME}}(T) = 0.103 - \frac{43.0\text{ K}}{T}.$$

Some illustrative values for particular temperatures are

$$\begin{aligned}\chi_{\text{PS-PVME}}(T = 10\text{ }^\circ\text{C}) &= -0.04886, & \chi_{\text{PS-PVME}}(T = 25\text{ }^\circ\text{C}) &= -0.04122, \\ \chi_{\text{PS-PVME}}(T = 100\text{ }^\circ\text{C}) &= -0.01223.\end{aligned}$$

Polypropylene - Saturated Polybutadiene

Polypropylene (PP) is a popular plastic that is extensively used in manufacturing - for example, it is used in packaging manufacture, in numerous household items such as furniture fittings, and in a wide variety of medical products. Polybutadiene (SPB₉₇) is a synthetic rubber that is commonly used in the manufacture of tires. The interaction parameter for the PP-SPB₉₇ blend has been given by ([92])

$$\chi_{\text{PP-SPB}_{97}}(T) = 0.00349 - \frac{3.99\text{ K}}{T} + \frac{1208.0\text{ K}^2}{T^2}.$$

Illustrative values are

$$\begin{aligned}\chi_{\text{PP-SPB}_{97}}(T = 10\text{ }^\circ\text{C}) &= 0.00447, & \chi_{\text{PP-SPB}_{97}}(T = 25\text{ }^\circ\text{C}) &= 0.00370, \\ \chi_{\text{PP-SPB}_{97}}(T = 100\text{ }^\circ\text{C}) &= 0.00147.\end{aligned}$$

Head-To-Head-Polypropylene - Poly(ethyl butylene)

Poly(ethyl butylene) (PEB) is a biodegradable polymer resin that is a promising alternative material to some plastics. For the Head-To-Head Polypropylene (HHPP) - PEB blend, the following form has been proposed ([92])

$$\chi_{\text{HHPP-PEB}}(T) = 0.00185 - \frac{1.41\text{ K}}{T} + \frac{370.0\text{ K}^2}{T^2}.$$

Some illustrative values are

$$\begin{aligned}\chi_{\text{HHPP-PEB}}(T = 10^\circ\text{C}) &= 0.001458, & \chi_{\text{HHPP-PEB}}(T = 25^\circ\text{C}) &= 0.001283, \\ \chi_{\text{HHPP-PEB}}(T = 100^\circ\text{C}) &= 0.000729.\end{aligned}$$

4.4 Analysis And Results

I now analyse the stability behaviour of P-P-D systems for various interaction parameter regimes. The stability of the system is assessed by plotting phase diagrams, as discussed in the earlier chapters of this study. Much of the analysis will rely on an asymptotic argument that exploits the fact that the polymers typically have a much larger molar volume than that of the drug. In particular, I will derive asymptotic approximations for the location of the plait point. The plait point lies on both the spinodal and binodal curves and determining its location often reveals a lot of information regarding the geometry of the phase diagram, particularly when it is combined with information about the spinodal curve. I will also plot numerically calculated spinodal curves, guided by the asymptotic results. I will not display binodal curves in the current chapter since their calculation is labour intensive and much of the key behaviour is revealed by the spinodal curves. However, in Chapter 6, I will plot some binodal curves for selected parameter values when considering phase separation kinetics.

Before considering the asymptotics, it is worth recalling here the equations for the plait points and the spinodal curve for ternary systems in terms of the volume fractions. These formulae were derived in Chapter 3. Denoting a point on the ternary spinodal curve by $(\phi_1^s, \phi_2^s, \phi_3^s)$, I have that

$$\begin{aligned}\phi_1^s + \phi_2^s + \phi_3^s &= 1, \\ \frac{m_1\phi_1^s}{1 - 2\chi_1 m_1\phi_1^s} + \frac{m_2\phi_2^s}{1 - 2\chi_2 m_2\phi_2^s} + \frac{m_3\phi_3^s}{1 - 2\chi_3 m_3\phi_3^s} &= 0.\end{aligned}\tag{4.6}$$

These two equations in three unknowns $(\phi_1^s, \phi_2^s, \phi_3^s)$ determine the spinodal curve. The plait points $(\phi_1^p, \phi_2^p, \phi_3^p)$ are determined from

$$\begin{aligned}\phi_1^p + \phi_2^p + \phi_3^p &= 1, \\ \frac{m_1\phi_1^p}{1 - 2\chi_1 m_1\phi_1^p} + \frac{m_2\phi_2^p}{1 - 2\chi_2 m_2\phi_2^p} + \frac{m_3\phi_3^p}{1 - 2\chi_3 m_3\phi_3^p} &= 0, \\ \frac{m_1^2\phi_1^p}{(1 - 2\chi_1 m_1\phi_1^p)^3} + \frac{m_2^2\phi_2^p}{(1 - 2\chi_2 m_2\phi_2^p)^3} + \frac{m_3^2\phi_3^p}{(1 - 2\chi_3 m_3\phi_3^p)^3} &= 0.\end{aligned}\tag{4.7}$$

These three equations in three unknowns $(\phi_1^p, \phi_2^p, \phi_3^p)$ determine the plait points.

I now consider the asymptotic behaviour of the spinodal curve and the plait points in the limit

$$m_1 \gg 1, \quad m_2 = O(m_1), \quad m_3 = 1.$$

This is the natural limit to consider since it corresponds to the case of the molecular

weight of the two polymers being much larger than that of the drug, which of course is normally the case. I write

$$m_1 = \frac{1}{\varepsilon}, \quad m_2 = \frac{\bar{m}_2}{\varepsilon}, \quad m_3 = 1,$$

with $\varepsilon \ll 1$ and $\bar{m}_2 = O(1)$. Using this notation, equations (4.6) and (4.7) become

$$\begin{aligned} \phi_1^s + \phi_2^s + \phi_3^s &= 1, \\ \frac{\phi_1^s}{\varepsilon - 2\chi_1\phi_1^s} + \frac{\bar{m}_2\phi_2^s}{\varepsilon - 2\chi_2\bar{m}_2\phi_2^s} + \frac{\phi_3^s}{1 - 2\chi_3\phi_3^s} &= 0, \end{aligned} \quad (4.8)$$

and

$$\begin{aligned} \phi_1^p + \phi_2^p + \phi_3^p &= 1, \\ \frac{\phi_1^p}{\varepsilon - 2\chi_1\phi_1^p} + \frac{\bar{m}_2\phi_2^p}{\varepsilon - 2\chi_2\bar{m}_2\phi_2^p} + \frac{\phi_3^p}{1 - 2\chi_3\phi_3^p} &= 0, \\ \frac{\varepsilon\phi_1^p}{(\varepsilon - 2\chi_1\phi_1^p)^3} + \frac{\varepsilon\bar{m}_2^2\phi_2^p}{(\varepsilon - 2\chi_2\bar{m}_2\phi_2^p)^3} + \frac{\phi_3^p}{(1 - 2\chi_3\phi_3^p)^3} &= 0, \end{aligned} \quad (4.9)$$

respectively. For convenience, I also recall here the equations for χ_1, χ_2, χ_3 :

$$\begin{aligned} \chi_1 &= \frac{1}{2}(\chi_{12} + \chi_{13} - \chi_{23}), \\ \chi_2 &= \frac{1}{2}(\chi_{12} + \chi_{23} - \chi_{13}), \\ \chi_3 &= \frac{1}{2}(\chi_{13} + \chi_{23} - \chi_{12}). \end{aligned} \quad (4.10)$$

I consider three cases. The first case shows that polymers with poor compatibility typically lead to immiscible ternary mixtures.

4.4.1 Case I: $\chi_{12} > 0, \chi_{12} = O(1)$

I shall show that the case $\chi_{12} > 0, \chi_{12} = O(1)$ leads to incompatibility of the ternary mixture for most compositions. This is as would be expected as $\chi_{12} > 0, \chi_{12} = O(1)$ corresponds to like-like interactions for the two polymers being on average clearly energetically favoured over like-unlike interactions. The analysis here will be cursory because the key features of the ternary diagram quickly become apparent.

For this case, we have

$$\chi_1, \chi_2, \chi_3 = O(1), \quad (4.11)$$

apart from some special cases, such as $\chi_3 = 0$ which would arise if the parameters were such that $\chi_{12} = \chi_{13} + \chi_{23}$.

The Plait Points

Considering equations (4.9) in the limit $\varepsilon \rightarrow 0$, it is readily seen that

$$\phi_1^p, \phi_2^p = O(\varepsilon), \quad \phi_3^p \sim 1, \quad (4.12)$$

so that plait point occurs near the apex of the polymer-polymer-drug ternary diagram, as illustrated in the example shown in Figure 4.6. The plait point lies on the spinodal curve.

The Spinodal Curve

The spinodal intersects the polymer-polymer binary line at $\phi_3 = 0$, and these points are determined by simultaneously solving the equations (see (4.8))

$$\begin{aligned} \phi_1^s + \phi_2^s &= 1, \\ \frac{\phi_1^s}{\varepsilon - 2\chi_1\phi_1^s} + \frac{\bar{m}_2\phi_2^s}{\varepsilon - 2\chi_2\bar{m}_2\phi_2^s} &= 0, \end{aligned} \quad (4.13)$$

where the superscript s here denotes spinodal. Equations (4.13) lead to a quadratic equation which is readily solved. However, it sufficient for my purposes here to note that as $\varepsilon \rightarrow 0$, the two solutions to (4.13) take the form

$$\phi_{1L}^s \sim 1, \quad \phi_{2L}^s = O(\varepsilon), \quad \phi_{3L}^s = 0, \quad (4.14)$$

and

$$\phi_{1R}^s = O(\varepsilon), \quad \phi_{2R}^s \sim 1, \quad \phi_{3R}^s = 0, \quad (4.15)$$

where here L refers to the left intersect of the spinodal with the polymer-polymer binodal and R denotes the right intersect. The triangle defined by the three points (4.12), (4.14) and (4.15) approximates the unstable region, and almost fills the entire ternary phase diagram.

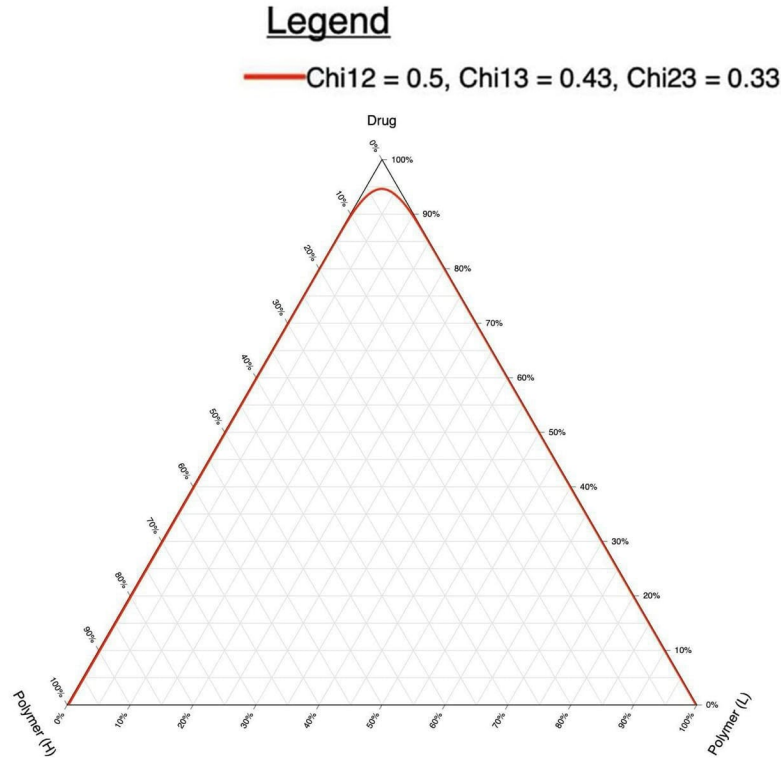


Figure 4.1: A spinodal curve for a Polymer-Polymer-Drug system illustrating Case I in the main text. Here $m_1 = 1000$, $m_2 = 500$ and $m_3 = 1$, and the remaining parameter values are given on the figure legend. It is clear here that almost the entire composition domain is unstable, showing that the case $\chi_{12} = O(1)$, $\chi_{12} > 0$ has undesirable stability properties.¹

This indicates (at least within the context of Flory-Huggins theory) that using incompatible polymers leads to unfavorable stability properties for the dispersion irrespective of the interaction properties of the drug with the polymers. The mixture is only miscible when one or both of the polymers has a very low volume fraction. Figure 4.1 shows an example of a spinodal curve for this case, and it is clear that the unstable region occupies almost the entirety of the ternary diagram.

4.4.2 Case II: $\chi_{12} = O(1/m_1)$, $\chi_{12} > 0$, $\chi_{13} - \chi_{23} = O(1/m_1)$

I now consider the limit $\varepsilon = 1/m_1 \rightarrow 0$ with $\chi_{12} = O(\varepsilon)$ and $\chi_{13} - \chi_{23} = O(\varepsilon)$. The condition $\chi_{12} = O(\varepsilon)$, $\chi_{12} > 0$ implies that for the polymers like-like interactions are marginally favoured over like-unlike interactions. $\chi_{13} - \chi_{23} = O(\varepsilon)$ implies that there is a weak asymmetry in the manner the two polymers interact with the drug. I shall show that for this case favourable stability properties are possible for certain parameter values.

¹Created using the software on the website TernaryPlot.com

Asymptotic Analysis

I begin by giving the mathematical analysis, and then move onto discuss its implications for the stability behaviour of the ternary mixture. In the limit $\varepsilon \rightarrow 0$, I write

$$\chi_{12} = \frac{1}{m_1} \bar{\chi}_{12} = \varepsilon \bar{\chi}_{12}, \quad \chi_{13} - \chi_{23} = \frac{1}{m_1} \bar{\chi}_d = \varepsilon \bar{\chi}_d,$$

with $\bar{\chi}_{12}, \bar{\chi}_d = O(1)$, $\bar{\chi}_{12} > 0$. Using (4.10) now gives that

$$\begin{aligned} \chi_1 &= \frac{\varepsilon}{2} (\bar{\chi}_{12} + \bar{\chi}_d), \\ \chi_2 &= \frac{\varepsilon}{2} (\bar{\chi}_{12} - \bar{\chi}_d), \\ \chi_3 &= \chi_{23} + \frac{\varepsilon}{2} (\bar{\chi}_d - \bar{\chi}_{12}), \end{aligned} \tag{4.16}$$

and the equations determining the plait points are then given by

$$\begin{aligned} \phi_1^p + \phi_2^p + \phi_3^p &= 1, \\ \frac{\phi_1^p}{1 - (\bar{\chi}_{12} + \bar{\chi}_d)\phi_1^p} + \frac{\bar{m}_2\phi_2^p}{1 - \bar{m}_2(\bar{\chi}_{12} - \bar{\chi}_d)\phi_2^p} + \frac{\varepsilon\phi_3^p}{1 - (2\chi_{23} + \varepsilon(\bar{\chi}_d - \bar{\chi}_{12}))\phi_3^p} &= 0, \\ \frac{\phi_1^p}{(1 - (\bar{\chi}_{12} + \bar{\chi}_d)\phi_1^p)^3} + \frac{\bar{m}_2^2\phi_2^p}{(1 - \bar{m}_2(\bar{\chi}_{12} - \bar{\chi}_d)\phi_2^p)^3} + \frac{\varepsilon^2\phi_3^p}{(1 - (2\chi_{23} + \varepsilon(\bar{\chi}_d - \bar{\chi}_{12}))\phi_3^p)^3} &= 0. \end{aligned} \tag{4.17}$$

The Plait Points

In the limit $\varepsilon \rightarrow 0$, pose

$$\phi_1^p \sim \phi_{10}^p, \quad \phi_2^p \sim \phi_{20}^p, \quad \phi_3^p \sim \phi_{30}^p,$$

to obtain the leading order equations

$$\begin{aligned} \phi_{10}^p + \phi_{20}^p + \phi_{30}^p &= 1, \\ \frac{\phi_{10}^p}{1 - (\bar{\chi}_{12} + \bar{\chi}_d)\phi_{10}^p} &= -\frac{\bar{m}_2\phi_{20}^p}{1 - \bar{m}_2(\bar{\chi}_{12} - \bar{\chi}_d)\phi_{20}^p}, \\ \frac{\phi_{10}^p}{(1 - (\bar{\chi}_{12} + \bar{\chi}_d)\phi_{10}^p)^3} &= -\frac{\bar{m}_2^2\phi_{20}^p}{(1 - \bar{m}_2(\bar{\chi}_{12} - \bar{\chi}_d)\phi_{20}^p)^3}. \end{aligned} \tag{4.18}$$

These equations are readily solved (for example, by dividing the cube of (4.18)₂ by (4.18)₃) to give

$$\phi_{10}^p = \frac{1 + \sqrt{\bar{m}_2}}{2\bar{\chi}_{12}\sqrt{\bar{m}_2}}, \quad \phi_{20}^p = \frac{1 + \sqrt{\bar{m}_2}}{2\bar{\chi}_{12}\bar{m}_2}, \quad \phi_{30}^p = 1 - \frac{(1 + \sqrt{\bar{m}_2})^2}{2\bar{\chi}_{12}\bar{m}_2}.$$

In dimensional terms, we thus have that in the current limit

$$\begin{aligned}\phi_1^p &\sim \frac{1}{2\chi_{12}\sqrt{m_1}} \left(\frac{1}{\sqrt{m_1}} + \frac{1}{\sqrt{m_2}} \right), \\ \phi_2^p &\sim \frac{1}{2\chi_{12}\sqrt{m_2}} \left(\frac{1}{\sqrt{m_1}} + \frac{1}{\sqrt{m_2}} \right), \\ \phi_3^p &\sim 1 - \frac{\chi_{12}^c}{\chi_{12}},\end{aligned}\tag{4.19}$$

where

$$\chi_{12}^c = \frac{1}{2} \left(\frac{1}{\sqrt{m_1}} + \frac{1}{\sqrt{m_2}} \right)^2,\tag{4.20}$$

is a critical value for the polymer-polymer interaction parameter. By critical, I mean here that in the current limit, the spinodal (unstable) domain in the ternary diagram vanishes as χ_{12} drops below the value χ_{12}^c ; I shall return to this issue in the discussion below. Further discussion of this parameter in the context of binary mixtures is given in the books by Rubinstein & Colby [72] (Section 4.4) and Hiemenz [33] (Section 7.5.5).

The Spinodal Curve

It is also worth considering the asymptotic behaviour of the spinodal curve in the current limit. Denoting a point on the spinodal curve by $(\phi_1^s, \phi_2^s, \phi_3^s)$, I pose

$$\phi_1^s \sim \phi_{10}^s, \quad \phi_2^s \sim \phi_{20}^s, \quad \phi_3^s \sim \phi_{30}^s,$$

as $\varepsilon \rightarrow 0$ to obtain the leading order equations

$$\begin{aligned}\phi_{10}^s + \phi_{20}^s + \phi_{30}^s &= 1, \\ \frac{\phi_{10}^s}{1 - (\bar{\chi}_{12} + \bar{\chi}_d)\phi_{10}^s} &= -\frac{\bar{m}_2\phi_{20}^s}{1 - \bar{m}_2(\bar{\chi}_{12} - \bar{\chi}_d)\phi_{20}^s}.\end{aligned}\tag{4.21}$$

The second of these equations can be re-cast in the form

$$\phi_{10}^s - 2\bar{\chi}_{12}\bar{m}_2\phi_{10}^s\phi_{20}^s + \bar{m}_2\phi_{20}^s = 0.\tag{4.22}$$

The location of the intercepts of the spinodal curve with the binary $\phi_3 = 0$ is discussed in Section 3.3.1.

I now discuss the implications of these results with the aid of some numerical illustrations.

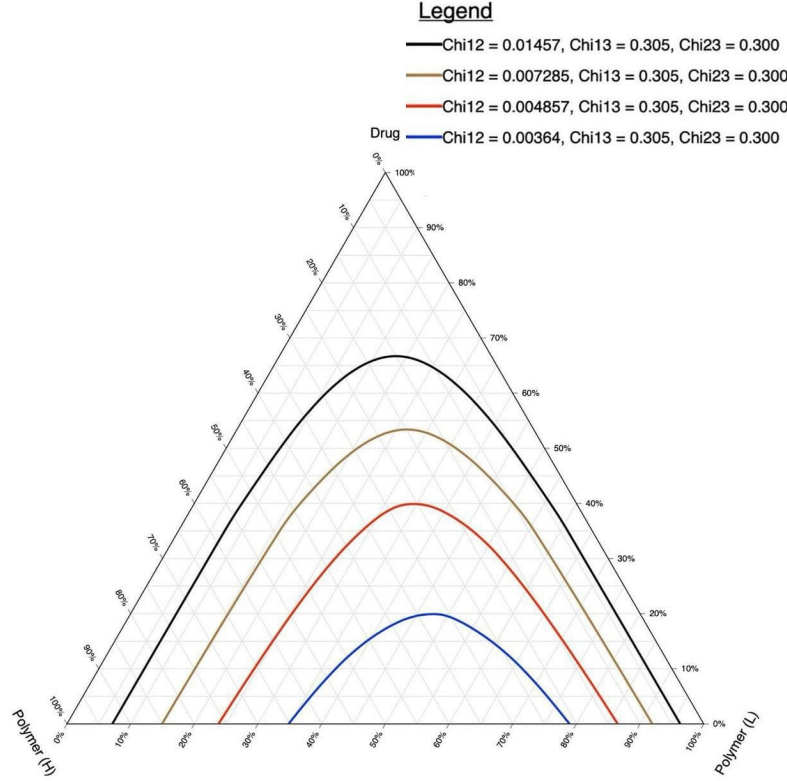


Figure 4.2: Spinodal curves illustrating Case II in the main text. Here $m_1 = 1000$, $m_2 = 500$ and $m_3 = 1$, with the remaining parameter values being given on the figure legend. This figure shows the effect of varying the value of the polymer-polymer interaction parameter χ_{12} with $m_1 \gg 1$, $m_2 = O(m_1)$ and $\chi_{13} - \chi_{23} = O(1/m_1)$.¹

Case II: Figure 4.2: The Effect Of Varying $\chi_{12} = O(1/m_1)$

I now show that even slight changes to the value of $\chi_{12} = O(1/m_1)$ for the weakly asymmetric case $\chi_{13} - \chi_{23} = O(1/m_1)$ can significantly affect the stability of the ternary mixture. The choices for χ_{12} in Figure 4.2 were guided by the third equation in (4.19), given by

$$\phi_3^p \sim 1 - \chi_{12}^c / \chi_{12}, \quad (4.23)$$

where χ_{12}^c is given by (4.20). Recall that ϕ_3^p measures the perpendicular distance from the plait point to the polymer-polymer binary base, and it yields valuable qualitative information about the character of the phase diagram. Consider, for example, the red curve displayed in Figure 4.2. The χ_{12} value chosen to obtain this curve was selected by setting $\phi_3^p = 0.4$, and so using (4.23), $1 - \chi_{12}^c / \chi_{12} \approx 0.4$ or $\chi_{12} \approx \chi_{12}^c / 0.6 = 0.004857$. The χ_{12} values for the other curves displayed were chosen similarly.

Notice that for $\chi_{12} < \chi_{12}^c$, the plait point and spinodal region vanish from the ternary triangle. Hence, we have identified the following parameter regime that

¹Created using the software on the website TernaryPlot.com

leads to favourable stability behaviour (in terms of m_1 and m_2):

$$\chi_{12} < \frac{1}{2} \left(\frac{1}{\sqrt{m_1}} + \frac{1}{\sqrt{m_2}} \right)^2, \quad \chi_{13} - \chi_{23} = O(1/m_1).$$

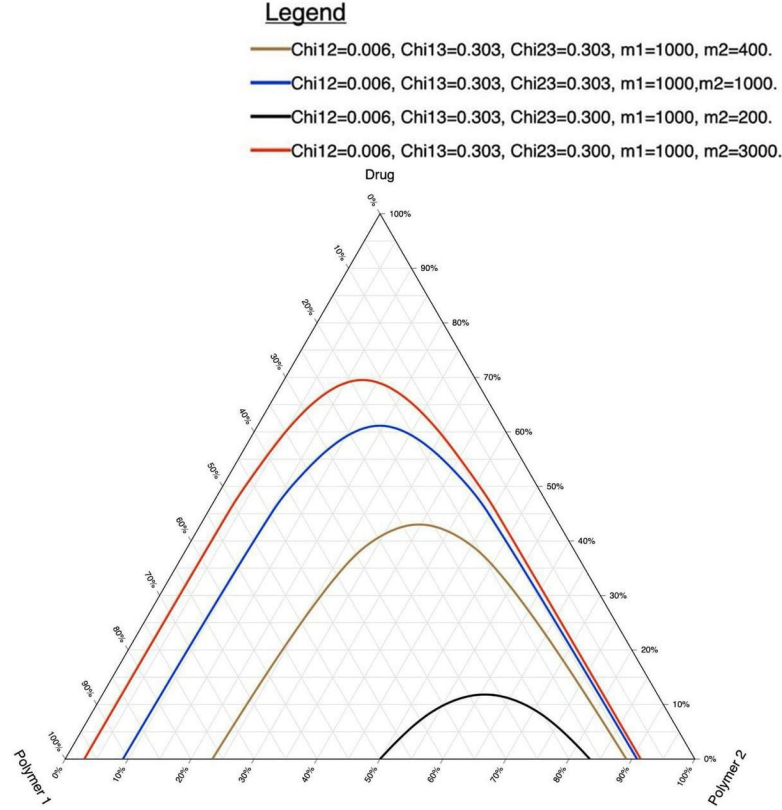


Figure 4.3: Spinodal curves illustrating Case II in the main text. Here $m_1 = 1000$ and $m_3 = 1$, with the remaining parameter values being given on the figure legend. This figure shows the effect of varying the molar volume of the second polymer with $m_1 \gg 1$, $m_2 = O(m_1)$ and $\chi_{13} - \chi_{23} = O(1/m_1)$.¹

Case II: Figure 4.3: The Effect Of Varying The Molar Volume Of One Of The Polymers

In Figure 4.3, we evaluate the effect of varying the molar volume of one of the two polymers within the context of the Case II limit. This is another parameter that can in principle be tuned by a manufacturer to produce a dispersion with advantageous stability behaviour.

I begin by noting that (4.23) can be re-written in the form

$$\phi_3^p \sim 1 - \frac{1}{2\chi_{12}} \left(\frac{1}{\sqrt{m_1}} + \frac{1}{\sqrt{m_2}} \right)^2, \quad (4.24)$$

¹Created using the software on the website TernaryPlot.com

from which it is clear that ϕ_3^p increases as m_2 increases. Hence the perpendicular distance from the plait point to the polymer-polymer binodal base increases with increasing m_2 , and this behaviour is clearly seen in Figure 4.3.

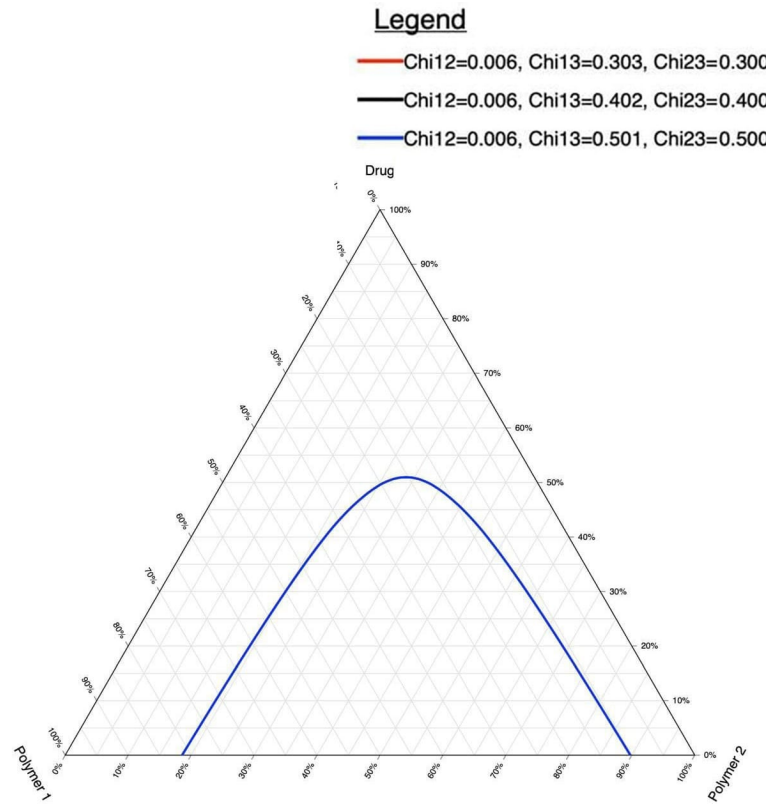


Figure 4.4: Spinodal curves illustrating Case II in the main text. Here $m_1 = 1000$, $m_2 = 500$ and $m_3 = 1$, with the remaining parameter values being given on the figure legend. Despite appearances, there are actually three indistinguishable curves on this figure. This figure shows that for the limit considered in Case II, and holding the m_i and χ_{12} values fixed, the behaviour does not depend on the values of χ_{13} and χ_{23} provided $\chi_{13} - \chi_{23} = O(1/m_1)$.¹

Case II: Figure 4.4: The Effect Of Varying χ_{13}, χ_{23}

I now evaluate the effect on stability (or the lack thereof more correctly) of varying the values of χ_{13} and χ_{23} within the context of the Case II limit. Note that equations (4.21)₁ and (4.22), which together determine the spinodal curve, do not depend on the value of either χ_{13} or χ_{23} . This implies that for the Case II limit, the spinodal curves do not (to leading order) depend on the values of χ_{13}, χ_{23} . This prediction is supported by the numerical results displayed in Figure 4.4, where three spinodals are plotted for a fixed value of $\chi_{12} = O(\varepsilon)$ and varying values of χ_{13}, χ_{23} with $\chi_{13} - \chi_{23} = O(\varepsilon)$ (but apart from this, there is nothing special about the values chosen here). Even though three different sets of values for χ_{13}, χ_{23} are used in

¹Created using the software on the website TernaryPlot.com

Figure 4.4, the three curves they generate are indistinguishable - they appear as a single curve.

This effect has essentially been noted before in the context of polymer-polymer-solvent ternary mixtures ([78], [64], [39]), where for symmetric polymer-solvent interactions $\chi_{13} = \chi_{23}$, the behaviour was shown to not otherwise depend on the values of χ_{13}, χ_{23} (provided the Case II limit applies). Here we have extended this result somewhat to include the cases $\chi_{13} - \chi_{23} = O(\varepsilon)$, and have also explained the behaviour mathematically using an asymptotic argument that relies on the fact that the molar volume of a polymer is usually much larger than that of a drug.

4.4.3 Case III: $\chi_{12} = O(1/m_1), \chi_{12} > 0, \chi_{13} - \chi_{23} = O(1/\sqrt{m_1})$

In this limit, I again have $\chi_{12} = O(1/m_1)$ so that for the two polymers, like-like contacts are slightly favoured over like-unlike contacts. However, the difference with Case II is that the asymmetry in the interaction of the two polymers with the drug is now stronger, with $\chi_{13} - \chi_{23} = O(1/\sqrt{m_1})$. I shall show that this seemingly small difference with Case II can lead to interesting new behaviour, including closed loops of immiscibility. As for Case II, I begin with an asymptotic analysis and then consider its consequences.

Asymptotic Analysis

I now consider the limit $m_1 \rightarrow \infty$ with $\chi_{12} = O(1/m_1)$ and $\chi_{13} - \chi_{23} = O(1/\sqrt{m_1})$. I again write $\varepsilon = 1/m_1$ and let

$$\chi_{12} = \varepsilon \bar{\chi}_{12}, \quad \chi_{13} - \chi_{23} = \sqrt{\varepsilon} \bar{\chi}_d.$$

From (4.10), it is clear that

$$\begin{aligned} \chi_1 &= \frac{1}{2} (\varepsilon \bar{\chi}_{12} + \sqrt{\varepsilon} \bar{\chi}_d), \\ \chi_2 &= \frac{1}{2} (\varepsilon \bar{\chi}_{12} - \sqrt{\varepsilon} \bar{\chi}_d), \\ \chi_3 &= \chi_{23} + \frac{1}{2} (\sqrt{\varepsilon} \bar{\chi}_d - \varepsilon \bar{\chi}_{12}). \end{aligned}$$

The Plait Points

The governing equations for the plait points $(\phi_1^p, \phi_2^p, \phi_3^p)$ are now

$$\begin{aligned} \phi_1^p + \phi_2^p + \phi_3^p &= 1, \\ \frac{\phi_1^p}{\sqrt{\varepsilon} - (\sqrt{\varepsilon} \bar{\chi}_{12} + \bar{\chi}_d) \phi_1^p} + \frac{\bar{m}_2 \phi_2^p}{\sqrt{\varepsilon} - (\sqrt{\varepsilon} \bar{\chi}_{12} - \bar{\chi}_d) \bar{m}_2 \phi_2^p} + \frac{\sqrt{\varepsilon} \phi_3^p}{1 - (2\bar{\chi}_{23} + (\sqrt{\varepsilon} \bar{\chi}_d - \varepsilon \bar{\chi}_{12})) \phi_3^p} &= 0, \quad (4.25) \\ \frac{\phi_1^p}{(\sqrt{\varepsilon} - (\sqrt{\varepsilon} \bar{\chi}_{12} + \bar{\chi}_d) \phi_1^p)^3} + \frac{\bar{m}_2^2 \phi_2^p}{(\sqrt{\varepsilon} - (\sqrt{\varepsilon} \bar{\chi}_{12} - \bar{\chi}_d) \bar{m}_2 \phi_2^p)^3} + \frac{\sqrt{\varepsilon} \phi_3^p}{(1 - (2\bar{\chi}_{23} + (\sqrt{\varepsilon} \bar{\chi}_d - \varepsilon \bar{\chi}_{12})) \phi_3^p)^3} &= 0. \end{aligned}$$

In the limit $\varepsilon \rightarrow 0$, I pose

$$\phi_1^p \sim \phi_{10}^p, \quad \phi_2^p \sim \phi_{20}^p, \quad \phi_3^p \sim \phi_{30}^p,$$

to obtain the leading order equations (after some algebra)

$$\begin{aligned} \phi_{10}^p + \phi_{20}^p + \phi_{30}^p &= 1, \\ \frac{\phi_{30}^p}{1 - 2\chi_{23}\phi_{30}^p} &= \frac{1}{\bar{\chi}_d^2} \left(\frac{1}{\phi_{10}^p} + \frac{1}{\bar{m}_2\phi_{20}^p} - 2\bar{\chi}_{12} \right), \\ \phi_{10}^p &= \sqrt{\bar{m}_2}\phi_{20}^p. \end{aligned} \quad (4.26)$$

Equations (4.26) are readily re-cast in the form

$$\phi_{10}^p = \sqrt{\bar{m}_2}\phi_{20}^p, \quad \phi_{30}^p = 1 - (\sqrt{\bar{m}_2} + 1)\phi_{20}^p,$$

where ϕ_{20}^p satisfies the quadratic equation

$$(\phi_{20}^p)^2 - B\phi_{20}^p + C = 0, \quad (4.27)$$

where

$$\begin{aligned} B &= \frac{\bar{m}_2\bar{\chi}_d^2 \left(1 - \frac{4\chi_{23}\bar{\chi}_{12}}{\bar{\chi}_d^2} + \frac{2\bar{\chi}_{12}}{\bar{\chi}_d^2} \right) - 2\chi_{23}(1 + \sqrt{\bar{m}_2})^2}{\bar{m}_2(1 + \sqrt{\bar{m}_2})\bar{\chi}_d^2 \left(1 - \frac{4\chi_{23}\bar{\chi}_{12}}{\bar{\chi}_d^2} \right)}, \\ C &= \frac{1 - 2\chi_{23}}{\bar{m}_2\bar{\chi}_d^2 \left(1 - \frac{4\chi_{23}\bar{\chi}_{12}}{\bar{\chi}_d^2} \right)}. \end{aligned} \quad (4.28)$$

Notice that two physically meaningful solutions for ϕ_{20}^p can exist if

$$B > 0, \quad C > 0, \quad B^2 > 4C. \quad (4.29)$$

For the case of (4.29), I denote the two solutions of (4.27) by

$$(\phi_{20}^p)^- = \frac{1}{2} \left(B - \sqrt{B^2 - 4C} \right)$$

and

$$(\phi_{20}^p)^+ = \frac{1}{2} \left(B + \sqrt{B^2 - 4C} \right)$$

and also write

$$(\phi_{30}^p)^T = 1 - (\sqrt{\bar{m}_2} + 1)(\phi_{20}^p)^- \quad (4.30)$$

and

$$(\phi_{30}^p)^B = 1 - (\sqrt{\bar{m}_2} + 1)(\phi_{20}^p)^+. \quad (4.31)$$

where here T refers to the top plait point and B the bottom. If $0 \leq (\phi_{30}^p)^B \leq (\phi_{30}^p)^T \leq 1$, then (4.30) and (4.31) give the bottom and top plait points of a closed loop of immiscibility in the polymer-polymer-drug ternary diagram (see Figure 4.5). The loop of immiscibility can be made to vanish (to leading order at least) by choosing parameters so that

$$(\phi_{30}^p)^B \rightarrow (\phi_{30}^p)^T$$

or, equivalently,

$$(\phi_{20}^p)^- \rightarrow (\phi_{20}^p)^+$$

so that the top and bottom plait points coalesce. This last condition becomes true in the limit

$$B^2 \rightarrow 4C,$$

where B and C are given in (4.28). Hence, for the current limit, a favourable parameters choice is given by $B^2 = 4C$, or

$$\left(\bar{\chi}_d^2 \left(1 - \frac{4\chi_{23}\bar{\chi}_{12}}{\bar{\chi}_d^2} + \frac{2\bar{\chi}_{12}}{\bar{\chi}_d^2} \right) - \frac{2\chi_{23}}{\bar{m}_2} (1 + \sqrt{m_2})^2 \right)^2 = \frac{4(1 - 2\chi_{23})(1 + \sqrt{m_2})^2 \bar{\chi}_d^2 \left(1 - \frac{4\chi_{23}\bar{\chi}_{12}}{\bar{\chi}_d^2} \right)}{\bar{m}_2}.$$

The Spinodal Curve

Denoting the points on the spinodal curve by $(\phi_1^s, \phi_2^s, \phi_3^s)$, we have that

$$\begin{aligned} \phi_1^s + \phi_2^s + \phi_3^s &= 1, \\ \frac{\phi_1^s}{\sqrt{\varepsilon} - (\sqrt{\varepsilon}\bar{\chi}_{12} + \bar{\chi}_d)\phi_1^s} + \frac{\bar{m}_2\phi_2^s}{\sqrt{\varepsilon} - (\sqrt{\varepsilon}\bar{\chi}_{12} - \bar{\chi}_d)\bar{m}_2\phi_2^s} + \frac{\sqrt{\varepsilon}\phi_3^s}{1 - (2\bar{\chi}_{23} + (\sqrt{\varepsilon}\bar{\chi}_d - \varepsilon\bar{\chi}_{12}))\phi_3^s} &= 0. \end{aligned} \quad (4.32)$$

In the limit $\varepsilon \rightarrow 0$, I pose

$$\phi_1^s \sim \phi_{10}^s, \quad \phi_2^s \sim \phi_{20}^s, \quad \phi_3^s \sim \phi_{30}^s,$$

to obtain the leading order equations (in the same way as for the plait points)

$$\begin{aligned} \phi_{10}^s + \phi_{20}^s + \phi_{30}^s &= 1, \\ \frac{\phi_{30}^s}{1 - 2\chi_{23}\phi_{30}^s} &= \frac{1}{\bar{\chi}_d^2} \left(\frac{1}{\phi_{10}^s} + \frac{1}{\bar{m}_2\phi_{20}^s} - 2\bar{\chi}_{12} \right). \end{aligned} \quad (4.33)$$

I now discuss the implications of these results with the aid of numerical results.

Case III: Figure 4.5: Closed Loops Of Immiscibility

Consider first the red curve in Figure 4.5, which has $\chi_{12} = 0.001$, $\chi_{13} = 0.26$ and $\chi_{23} = 0.49$. These parameter values are chosen so that $\chi_{12} = O(\varepsilon)$ and $\chi_{12} - \chi_{13} = O(\sqrt{\varepsilon})$, and to ensure that the quadratic equation (4.27) has two physically meaningful solutions. For these parameter values, the quadratic equation (4.27) becomes

$$(\phi_{20}^p)^2 - 0.543102\phi_{20}^p + 0.000785 = 0,$$

and this has solutions

$$(\phi_{20}^p)^- = 0.001450, \quad (\phi_{20}^p)^+ = 0.541652,$$

so that

$$(\phi_{30}^p)^B = 0.075342, \quad (\phi_{30}^p)^T = 0.997525,$$

and these asymptotic predictions agree well with the relevant numerical curve (the red one) in Figure 4.5. The asymptotic analysis indicates that the discrepancy between the asymptotic predictions and the numerical results can be $O(\sqrt{\varepsilon})$, and this is consistent with our numerical findings.

Repeating these calculations for the blue curve in Figure 4.5 (which has the same parameter values as the red curve apart from $\chi_{13} = 0.38$) gives

$$(\phi_{30}^p)^B = 0.384746, \quad (\phi_{30}^p)^T = 0.981315,$$

which is again in good agreement with the numerical profile.

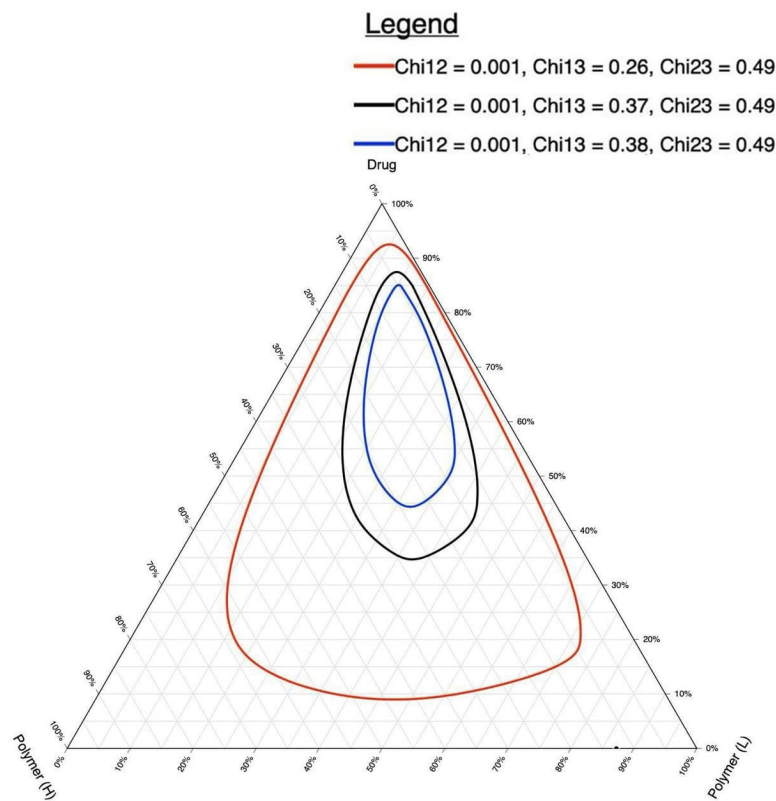


Figure 4.5: Spinodal curves illustrating Case III in the main text, which has $\chi_{12} = O(1/m_1)$, $\chi_{12} > 0$ and $\chi_{13} - \chi_{23} = O(1/\sqrt{m_1})$. Here $m_1 = 1000$, $m_2 = 500$ and $m_3 = 1$, with the remaining parameter values been given on the figure legend. In the figure, χ_{12} and χ_{23} are fixed and χ_{13} varies, and the parameter values have been chosen to illustrate closed loops of immiscibility.¹

It should be noted that closed loops of immiscibility have been experimentally observed for some ternary polymer blends; see, for example, the papers by Rabeony *et al.* [69] and Hong *et al.* [38]. However, I am unaware of any such observations in the context of ternary solid dispersions.

¹Created using the software on the website TernaryPlot.com

Case III: Figure 4.6: A Single Plait Point

Consider the green curve in Figure 4.6, which has $\chi_{12} = 0.009$, $\chi_{13} = 0.10$ and $\chi_{23} = 0.12$. The quadratic equation (4.27) for these parameter values is

$$(\phi_{20}^p)^2 + 1.895016\phi_{20}^p - 0.387755 = 0,$$

and this has solutions

$$(\phi_{20}^p)^- = -2.081318, \quad (\phi_{20}^p)^+ = 0.186302,$$

and clearly only the second of these $(\phi_{20}^p)^+$ is physically relevant, so that there is only one meaningful plait point. For this value, it follows that

$$(\phi_{30}^p)^+ = 0.681962,$$

which agrees well with the numerical curve. The other curves in Figure 4.6 similarly also give good agreement with the asymptotic predictions.

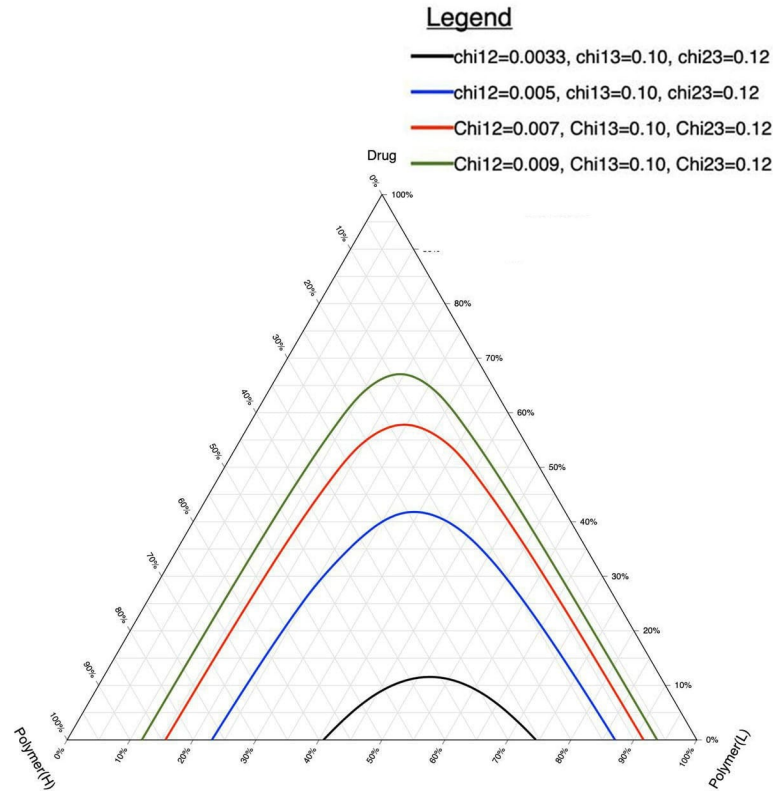


Figure 4.6: Spinodal curves illustrating Case III in the main text, which has $\chi_{12} = O(1/m_1)$, $\chi_{12} > 0$ and $\chi_{13} - \chi_{23} = O(1/\sqrt{m_1})$. Here $m_1 = 1000$, $m_2 = 500$ and $m_3 = 1$, with the remaining parameter values been given on the figure legend. In the figure, χ_{13} and χ_{23} are fixed and χ_{12} varies, and the parameter values have been chosen so that there is a single plait point.¹

¹Created using the software on the website TernaryPlot.com

4.5 Conclusions

I now summarise some of the notable predictions of the current chapter for polymer-polymer-drug ternary solid dispersions.

- If the two polymers are incompatible in the sense that $\chi_{12} = O(1)$, $\chi_{12} > 0$, then the system has unfavourable stability properties - most initial compositions lead to phase separation.
- If the two polymers are compatible in the sense that $\chi_{12} = O(1/m_1) \ll 1$, $\chi_{12} > 0$, then the system can have favourable stability properties (depending on the values for the other parameters in the system).
- For $\chi_{12} = O(1/m_1) \ll 1$, $\chi_{12} > 0$, the stability behaviour of the system is sensitive to an asymmetry in how the two polymers interact with the drug; more precisely, the behaviour can be sensitive to a small change in the value of $|\chi_{13} - \chi_{23}|$. Two cases are explored in detail $\chi_{13} - \chi_{23} = O(1/m_1)$ and $\chi_{13} - \chi_{23} = O(1/\sqrt{m_1})$ with $m_1 \gg 1$.
- For $\chi_{12} = O(1/m_1) \ll 1$, $\chi_{12} > 0$ and $\chi_{13} - \chi_{23} = O(1/\sqrt{m_1})$, it has been shown that closed loops of immiscibility are theoretically possible.

Chapter 5

Analyzing The Stability Of Polymer-Surfactant-Drug Ternary Solid Dispersions

5.1 Introduction

In this chapter, I analyze the stability of some Polymer-Surfactant-Drug (P-S-D) ternary solid dispersions. The analysis mirrors that of Chapter 4 in that the stability of these ternary systems will be analyzed by constructing phase diagrams using standard thermodynamic methods and Flory-Huggins solution theory. Also, similar to Chapter 4, I will construct the phase diagrams using asymptotic and numerical methods. The asymptotics will yield insights into the underlying governing chemistry as well as providing a check on the accuracy of the numerical results. One of the principal aims again here is to identify parameter regimes that lead to desirable stability behaviour for products in storage, but also to identify parameter regimes that should be avoided. For example, we shall see from the results of this chapter that system stability may be enhanced by such factors as reducing the molecular weight of the surfactant, improving the compatibility of the surfactant and the drug, and improving the compatibility of the polymer and the drug.

I begin by giving some general discussion of P-S-D ternary solid dispersions.

5.2 Drug-Surfactant-Drug Ternary Solid Dispersions

Some Drug-Polymer-Surfactant ternary systems that have previously appeared in the literature are listed in Table 5.1. The list is not exhaustive and emphasizes stability studies.

In these Ternary Solid Dispersions (TSDs), a drug with low solubility is dispersed

in a hydrophilic polymer together with a suitable surfactant. In traditional drug-surfactant binary formulations, the purpose of the surfactant is to encapsulate poorly soluble drug and thereby improve its solubility. Popular surfactants used in TSDs are Tween 80 and Poloxamer 407.

However, it should be admitted that the literature regarding the mechanisms involved in drug-polymer-surfactant interactions is still quite limited. In fact, there is some evidence from binary studies that the presence of a surfactant can have negative consequences for dispersion stability. For example, there is evidence that the presence of a surfactant may reduce the glass transition temperature of the dispersion, leading to increased drug mobility at lower temperatures and accelerated phase separation - see, for example, the review by Li *et al.* [53]. For other studies that discuss the interactions between polymers and surfactants, I refer the interested reader to the references in Table 5.1.

Drug	Polymer	Surfactant	Purpose	Volume Fractions	References
Curcumin	PVP	Pluronic	Stability ↑	$m_1 \approx 118, m_2 \approx 45$	[45]
Itraconazole	PVP VA64	Myrj52	Stability ↑	$m_1 \approx 60, m_2 \approx 2$	[95]
Aprepitant	Soluplus	Poloxmer 188	Stability ↑	$m_1 \approx 216, m_2 \approx 25$	[62]
Valsartan	PEG6000	TPGS	Stability ↑	$m_1 \approx 17, m_2 \approx 5$	[51]
PBC	PVP K12	P407	Stability ↑	$m_1 \approx 6, m_2 \approx 26$	[32]
Celecoxid	PVP	SLS	Stability ↑	$m_1 \approx 9, m_2 \approx 2$	[60]
Paclitaxeel	PVP K30	SDS	Stability ↑ Solubility ↑	$m_1 \approx 90, m_2 \approx 0.5$	[74]
Clopidogrel	HPMC VA	Tween 80	Stability ↑ Solubility ↑	$m_1 \approx 26, m_2 \approx 5$	[46]
Efavirenz	PEG 800	Tween 80	Stability ↑ Solubility ↑	$m_1 \approx 32, m_2 \approx 6$	[48]

Table 5.1: Some Drug-Polymer-Surfactant ternary systems that have previously appeared in the literature. This list is not exhaustive and emphasizes stability studies. In the table, m_1 gives the ratio of the molar volume of the polymer and the drug, and m_2 gives the ratio of the molar volume of the surfactant and the drug.

5.3 Analysis And Results

As stated above, the analysis presented here mirrors that of Chapter 4 for Polymer-Polymer-Drug systems in a number of respects. The analysis is centred on calculating plait points and spinodal curves for various parameter regimes using asymptotic and numerical techniques, with a view to identifying regimes with favourable or unfavourable stability properties. I am assuming again here that the mixture may be adequately modelled using Flory-Huggins solution theory.

From Chapter 3, recall that

$$m_1 = \frac{V_1}{V^*}, \quad m_2 = \frac{V_2}{V^*}, \quad m_3 = \frac{V_3}{V^*},$$

where V_i is the molar volume of species i ($i = 1, 2, 3$) and V^* is some reference molar volume. I adopt the following notation for the current chapter -

$$1 = \text{polymer}, \quad 2 = \text{surfactant}, \quad 3 = \text{drug},$$

and I make the choice

$$V^* = V_3,$$

so that

$$m_1 = \frac{V_1}{V_3}, \quad m_2 = \frac{V_2}{V_3}, \quad m_3 = 1.$$

I begin by giving an asymptotic analysis of the plait points and spinodal curve, and then discuss the implications of its results. The results will be illustrated using numerical calculations generated by the mathematical package Maple.

5.3.1 Asymptotic Analysis

Inspecting the values for m_1 and m_2 in Table 5.1, an appropriate limit to consider is

$$m_1 \gg 1, \quad m_2 = O(1),$$

where here $m_1 \gg 1$ reflects the fact that polymer molecules are typically much larger than drug molecules. In Chapter 4, I have described how values for the molar volumes required for the calculation of m_1 and m_2 can be estimated. I write

$$m_1 = \frac{1}{\varepsilon}, \quad m_3 = 1,$$

and consider the limit $\varepsilon \rightarrow 0$.

The Plait Points

The governing equations for the plait points now take the form (see equations (4.7) in Chapter 4)

$$\begin{aligned} \phi_1^p + \phi_2^p + \phi_3^p &= 1, \\ \frac{\phi_1^p}{\varepsilon - 2\chi_1\phi_1^p} + \frac{m_2\phi_2^p}{1 - 2\chi_2m_2\phi_2^p} + \frac{\phi_3^p}{1 - 2\chi_3\phi_3^p} &= 0, \\ \frac{\varepsilon\phi_1^p}{(\varepsilon - 2\chi_1\phi_1^p)^3} + \frac{m_2^2\phi_2^p}{(1 - 2\chi_2m_2\phi_2^p)^3} + \frac{\phi_3^p}{(1 - 2\chi_3\phi_3^p)^3} &= 0, \end{aligned} \tag{5.1}$$

where the χ_i ($i = 1, 2, 3$) are given by (3.36) in Chapter 3. Inspecting these equations, I deduce that

$$\phi_1^p = O(\sqrt{\varepsilon}), \quad \phi_2^p = O(1), \quad \phi_3^p = O(1),$$

as $\varepsilon \rightarrow 0$. This implies that the plait points are close to the surfactant-drug binary on the ternary phase diagrams, a feature that is clearly visible in the numerical profiles displayed in Figures 5.1 - 5.5.

In the limit $\varepsilon \rightarrow 0$, I pose

$$\phi_1^p \sim \sqrt{\varepsilon}\phi_{10}^p, \quad \phi_2^p \sim \phi_{20}^p, \quad \phi_3^p \sim \phi_{30}^p,$$

to obtain the leading order equations

$$\begin{aligned} \phi_{20}^p + \phi_{30}^p &= 1, \\ \frac{m_2\phi_{20}^p}{1 - 2\chi_2 m_2\phi_{20}^p} + \frac{\phi_{30}^p}{1 - 2\chi_3\phi_{30}^p} &= \frac{1}{2\chi_1}, \\ \frac{m_2^2\phi_{20}^p}{(1 - 2\chi_2 m_2\phi_{20}^p)^3} + \frac{\phi_{30}^p}{(1 - 2\chi_3\phi_{30}^p)^3} &= \frac{1}{8\chi_1^3(\phi_{10}^p)^2}. \end{aligned} \quad (5.2)$$

These equations readily lead to the following quadratic equation for ϕ_{20}^p :

$$A(\phi_{20}^p)^2 - B\phi_{20}^p + C = 0, \quad (5.3)$$

where

$$\begin{aligned} A &= 4m_2(\chi_1\chi_3 + \chi_1\chi_2 + \chi_2\chi_3), \\ B &= -2m_2(\chi_1 + \chi_2) + 2(\chi_1 + \chi_3) + 4m_2(\chi_1\chi_3 + \chi_1\chi_2 + \chi_2\chi_3), \\ C &= 2(\chi_1 + \chi_3) - 1. \end{aligned} \quad (5.4)$$

Once ϕ_{20}^p has been determined, equations (5.2)₁ and (5.2)₃ may be used to determine ϕ_{30}^p and ϕ_{10}^p , respectively.

Solving the quadratic equation (5.3) gives solutions with a quite complex dependency on the parameter values χ_1 , χ_2 , χ_3 and m_2 . The number of physically meaningful solutions (if any) will clearly depend on the values for the parameters. Nevertheless, for a given set of values, equation (5.3) is trivial to solve and provides a useful first step in evaluating a particular system.

The Spinodal Curves

I now make a few remarks about the character of the spinodal curves in the limit $\varepsilon \rightarrow 0$, avoiding most mathematical details. Examples of these spinodals can be found in Figures 5.1 - 5.5. Inspecting these curves, it is clear that the right arms of these spinodals are very close to the surfactant-drug binary. In fact, in limit $\varepsilon \rightarrow 0$, the right arms of the spinodals have $\phi_1^s = O(\varepsilon)$, while the left arms have $\phi_1^s = O(1)$, and this is clear in the figures. Recall that the plait points have $\phi_1^p = O(\sqrt{\varepsilon})$ in the limit $\varepsilon \rightarrow 0$, so that these are also close to the surfactant-drug binary, though further from it than the right arms of the spinodal curves, another feature that is clearly visible on the figures.

It is also of interest to locate the points where the spinodal curve intersects the polymer-surfactant binary $\phi_3 = 0$, if it intersects it at all. I denote by $(\phi_1^L, \phi_2^L, 0)$

the left intersection point and by $(\phi_1^R, \phi_2^R, 0)$ the right intersection point. In the limit $\varepsilon \rightarrow 0$, it is easily seen that

$$\phi_1^L \sim 1 - \frac{1}{2m_2\chi_{12}}, \quad \phi_2^L \sim \frac{1}{2m_2\chi_{12}},$$

and

$$\phi_1^R = O(\varepsilon), \quad \phi_2^R \sim 1.$$

Clearly, a physically meaningful value for $(\phi_1^L, \phi_2^L, 0)$ only exists for

$$\chi_{12} \geq \frac{1}{2m_2}.$$

Hence, there will not be an unstable region on the polymer-surfactant binary if the polymer and surfactant are sufficiently compatible (more precisely, if $\chi_{12} \leq 1/(2m_2)$). All of these predictions are borne out in the numerical curves displayed in Figures 5.1-5.4.

The intersections (if they exist) of the spinodals with the polymer-drug binary $\phi_2 = 0$ are similarly analyzed. Using the same notation as for the $\phi_3 = 0$ intersects, I have that

$$\phi_1^L \sim 1 - \frac{1}{2\chi_{13}}, \quad \phi_3^L \sim \frac{1}{\chi_{13}},$$

and

$$\phi_1^R = O(\varepsilon), \quad \phi_3^R \sim 1,$$

as $\varepsilon \rightarrow 0$. Clearly, a physically meaningful value for $(\phi_1^L, 0, \phi_3^L)$ only exists for

$$\chi_{13} \geq \frac{1}{2},$$

which is quite a severe restriction on the compatibility properties of the polymer and the drug. A numerical example of this case can be found in Figure 5.5.

5.3.2 Numerical Results

I now describe some numerical results for the spinodal curves for polymer-ternary-drug systems. The spinodal curves are calculated using the mathematical package Maple, as previously described in Chapter 3. Throughout the numerical results, I fix the value of m_1 to be $m_1 = 1000 \gg 1$. This still leaves four parameters that can be independently varied - χ_{12} , χ_{13} , χ_{23} and m_2 , and it is too large a task to numerically explore the entire parameter space. However, the foregoing asymptotic analysis helps identify parameter regimes of particular interest and relevance.

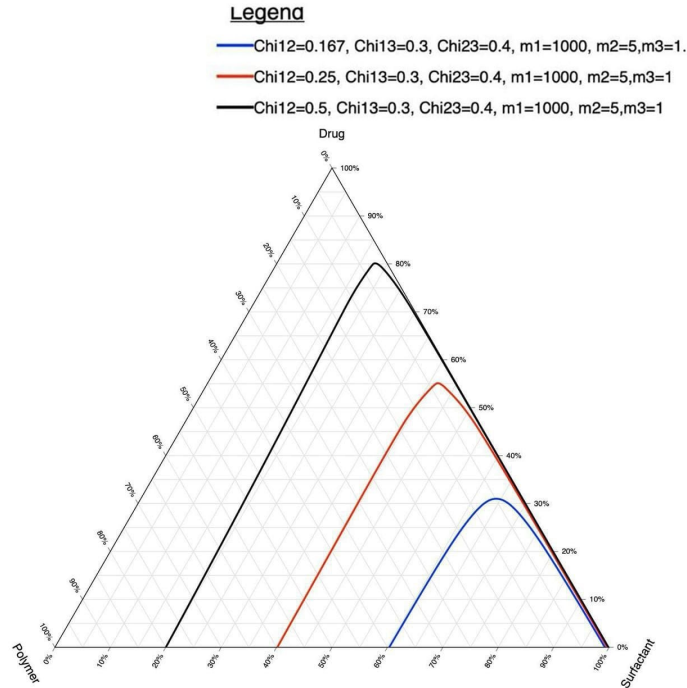


Figure 5.1: Spinodal curves for a polymer-surfactant-drug system. Here $m_1 = 1000$, $m_2 = 5$ and $m_3 = 1$, and the remaining parameter values are given on the figure legend. These curves show the effect on stability of varying the parameter χ_{12} , the polymer-surfactant interaction parameter. The figure is further discussed in the main text.¹

Figure 5.1: The Effect Of Varying The Polymer-Surfactant Interaction Parameter χ_{12}

In Figure 5.1, I display spinodals for various values of χ_{12} , the interaction parameter for the polymer and the surfactant. The parameter values are chosen here so that the spinodals only intersect the polymer-surfactant binary - this is achieved by choosing $\chi_{12} > 1/(2m_2)$ and sufficiently small values of χ_{13} and χ_{23} , as guided by the asymptotic analysis above. It is noteworthy from the figure that the unstable region grows as χ_{12} increases (that is, as the polymer and surfactant become more incompatible), as might be expected. For the current parameter regime, the unstable region vanishes as $\chi_{12} \rightarrow 0.1^+$. Hence, in the current context, there is no unstable region for polymer-surfactant pairings with $\chi_{12} < 0.1$.

¹Created using the software on the website TernaryPlot.com

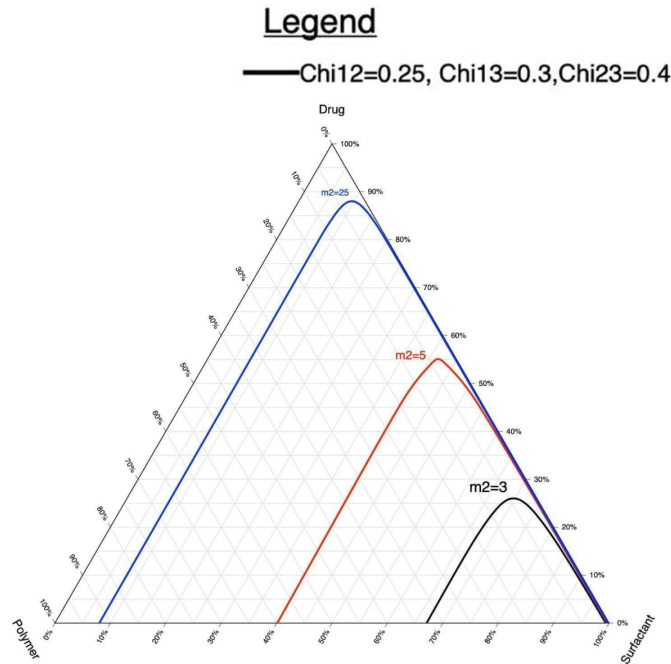


Figure 5.2: Spinodal curves for a polymer-surfactant-drug system. Here $m_1 = 1000$, $m_3 = 1$, with the remaining parameter values being given on the figure. These curves show the effect on dispersion stability of varying m_2 , the ratio of the molar volume of the surfactant to that of the drug. The figure is further discussed in the main text.¹

Figure 5.2: The Effect Of Varying The Surfactant Molar Volume m_2

In Figure 5.2, I display numerically calculated spinodal curves that show the effect on stability of varying m_2 , the ratio of the molar volume of the polymer to that of the drug. The parameter values are again chosen here so that the spinodals only intersect the polymer-surfactant binary. For a fixed drug, increasing m_2 corresponds to increasing the molar volume (or molecular weight) of the surfactant. Inspecting the curves in Figure 5.2, it is clear that the unstable region grows as m_2 increases, so that the molecular weight of the surfactant may have a significant effect on the stability of a dispersion. For the current parameter regime, the unstable region vanishes as $m_2 \rightarrow 2^+$.

¹Created using the software on the website TernaryPlot.com

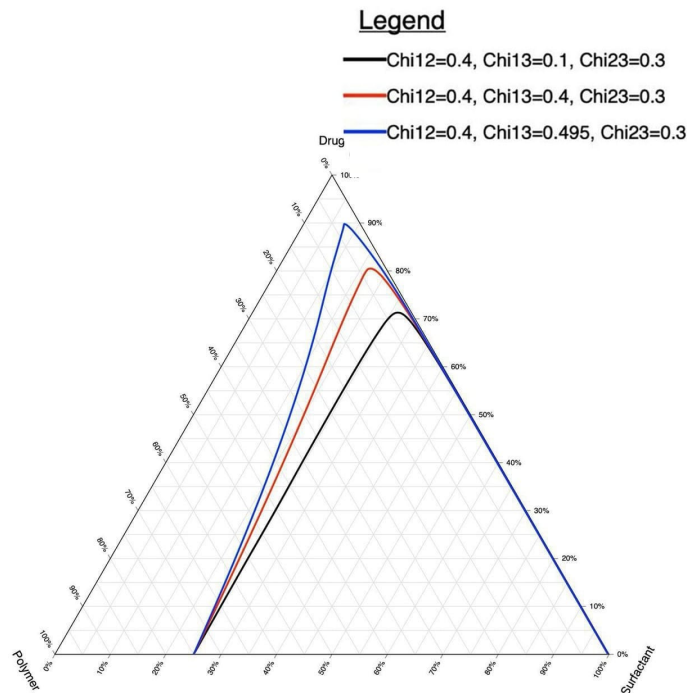


Figure 5.3: Spinodal curves for a polymer-surfactant-drug system. Here $m_1 = 1000$, $m_2 = 5$, $m_3 = 1$, and the remaining parameter values are given on the figure legend. These curves show the effect on stability of varying χ_{13} , the polymer-drug interaction parameter. The figure is further discussed in the main text.¹

Figure 5.3: The Effect Of Varying The Polymer-Drug Interaction Parameter χ_{13}

In Figure 5.3, spinodal curves are plotted that show the effect of varying the polymer-drug interaction parameter χ_{13} . The parameter values are again chosen so that the spinodals intersect the polymer-surfactant binary only. Inspecting the curves, we see that the unstable region grows larger as χ_{13} increases, though the effect is quite weak. It is also noteworthy that the spinodals all intersect the polymer-surfactant binary at approximately the same points - this is consistent with the asymptotic predictions of Section 5.3.1 (recall that, to leading order as $1/m_1 \rightarrow 0$, the left intersection point for the spinodals depends only on the values of m_2 and χ_{12}).

¹Created using the software on the website TernaryPlot.com

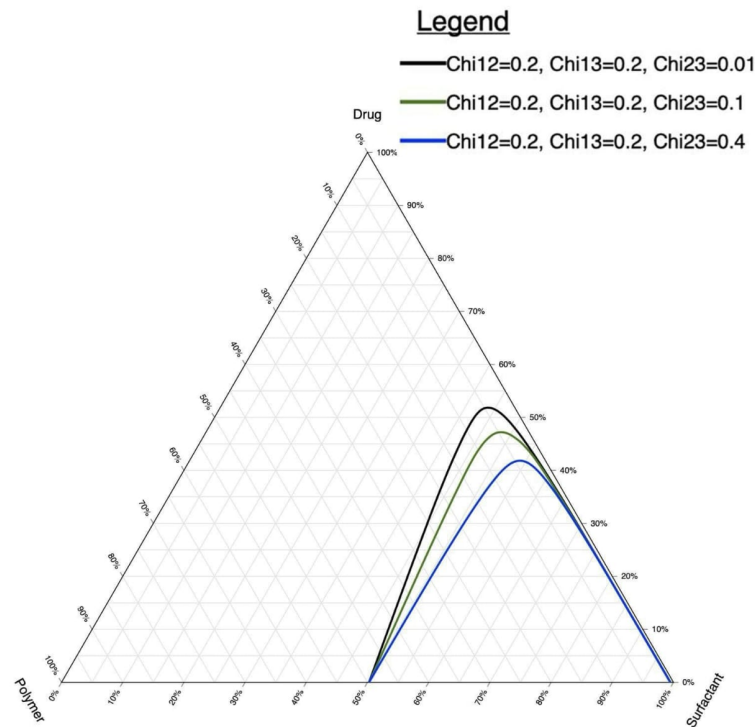


Figure 5.4: Spinodal curves for a polymer-surfactant-drug system. Here $m_1 = 1000$, $m_2 = 5$, $m_3 = 1$, and the remaining parameter values are given on the figure legend. These curves show the effect on stability of varying χ_{23} , the surfactant-drug interaction parameter. The figure is further discussed in the main text.¹

Figure 5.4: The Effect Of Varying The Surfactant-Drug Interaction Parameter χ_{23}

In Figure 5.4, I display numerical spinodal curves that show the effect of varying the surfactant-drug interaction parameter χ_{23} . Interestingly, for the current parameter choice, we observe that the unstable region shrinks as χ_{23} increases. Hence, for the current parameter choice, the stability properties of the dispersion marginally improve as the surfactant and drug become less compatible.

¹Created using the software on the website TernaryPlot.com

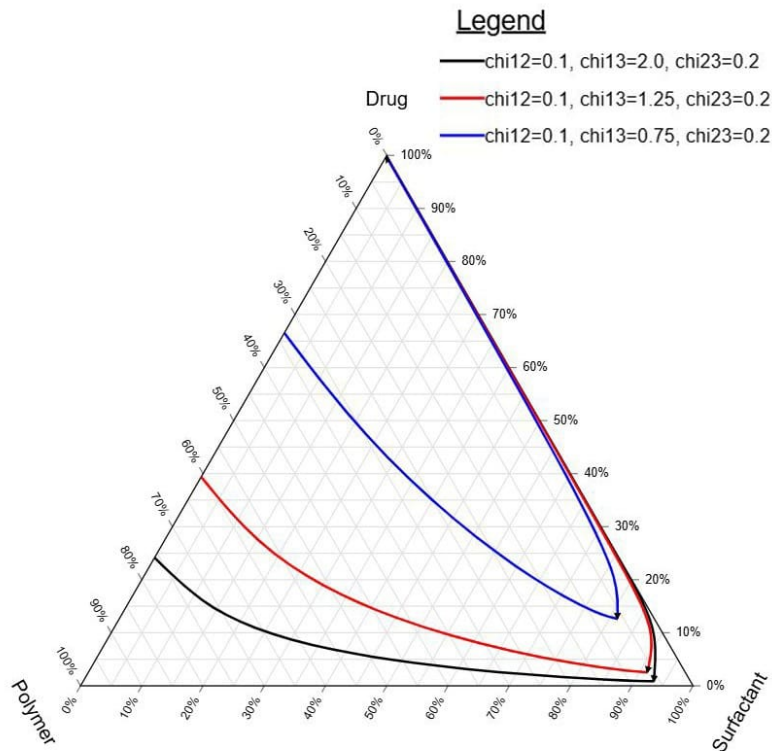


Figure 5.5: Spinodal curves for a polymer-surfactant-drug system. Here $m_1 = 1000$, $m_2 = 5$, $m_3 = 1$, and the remaining parameter values are given on the figure legend. These curves show spinodals that intersect the polymer-drug binary, with varying χ_{13} . The figure is further discussed in the main text.¹

Figure 5.5: Spinodals Of A Different Character Are Also Possible

The spinodals we have encountered thus far do not exhaust all of the possibilities. In Figure 5.5, I display spinodal curves that intersect the polymer-drug binary only. These curves are obtained by choosing parameter values with $\chi_{13} > 1/2$ and χ_{12} , χ_{23} sufficiently small. Spinodals that intersect the surfactant-drug binary only or more than one binary are also possible - see Figure 5.6.

¹Created using the software on the website TernaryPlot.com

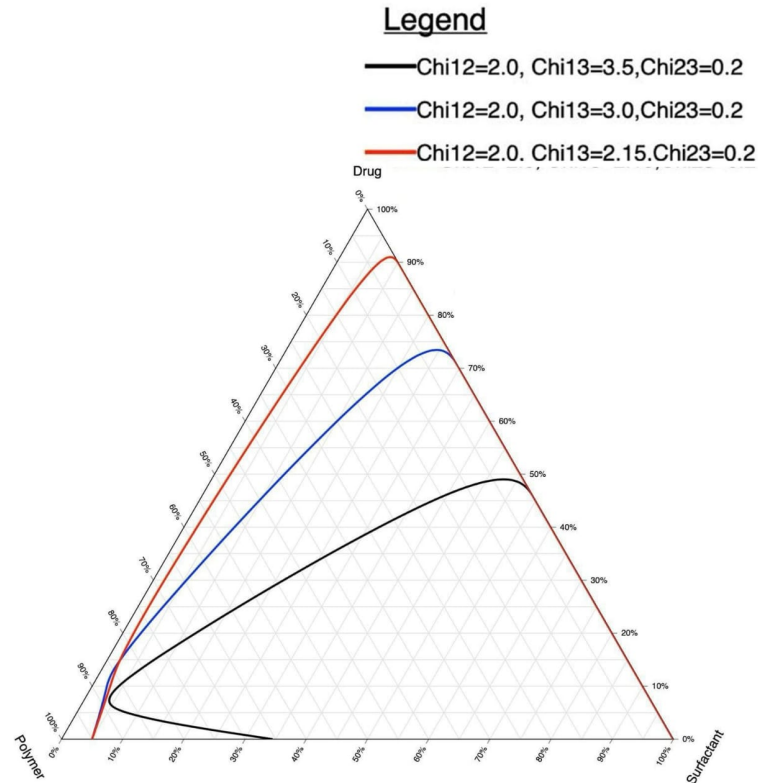


Figure 5.6: Spinodal curves for a polymer-surfactant-drug system. Here $m_1 = 1000$, $m_2 = 5$, $m_3 = 1$, and the remaining parameter values are given on the figure legend. These curves show spinodals that intersect both the surfactant-polymer and surfactant-drug binaries.¹

5.4 Conclusions

I now summarise some of the notable predictions of the current chapter for polymer-surfactant-drug ternary solid dispersions.

- Making the weak assumption that the polymer has by far the largest molar volume of the three components ($m_1 \gg 1$, $m_2 = O(1)$, $m_3 = 1$), estimating the location of the plait points has been reduced to solving a quadratic equation. Useful information regarding the character of the spinodals in this limit has also been extracted.
- Aided by an asymptotic analysis, the effect on stability of varying the various parameters in the system has been numerically investigated. In particular, the effect of changing the polymer-surfactant interaction (χ_{12}), the polymer-drug interaction (χ_{13}), and the surfactant-drug interaction (χ_{23}) have been evaluated.

¹Created using the software on the website TernaryPlot.com

-
- The results of the analysis suggest that system stability is enhanced by such factors as reducing the molecular weight of the surfactant, improving the compatibility of the surfactant and the drug, and improving the compatibility of the polymer and the drug.
 - One somewhat counter-intuitive result of the current analysis is that the stability properties of the system may be improved by making the surfactant and drug less compatible (that is, by increasing χ_{23}).

It is my hope that some of these predictions will be tested in future experimental studies of these ternary systems, and will provide a guide for system design.

Chapter 6

A Diffusion Model For A Ternary Solid Dispersion

6.1 Introduction

In this chapter, I develop a multicomponent diffusion model that describes the evolution of a solid dispersion. The model will consist of a coupled system of nonlinear partial differential equations, and has close parallels with a model developed by Meere, Pontrelli & McGinty [58]. The added value of this type of modelling is that it allows us to track the detailed evolution of the dispersion to its final fate, and not just the final character of the dispersion as predicted by thermodynamic theory.

6.2 Model Formulation

To begin with, I suppose that there are p components in the dispersion. However, in the current thesis, I will ultimately specialize to the case of ternary systems which have $p = 3$. The chemical potential μ_i (J/mole) of species i ($i = 1, 2, \dots, p$) gives the Gibbs free energy per mole of species i , and is given here by ([82])

$$\mu_i = \mu_i^b - \epsilon_i^2 \nabla^2 X_i \quad (6.1)$$

where

$$\mu_i^b = \mu_i^0 + RT \ln(a_i) \quad (6.2)$$

and where μ_i^b is the bulk chemical potential of species i , μ_{i0} is the chemical potential of species i in the pure state, a_i is the activity of species i , and the term involving $\epsilon_i^2 > 0$ (m²J/mole) penalises the formation of phase boundaries ([76], [75],[100],[99]). The parameters ϵ_i^2 are referred to as gradient energy coefficients ([16], [25]). Here X_i is the molar fraction of species i ($i = 1, 2, \dots, p$), and the activities can depend on these molar fractions, so that

$$a_i = a_i(X_1, X_2, \dots, X_p).$$

The molar fraction is related to the molar concentration via

$$X_i = V_i c_i \quad (6.3)$$

where V_i (molar⁻¹) is the molar volume of species i . The flux of species i (molar·m/s) is given by

$$\mathbf{J}_i = c_i \mathbf{v}_i \quad (6.4)$$

where c_i (molar), \mathbf{v}_i (m/s) give the molar concentration and drift velocity, respectively, of species i . The drift velocity \mathbf{v}_i gives the average velocity a particle of species i attains due to the diffusion force acting on it, and is given here by

$$\mathbf{v}_i = M_i \mathcal{F}_i = -M_i \nabla \mu_i \quad (6.5)$$

where M_i (mole·s/kg), \mathcal{F}_i (J/[m·mole]) give the mobility and diffusion force, respectively, for species i . Equations (6.4) and (6.5) give

$$\mathbf{J}_i = -M_i c_i \nabla \mu_i. \quad (6.6)$$

Conservation of mass for species i implies that

$$\frac{\partial c_i}{\partial t} + \nabla \cdot \mathbf{J}_i = 0 \quad (6.7)$$

and using (6.6) now gives

$$\frac{\partial c_i}{\partial t} = \nabla \cdot (M_i c_i \nabla \mu_i)$$

or equivalently

$$\frac{\partial X_i}{\partial t} = \nabla \cdot \left(D_i X_i \nabla \left\{ \frac{\mu_i - \mu_{i0}}{RT} \right\} \right) \quad (6.8)$$

with

$$\frac{\mu_i - \mu_{i0}}{RT} = \ln(a_i) - \delta_i^2 \nabla^2 X_i \quad (6.9)$$

for $i = 1, 2, \dots, p$, and where $\delta_i^2 = \epsilon_i^2 / RT > 0$ (m²/molar), and

$$D_i = M_i RT \quad (\text{Einstein relation})$$

is the self-diffusion coefficient for species i .

It is also of value to develop a formulation involving diffusion coefficients since these yield immediate information regarding timescales for transport processes, and will also enable the development of analytical results via a linearization process.

Diffusion Coefficients

Using (6.1), (6.2) and (6.6) gives

$$\mathbf{J}_i = -M_i c_i \nabla \mu_i = -M_i c_i \left(\frac{RT}{a_i} \nabla a_i - \epsilon_i^2 \nabla (\nabla^2 X_i) \right)$$

and then using the fact that the activities depend on the molar fractions gives

$$\mathbf{J}_i = -M_i c_i \left(\frac{RT}{a_i} \sum_{j=1}^p \frac{\partial a_i}{\partial X_j} \nabla X_j - \epsilon_i^2 \nabla(\nabla^2 X_i) \right). \quad (6.10)$$

Using (6.3), we can now write (6.10) as

$$\mathbf{J}_i = - \sum_{j=1}^p D_{ij} \nabla c_j + D_i \epsilon_i^2 c_i \nabla(\nabla^2 c_i) \quad (6.11)$$

where $\epsilon_i^2 = V_i \delta_i^2$ and where the diffusion coefficients D_{ij} (m²/s) are given by

$$D_{ij} = D_i \frac{V_j X_i}{V_i a_i} \frac{\partial a_i}{\partial X_j}. \quad i, j = 1, 2, \dots, p \quad (6.12)$$

Conservation of mass (6.7) then implies that (reverting to molar fractions)

$$\frac{\partial X_i}{\partial t} = \nabla \cdot \left(\sum_{j=1}^p \frac{V_i}{V_j} D_{ij}(\mathbf{X}) \nabla X_j - D_i \delta_i^2 X_i \nabla(\nabla^2 X_i) \right) \quad i = 1, 2, \dots, p \quad (6.13)$$

where $\mathbf{X} = (X_1, X_2, \dots, X_p)$, and where we have included the concentration dependence of the diffusion coefficients D_{ij} here to emphasise that this system is in general a coupled system of nonlinear diffusion equations. It should be noted that the equations (6.13) are not independent since $\sum_{i=1}^p X_i = 1$, and so it is sufficient to solve for $p - 1$ concentrations only.

6.2.1 Activity coefficients

The activities a_i are usually written as

$$a_i = \gamma_i X_i,$$

where the $\gamma_i = \gamma_i(X_1, X_2, \dots, X_p)$ are referred to as *activity coefficients*. Equations (6.12) now give

$$D_{ij} = D_i \frac{V_j}{V_i} \left(\delta_{ij} + \frac{X_i}{\gamma_i} \frac{\partial \gamma_i}{\partial X_j} \right) \quad i, j = 1, 2, \dots, p \quad (6.14)$$

where δ_{ij} is the Kronecker delta.

The details of the interactions between the species in solution are captured in the modelling by choosing appropriate forms for the activity coefficients $\gamma_i = \gamma_i(X_1, X_2, \dots, X_p)$. The construction of appropriate forms for the γ_i for various solutions is a large subject with a large literature; see, for example, the books [49] and [67].

6.2.2 Ternary Systems

In this chapter, I consider the behaviour of ternary solid dispersions. The problems I consider will be one-dimensional, and I denote the single spatial variable by x . Ternary systems have $p = 3$, so that

$$X_1 + X_2 + X_3 = 1.$$

Recalling that $X_i = c_i V_i$ then gives

$$V_1 c_1 + V_2 c_2 + V_3 c_3 = 1,$$

so that

$$c_1 = \frac{1}{V_1} - \frac{m_2}{m_1} c_2 - \frac{m_3}{m_1} c_3. \quad (6.15)$$

Hence, it sufficient here to solve for c_2 and c_3 only.

Conservation of mass for species i for one spatial dimension x implies that

$$\frac{\partial c_i}{\partial t} + \frac{\partial J_i}{\partial x} = 0 \quad \text{for } i = 1, 2, 3, \quad (6.16)$$

where here

$$J_i = - \sum_{j=1}^3 D_{ij} \frac{\partial c_j}{\partial x} + D_i \varepsilon_i^2 c_i \frac{\partial^3 c_i}{\partial x^3} \quad \text{for } i = 1, 2, 3, \quad (6.17)$$

and where the diffusion coefficients D_{ij} are given by

$$D_{ij} = D_i \frac{V_j}{V_i} X_i \frac{\partial}{\partial X_j} \ln(a_i). \quad (6.18)$$

Here the activities a_i are related to the bulk chemical potentials μ_i^b via

$$\frac{\Delta \mu_i^b}{RT} = \ln(a_i). \quad (6.19)$$

Using (6.15) and (6.17) now gives

$$J_2 = - \left(D_{22} - \frac{m_2}{m_1} D_{21} \right) \frac{\partial c_2}{\partial x} - \left(D_{23} - \frac{m_3}{m_1} D_{21} \right) \frac{\partial c_3}{\partial x} + D_2 \varepsilon_2^2 c_2 \frac{\partial^3 c_2}{\partial x^3}. \quad (6.20)$$

Using (6.17), the flux for species three can similarly be written as

$$J_3 = - \left(D_{32} - \frac{m_2}{m_1} D_{31} \right) \frac{\partial c_2}{\partial x} - \left(D_{33} - \frac{m_3}{m_1} D_{31} \right) \frac{\partial c_3}{\partial x} + D_3 \varepsilon_3^2 c_3 \frac{\partial^3 c_3}{\partial x^3}. \quad (6.21)$$

The Diffusion Coefficients In Terms Of Volume Fractions

I now derive expressions for the composition-dependent diffusion coefficients D_{ij} in terms of volume fractions, beginning with D_{12} . Combining equations (6.18) and

(6.19) gives

$$D_{21} = D_2 \frac{V_1}{V_2} X_2 \frac{\partial}{\partial X_1} \left(\frac{\Delta\mu_2^b}{RT} \right). \quad (6.22)$$

Also, from (3.38), I have that

$$\begin{aligned} \frac{\partial}{\partial X_1} \left(\frac{\Delta\mu_2^b}{RT} \right) &= \frac{1}{\phi_2} \frac{\partial\phi_2}{\partial X_1} + \left(1 - \frac{m_2}{m_1}\right) \frac{\partial\phi_1}{\partial X_1} + \left(1 - \frac{m_2}{m_3}\right) \frac{\partial\phi_3}{\partial X_1} + 2m_2 \left(\chi_2(\phi_1 + \phi_3) \right. \\ &\quad \left. \left(\frac{\partial\phi_1}{\partial X_1} + \frac{\partial\phi_3}{\partial X_1} \right) + \chi_1\phi_1 \frac{\partial\phi_1}{\partial X_1} + \chi_3\phi_3 \frac{\partial\phi_3}{\partial X_1} \right). \end{aligned} \quad (6.23)$$

Recalling that

$$\phi_i = \frac{m_i X_i}{m_1 X_1 + m_2 X_2 + m_3 X_3} \quad \text{for } i = 1, 2, 3,$$

and substituting (6.23) into (6.22), now gives

$$\begin{aligned} D_{21} &= D_{21}(\phi_1, \phi_2, \phi_3) = D_2 \left(\frac{m_1}{m_2} \right)^2 \phi_2 \left(-1 + \left(1 - \frac{m_2}{m_1}\right) (\phi_2 + \phi_3) - \left(1 - \frac{m_2}{m_3}\right) \phi_3 \right. \\ &\quad \left. + 2m_2 \left(\chi_2(1 - \phi_2)\phi_2 + \chi_1\phi_1(1 - \phi_1) - \chi_3\phi_3^2 \right) \right). \end{aligned}$$

I now carry out a similar calculation for D_{22} . I have that

$$D_{22} = D_2 \frac{V_2}{V_2} X_2 \frac{\partial}{\partial X_2} \left(\frac{\Delta\mu_2^b}{RT} \right), \quad (6.24)$$

where, using (3.38),

$$\begin{aligned} \frac{\partial}{\partial X_2} \left(\frac{\Delta\mu_2^b}{RT} \right) &= \frac{1}{\phi_2} \frac{\partial\phi_2}{\partial X_2} + \left(1 - \frac{m_2}{m_1}\right) \frac{\partial\phi_1}{\partial X_2} + \left(1 - \frac{m_2}{m_3}\right) \frac{\partial\phi_3}{\partial X_2} + 2m_2 \left(\chi_2(\phi_1 + \phi_3) \right. \\ &\quad \left. \left(\frac{\partial\phi_1}{\partial X_2} + \frac{\partial\phi_3}{\partial X_2} \right) + \chi_1\phi_1 \frac{\partial\phi_1}{\partial X_2} + \chi_3\phi_3 \frac{\partial\phi_3}{\partial X_2} \right). \end{aligned} \quad (6.25)$$

Substituting (6.25) into (6.24) now gives

$$\begin{aligned} D_{22} &= D_{22}(\phi_1, \phi_1, \phi_1) \\ &= D_2 \left((1 - \phi_2) \left(1 + \left(1 - \frac{m_2}{m_1}\right) \phi_1 \right. \right. \\ &\quad \left. \left. + \left(1 - \frac{m_2}{m_3}\right) \phi_3 + 2m_2 \left(\chi_2(\phi_1 + \phi_3)^2 + \chi_1\phi_1^2 + \chi_3\phi_3^2 \right) \right) \right). \end{aligned}$$

The remaining diffusion coefficients D_{23} , D_{31} , D_{32} and D_{33} are calculated similarly.

I omit the details of their derivation here, and simply display the results.

$$\begin{aligned}
D_{21} &= D_2 \left(\frac{m_1}{m_2} \right)^2 \phi_2 \left(-1 + \left(1 - \frac{m_2}{m_1} \right) (\phi_2 + \phi_3) - \left(1 - \frac{m_2}{m_3} \right) \phi_3 \right. \\
&\quad \left. + 2m_2 \left(\chi_2(1 - \phi_2)\phi_2 + \chi_1\phi_1(1 - \phi_1) - \chi_3\phi_3^2 \right) \right), \\
D_{22} &= D_2 \left((1 - \phi_2) \left(1 + \left(1 - \frac{m_2}{m_1} \right) \phi_1 + \left(1 - \frac{m_2}{m_3} \right) \phi_3 \right) \right. \\
&\quad \left. + 2m_2 \left(\chi_2(\phi_1 + \phi_3)^2 + \chi_1\phi_1^2 + \chi_3\phi_3^2 \right) \right), \\
D_{23} &= D_2 \left(\frac{m_3}{m_2} \right)^2 \phi_2 \left(-1 - \left(1 - \frac{m_2}{m_1} \right) \phi_1 + \left(1 - \frac{m_2}{m_3} \right) (\phi_1 + \phi_2) \right. \\
&\quad \left. + 2m_2 \left(\chi_2\phi_2(1 - \phi_2) - \chi_1\phi_1^2 + \chi_3(1 - \phi_3)\phi_3 \right) \right), \\
D_{31} &= D_3 \left(\frac{m_1}{m_3} \right)^2 \phi_3 \left(-1 + \left(1 - \frac{m_3}{m_1} \right) (\phi_2 + \phi_3) - \left(1 - \frac{m_3}{m_2} \right) \phi_2 \right. \\
&\quad \left. + 2m_3 \left(\chi_3(1 - \phi_3)\phi_2 + \chi_1\phi_1(1 - \phi_1) - \chi_2\phi_2^2 \right) \right), \\
D_{32} &= D_3 \left(\frac{m_2}{m_3} \right)^2 \phi_3 \left(-1 - \left(1 - \frac{m_3}{m_1} \right) \phi_1 + \left(1 - \frac{m_3}{m_2} \right) (\phi_1 + \phi_3) \right. \\
&\quad \left. + 2m_3 \left(\chi_3(1 - \phi_3) - \chi_1\phi_1^2 + \chi_2(1 - \phi_2)\phi_2 \right) \right), \\
D_{33} &= D_3 \left((1 - \phi_3) \left(1 + \left(1 - \frac{m_3}{m_2} \right) \phi_2 + \left(1 - \frac{m_3}{m_1} \right) \phi_1 \right) \right. \\
&\quad \left. + 2m_3 \left(\chi_3(\phi_1 + \phi_2)^2 + \chi_1\phi_1^2 + \chi_2\phi_2^2 \right) \right).
\end{aligned}$$

Using (6.16), the equations for the concentrations c_2 and c_3 are now given by

$$\begin{aligned}
\frac{\partial c_2}{\partial t} &= \frac{\partial}{\partial x} \left(\left(D_{22} - \frac{m_2}{m_1} D_{21} \right) \frac{\partial c_2}{\partial x} + \left(D_{23} - \frac{m_3}{m_1} D_{21} \right) \frac{\partial c_3}{\partial x} - D_2 \varepsilon_2^2 c_2 \frac{\partial^3 c_2}{\partial x^3} \right), \\
\frac{\partial c_3}{\partial t} &= \frac{\partial}{\partial x} \left(\left(D_{32} - \frac{m_2}{m_1} D_{31} \right) \frac{\partial c_2}{\partial x} + \left(D_{33} - \frac{m_3}{m_1} D_{31} \right) \frac{\partial c_3}{\partial x} - D_3 \varepsilon_3^2 c_3 \frac{\partial^3 c_3}{\partial x^3} \right).
\end{aligned}$$

However, for the purposes of numerical solution, it is more convenient to work with the molar fractions $X_i = c_i V_i$. In terms of these quantities, the governing equations immediately above become

$$\begin{aligned}
\frac{\partial X_2}{\partial t} &= \frac{\partial}{\partial x} \left(\left(D_{22} - \frac{m_2}{m_1} D_{21} \right) \frac{\partial X_2}{\partial x} + \left(\frac{m_2}{m_3} D_{23} - \frac{m_2}{m_1} D_{21} \right) \frac{\partial X_3}{\partial x} - D_2 \delta_2^2 X_2 \frac{\partial^3 X_2}{\partial x^3} \right), \\
\frac{\partial X_3}{\partial t} &= \frac{\partial}{\partial x} \left(\left(\frac{m_3}{m_2} D_{32} - \frac{m_3}{m_1} D_{31} \right) \frac{\partial X_2}{\partial x} + \left(D_{33} - \frac{m_3}{m_1} D_{31} \right) \frac{\partial X_3}{\partial x} - D_3 \delta_3^2 X_3 \frac{\partial^3 X_3}{\partial x^3} \right).
\end{aligned} \tag{6.26}$$

6.2.3 Using Maple To Numerically Integrate The PDEs

To solve the governing equations (6.26), I need to supplement them with appropriate boundary and initial conditions. In this chapter, I consider a one-dimensional domain occupying $0 < x < L$, so that the boundary points are given by $x = 0$ and $x = L$. I will analyze the stability of initially homogeneous mixtures. To model this behaviour, I choose the initial conditions

$$X_1 = X_1^0 + \hat{X}_1(x, 0), \quad X_2 = X_2^0 + \hat{X}_2(x, 0), \quad X_3 = X_3^0 + \hat{X}_3(x, 0), \quad (6.27)$$

for $0 < x < L$ and where (X_1^0, X_2^0, X_3^0) are the initial constant molar fractions of the mixture, and $(\hat{X}_1(x, 0), \hat{X}_2(x, 0), \hat{X}_3(x, 0))$ give an initial small perturbation from these. Hence I assume here that

$$|\hat{X}_1(x, 0)| \ll X_1^0, \quad |\hat{X}_2(x, 0)| \ll X_2^0, \quad |\hat{X}_3(x, 0)| \ll X_3^0.$$

I choose to impose no flux boundary conditions for both the drug and the polymer, so that

$$J_2^X(0, t) = J_2^X(L, t) = J_3^X(0, t) = J_3^X(L, t) = 0, \quad (6.28)$$

where here (see equations (6.26))

$$J_2^X = - \left(D_{22} - \frac{m_2}{m_1} D_{21} \right) \frac{\partial X_2}{\partial x} - \left(\frac{m_2}{m_3} D_{23} - \frac{m_2}{m_1} D_{21} \right) \frac{\partial X_3}{\partial x} + D_2 \delta_2^2 X_2 \frac{\partial^3 X_2}{\partial x^3},$$

$$J_3^X = - \left(\frac{m_3}{m_2} D_{32} - \frac{m_3}{m_1} D_{31} \right) \frac{\partial X_2}{\partial x} - \left(D_{33} - \frac{m_3}{m_1} D_{31} \right) \frac{\partial X_3}{\partial x} + D_3 \delta_3^2 X_3 \frac{\partial^3 X_3}{\partial x^3}.$$

The other boundary conditions I choose to use here are given by (zero slope)

$$\frac{\partial X_2}{\partial x}(0, t) = \frac{\partial X_2}{\partial x}(L, t) = \frac{\partial X_3}{\partial x}(0, t) = \frac{\partial X_3}{\partial x}(L, t) = 0. \quad (6.29)$$

The physical motivation for choosing the zero flux conditions (6.28) is obvious in this context - they model the presence of impenetrable boundaries. However, the motivation for the choice of the zero slope conditions (6.29) is less clear. In fact, they were chosen here to simplify the analysis. However, it is worth noting that zero slope conditions are frequently chosen for the analysis of the related Cahn-Hilliard equation (see [26] for example), and so they do represent a familiar choice in this context.

Equations (6.26), (6.27), (6.28) and (6.29) constitute a well-posed problem that I solved numerically using the mathematical package `Maple`.

However, before briefly describing the method of solution, I first introduce dimensionless quantities as these are more convenient to work with. I begin by introducing

the dimensionless diffusion coefficients D_{ij}^* as follows

$$\begin{aligned} D_{21}^* &= \frac{D_{21}}{D_2}, & D_{22}^* &= \frac{D_{22}}{D_2}, & D_{23}^* &= \frac{D_{23}}{D_2}, \\ D_{31}^* &= \frac{D_{31}}{D_3}, & D_{32}^* &= \frac{D_{32}}{D_3}, & D_{33}^* &= \frac{D_{33}}{D_3}. \end{aligned} \quad (6.30)$$

Non-dimensional space and time variables (x, t) are defined as follows

$$x^* = \frac{x}{L}, \quad t^* = \frac{t}{(L^2/D_3)}. \quad (6.31)$$

Using (6.30) and (6.31), the governing equations with boundary and initial conditions can be cast in the non-dimensional form ($0 \leq x^* \leq 1$)

$$\begin{aligned} \frac{\partial X_2}{\partial t^*} &= d^* \frac{\partial}{\partial x^*} \left(\left(D_{22}^* - \frac{m_2}{m_1} D_{21}^* \right) \frac{\partial X_2}{\partial x^*} + \left(\frac{m_2}{m_3} D_{23}^* - \frac{m_2}{m_1} D_{21}^* \right) \frac{\partial X_3}{\partial x^*} - \delta_2^{*2} X_2 \frac{\partial^3 X_2}{\partial x^{*3}} \right), \\ \frac{\partial X_3}{\partial t^*} &= \frac{\partial}{\partial x^*} \left(\left(\frac{m_3}{m_2} D_{32}^* - \frac{m_3}{m_1} D_{31}^* \right) \frac{\partial X_2}{\partial x^*} + \left(D_{33}^* - \frac{m_3}{m_1} D_{31}^* \right) \frac{\partial X_3}{\partial x^*} - \delta_3^{*2} X_3 \frac{\partial^3 X_3}{\partial x^{*3}} \right), \\ \frac{\partial X_2}{\partial x^*}(0, t^*) &= \frac{\partial X_2}{\partial x^*}(1, t^*) = \frac{\partial X_3}{\partial x^*}(0, t^*) = \frac{\partial X_3}{\partial x^*}(1, t^*) = 0, \\ \frac{\partial^3 X_2}{\partial x^{*3}}(0, t^*) &= \frac{\partial^3 X_2}{\partial x^{*3}}(1, t^*) = \frac{\partial^3 X_3}{\partial x^{*3}}(0, t^*) = \frac{\partial^3 X_3}{\partial x^{*3}}(1, t^*) = 0, \\ X_1(x^*, 0) &= X_1^0 + \hat{X}_1(x^*, 0), \quad X_2(x^*, 0) = X_2^0 + \hat{X}_2(x^*, 0), \quad X_3(x^*, 0) = X_3^0 + \hat{X}_3(x^*, 0), \end{aligned} \quad (6.32)$$

where here

$$d^* = \frac{D_3}{D_2}, \quad \delta_2^* = \frac{\delta_2}{L}, \quad \delta_3^* = \frac{\delta_3}{L},$$

are dimensionless parameters.

The `Maple` code used to solve the initial boundary value problem (6.32) can be found in Appendix A.4, and I will not discuss it in detail here. However, it is worth mentioning the solver that `Maple` employed to numerically integrate the partial differential equations. It used the

`pdsolve/numeric`

routine to numerically integrate the governing equations using finite difference methods. The default method used by the routine is a centered difference implicit scheme. More precisely, it uses backward difference approximations (making the scheme implicit) for the first order time derivatives, and standard centred-difference approximations for the second order spatial derivatives. To deal with the fourth order spatial derivatives that arise here, it employs centred-difference approximations twice. The line of code that calls the solver is

```
> pds := pdsolve(PDEsys, ICSSys, spacestep = 0.01, numeric)
```

In this command, `PDEsys` defines the system of differential equations to be solved and `ICSSys` defines the appropriate boundary and initial conditions.

Before presenting some numerical results, I first give a linearization analysis of the

governing equations as this will enable me to identify parameter regimes of particular interest. It will also yield insight into the character of the behaviour (for small times) for unstable regimes.

6.2.4 Linearizing The Governing Equations

In this section, I linearize the dimensional governing equations (6.26), (6.27), (6.28) and (6.29) about the homogeneous initial state. This will enable me to identify parameter regimes that lead to unstable behaviour when diffusion terms are included in the governing equations. It will also yield information about the character of the instability and, in particular, the wavelengths of the unstable modes.

I consider a small perturbation about an initial constant state, given by

$$X_1(x, t) = X_1^0 + \hat{X}_1(x, t), \quad X_2(x, t) = X_2^0 + \hat{X}_2(x, t), \quad X_3(x, t) = X_3^0 + \hat{X}_3(x, t). \quad (6.33)$$

with X_1^0, X_2^0, X_3^0 constant as before, and where here I am envisaging here that

$$|\hat{X}_1(x, t)| \ll X_1^0, \quad |\hat{X}_2(x, t)| \ll X_2^0, \quad |\hat{X}_3(x, t)| \ll X_3^0,$$

and so I will neglect quadratically small terms such as $\hat{X}_1\hat{X}_2$. For convenience, I write the initial volume fractions as

$$\phi_1^0 = \phi_1(X_1^0, X_2^0, X_3^0), \quad \phi_2^0 = \phi_2(X_1^0, X_2^0, X_3^0), \quad \phi_3^0 = \phi_3(X_1^0, X_2^0, X_3^0). \quad (6.34)$$

I also write

$$D_{ij}^0 = D_{ij}(\phi_1^0, \phi_2^0, \phi_3^0)$$

for the relevant values of i and j .

Substituting (6.33) into (6.26), and neglecting quadratically small terms, yields

$$\begin{aligned} \frac{\partial \hat{X}_2}{\partial t} &= \left(D_{22}^0 - \frac{m_2}{m_1} D_{21}^0 \right) \frac{\partial^2 \hat{X}_2}{\partial x^2} + \left(\frac{m_2}{m_3} D_{23}^0 - \frac{m_2}{m_1} D_{21}^0 \right) \frac{\partial^2 \hat{X}_3}{\partial x^2} - D_2 \delta_2^2 X_2^0 \frac{\partial^4 \hat{X}_2}{\partial x^4}, \\ \frac{\partial \hat{X}_3}{\partial t} &= \left(\frac{m_3}{m_2} D_{32}^0 - \frac{m_3}{m_1} D_{31}^0 \right) \frac{\partial^2 \hat{X}_2}{\partial x^2} + \left(D_{33}^0 - \frac{m_3}{m_1} D_{31}^0 \right) \frac{\partial^2 \hat{X}_3}{\partial x^2} - D_3 \delta_3^2 X_3^0 \frac{\partial^4 \hat{X}_3}{\partial x^4}. \end{aligned} \quad (6.35)$$

I will seek solutions to (6.35) of the form (chosen so as to satisfy the boundary conditions (6.28) and (6.29))

$$\hat{X}_2 = f_{2N}(t) \cos\left(\frac{N\pi x}{L}\right), \quad \hat{X}_3 = f_{3N}(t) \cos\left(\frac{N\pi x}{L}\right). \quad (6.36)$$

Substituting (6.36) into (6.35) gives

$$\begin{aligned} \frac{df_{2N}(t)}{dt} &= -\frac{N^2\pi^2}{L^2} \left\{ \left(D_{22}^0 - \frac{m_2}{m_1} D_{21}^0 \right) f_{2N} + \left(\frac{m_2}{m_3} D_{23}^0 - \frac{m_2}{m_1} D_{21}^0 \right) f_{3N} + D_2 \delta_2^2 X_2^0 \frac{N^2\pi^2}{L^2} f_{2N} \right\}, \\ \frac{df_{3N}(t)}{dt} &= -\frac{N^2\pi^2}{L^2} \left\{ \left(\frac{m_3}{m_2} D_{32}^0 - \frac{m_3}{m_1} D_{31}^0 \right) f_{2N} + \left(D_{33}^0 - \frac{m_3}{m_1} D_{31}^0 \right) f_{3N} + D_3 \delta_3^2 X_3^0 \frac{N^2\pi^2}{L^2} f_{3N} \right\}. \end{aligned}$$

These equations can be combined in matrix form as

$$\frac{d}{dt} \begin{pmatrix} f_{2N} \\ f_{3N} \end{pmatrix} = -\frac{N^2\pi^2}{L^2} \begin{pmatrix} \left(D_{22}^0 - \frac{m_2}{m_1} D_{21}^0 \right) + D_2 \delta_2^2 X_2^0 \frac{N^2\pi^2}{L^2} & \left(\frac{m_2}{m_3} D_{23}^0 - \frac{m_2}{m_1} D_{21}^0 \right) \\ \left(\frac{m_3}{m_2} D_{32}^0 - \frac{m_3}{m_1} D_{31}^0 \right) & \left(D_{33}^0 - \frac{m_3}{m_1} D_{31}^0 \right) + D_3 \delta_3^2 X_3^0 \frac{N^2\pi^2}{L^2} \end{pmatrix} \begin{pmatrix} f_{2N} \\ f_{3N} \end{pmatrix}. \quad (6.37)$$

Seeking solutions to (6.37) of the form

$$\begin{pmatrix} f_{2N} \\ f_{3N} \end{pmatrix} = \begin{pmatrix} \alpha_N \\ \beta_N \end{pmatrix} e^{-\frac{N^2\pi^2\lambda_N t}{L^2}} \quad (6.38)$$

with α_N, β_N constants, leads to

$$\begin{pmatrix} \left(D_{22}^0 - \frac{m_2}{m_1} D_{21}^0 \right) + D_2 \delta_2^2 X_2^0 \frac{N^2\pi^2}{L^2} - \lambda_N & \left(\frac{m_2}{m_3} D_{23}^0 - \frac{m_2}{m_1} D_{21}^0 \right) \\ \left(\frac{m_3}{m_2} D_{32}^0 - \frac{m_3}{m_1} D_{31}^0 \right) & \left(D_{33}^0 - \frac{m_3}{m_1} D_{31}^0 \right) + D_3 \delta_3^2 X_3^0 \frac{N^2\pi^2}{L^2} - \lambda_N \end{pmatrix} \begin{pmatrix} \alpha_N \\ \beta_N \end{pmatrix} = \begin{pmatrix} 0 \\ 0 \end{pmatrix}.$$

For non-trivial solutions to α_n, β_n , I now require that

$$\det \begin{pmatrix} \left(D_{22}^0 - \frac{m_2}{m_1} D_{21}^0 \right) + D_2 \delta_2^2 X_2^0 \frac{N^2\pi^2}{L^2} - \lambda_N & \left(\frac{m_2}{m_3} D_{23}^0 - \frac{m_2}{m_1} D_{21}^0 \right) \\ \left(\frac{m_3}{m_2} D_{32}^0 - \frac{m_3}{m_1} D_{31}^0 \right) & \left(D_{33}^0 - \frac{m_3}{m_1} D_{31}^0 \right) + D_3 \delta_3^2 X_3^0 \frac{N^2\pi^2}{L^2} - \lambda_N \end{pmatrix} = 0,$$

which leads to

$$\lambda_N^2 - A_N \lambda_N + B_N = 0, \quad (6.39)$$

where here

$$\begin{aligned} A_N &= D_{22}^0 + D_{33}^0 - \frac{m_2}{m_1} D_{21}^0 - \frac{m_3}{m_1} D_{31}^0 + \frac{N^2\pi^2}{L^2} (D_2 \delta_2^2 X_2^0 + D_3 \delta_3^2 X_3^0), \\ B_N &= \left(D_{22}^0 - \frac{m_2}{m_1} D_{21}^0 + D_2 \delta_2^2 X_2^0 \frac{N^2\pi^2}{L^2} \right) \left(D_{33}^0 - \frac{m_3}{m_1} D_{31}^0 + D_3 \delta_3^2 X_3^0 \frac{N^2\pi^2}{L^2} \right) \\ &\quad - \left(\frac{m_2}{m_3} D_{23}^0 - \frac{m_2}{m_1} D_{21}^0 \right) \left(\frac{m_3}{m_2} D_{32}^0 - \frac{m_3}{m_1} D_{31}^0 \right). \end{aligned}$$

Equation (6.39) is trivially solved for λ to give

$$\lambda_N^\pm = \frac{1}{2} \left(A_N \pm \sqrt{A_N^2 - 4B_N} \right). \quad (6.40)$$

Stable Modes

In view of (6.38), a mode N is stable if

$$\Re(\lambda_N^+) > 0 \quad \text{and} \quad \Re(\lambda_N^-) > 0.$$

Unstable Modes

In view of (6.38), a mode N is unstable if

$$\Re(\lambda_N^+) < 0 \quad \text{or} \quad \Re(\lambda_N^-) < 0.$$

6.3 Numerical Results

6.3.1 Parameter Values

I begin by briefly discussing the parameter values I used to generate the numerical results. The parameter values chosen here are not tied to any particular system, but are selected instead for illustrative purposes. I began by constructing a phase diagram for the values

$$m_1 = 1000, \quad m_2 = 500, \quad m_3 = 1,$$

and

$$\chi_{12} = 0.004857, \quad \chi_{13} = 0.305, \quad \chi_{23} = 0.300.$$

This choice for the parameters was chosen to correspond to Case II of Chapter 4 for a polymer-polymer-drug system. Also, the quite specific value for χ_{12} was chosen to make the height of the plait point above the polymer-polymer binary close to 0.4, and was guided by the asymptotic analysis. In Figure 6.1, I display a complete phase diagram for this set of parameter values. The method for constructing the binodal curve, the spinodal curve, and the plait point has already been discussed in detail in Chapter 3. On the figure, I also indicate the stable, metastable, and unstable regions, as previously described in Chapter 2.

However, to numerically integrate the PDE model, more parameter values are required to describe the kinetics. In the calculations I display here, I choose to use the values

$$d^* = \frac{D_3}{D_2} = 10, \quad \delta_2^* = 0.05, \quad \delta_3^* = 0.05, \quad \Delta x = 0.01,$$

where here Δx is the space step. Choosing $d^* = 10$ implies that I am taking the self-diffusion coefficient for the drug to be ten times larger than that of the second polymer - we expect the smaller drug molecules to be more mobile than the polymer molecules. Guided by Figure 6.1, I choose initial values for the volume fractions $(\phi_1^0, \phi_2^0, \phi_3^0)$ to illustrate stable and unstable behaviour. Once the values for $(\phi_1^0, \phi_2^0, \phi_3^0)$ have been chosen with the aid of Figure 6.1, the corresponding initial values for the molar fractions (X_1^0, X_2^0, X_3^0) can then be calculated using the relationships

$$X_i^0 = \frac{\phi_i^0/m_i}{\phi_1^0/m_1 + \phi_2^0/m_2 + \phi_3^0/m_3} \quad \text{for } i = 1, 2, 3.$$

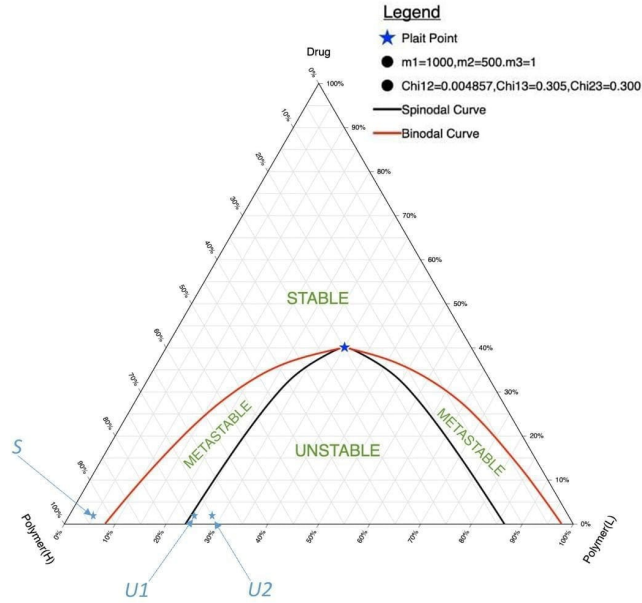


Figure 6.1: An illustrative ternary phase diagram with $m_1 = 1000$, $m_2 = 500$, $m_3 = 1$ and $\chi_{12} = 0.004857$, $\chi_{13} = 0.305$, $\chi_{23} = 0.300$. On the diagram are marked a stable point (S), and two unstable points ($U1$, $U2$).

A Stable Example (S)

In Figure 6.2, I show some numerical results for the PDE model for the choice of initial conditions

$$S : (\phi_1^0, \phi_2^0, \phi_3^0) = (0.941, 0.0588, 0.00011),$$

which corresponds to the initial molar fractions $(X_1^0, X_2^0, X_3^0) \approx (0.8, 0.1, 0.1)$, this point being chosen to lie in the stable regime of the ternary diagram.

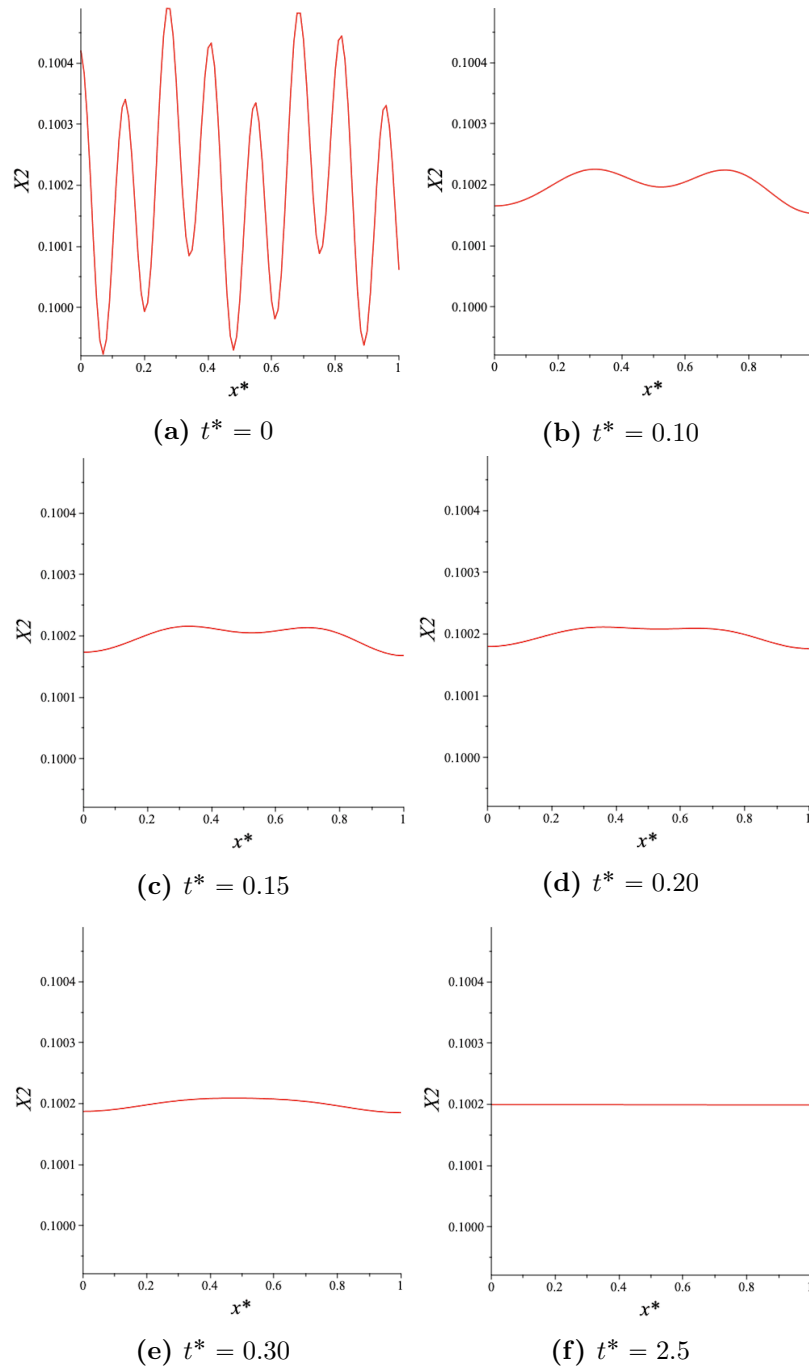


Figure 6.2: Plots of the concentration $X_2(x^*, t^*)$ for a stable case $S : (\phi_1^0, \phi_2^0, \phi_3^0) = (0.941, 0.0588, 0.00011)$ for various successive times. It is clear that the initial perturbation decays over time here, as would be expected.

This point S has been marked on the phase diagram displayed in Figure 6.1. Since this point lies in the stable regime, I expect the numerical results for the PDE model to show that an initial perturbation from uniform initial conditions decays over time. Referring back to the linearization analysis given in Section 6.2.4, the eigenvalues

for mode N are given here by

$$\lambda_N^+(N) = 0.001357N^2 + 0.595593 + \sqrt{2.722018 + 1.232833 \times 10^{-5}N^4 + 1.1583845 \times 10^{-3}N^2}, \quad (6.41)$$

$$\lambda_N^-(N) = 0.001357N^2 + 0.595593 - \sqrt{2.722018 + 1.232833 \times 10^{-5}N^4 + 1.1583845 \times 10^{-3}N^2}.$$

It is immediately clear that $\lambda_N^+(N) > 0$ for all N , and so these values cannot give rise to unstable modes. In Figure 6.3, I plot λ_N^- as a function of N , and this indicates that $\lambda_N^-(N) > 0$ as well for all N . Taken together, these results indicate stability, as would be expected here. This is confirmed by the numerical results shown in Figure 6.2, where we see that the initial perturbation to the initial values decays over time.

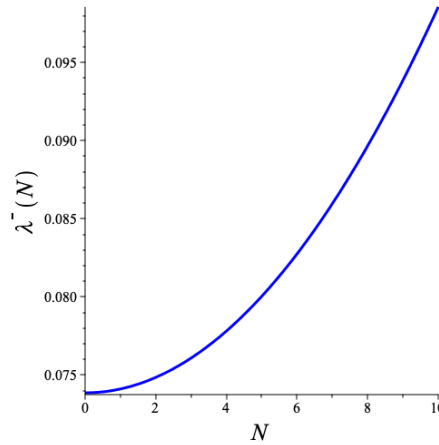


Figure 6.3: Plots of the eigenvalues λ_N^- for the stable case $S : (\phi_1^0, \phi_2^0, \phi_3^0) = (0.941, 0.0588, 0.00011)$. Notice that $\lambda_N^- > 0$ here, indicating stability.

An Unstable Case ($U1$: Two Modes Driven Unstable)

In Figure 6.4, I display some numerical results for the PDE model for the choice of initial conditions

$$U1 : (\phi_1^0, \phi_2^0, \phi_3^0) = (0.7495, 0.2498, 0.00053).$$

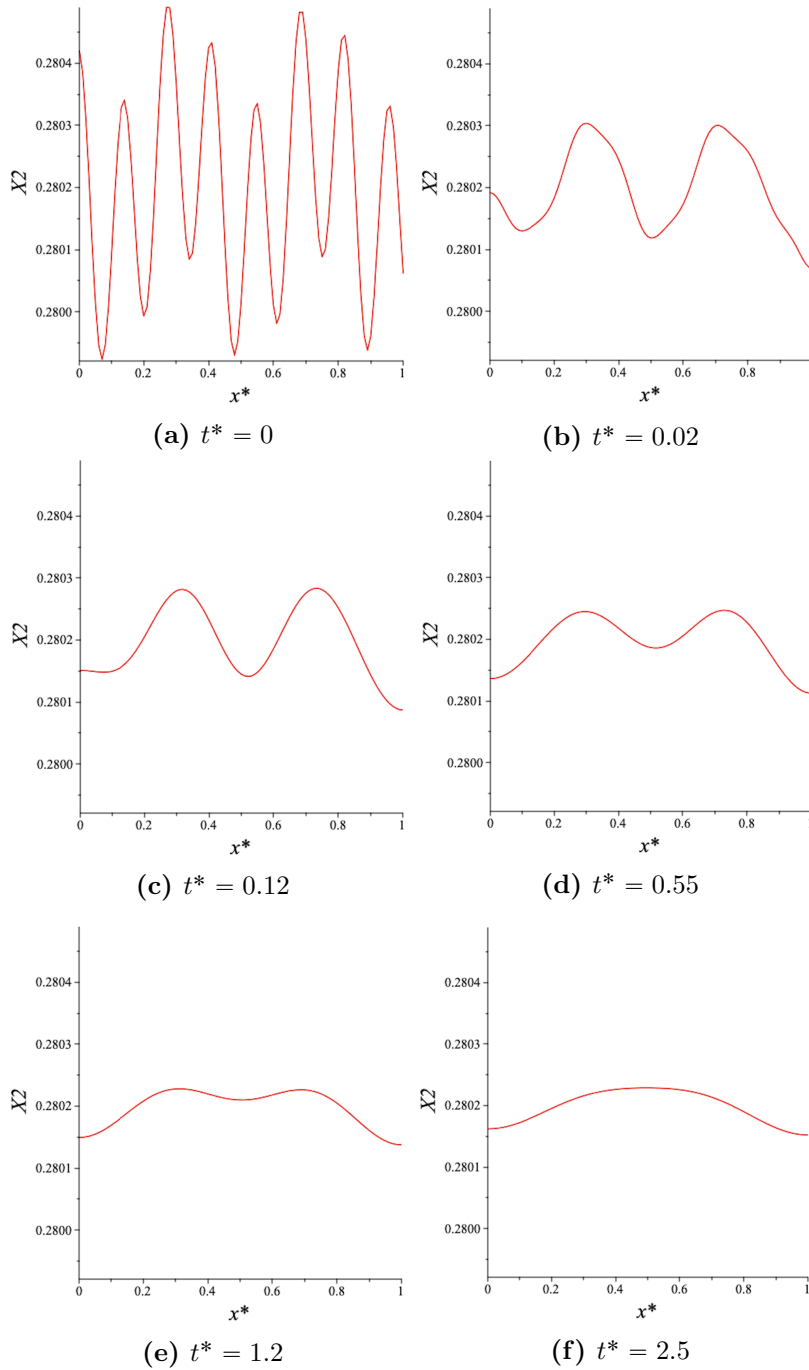


Figure 6.4: Plots of the concentration $X_2(x^*, t^*)$ for successive times for the unstable case $U1 : (\phi_1^0, \phi_2^0, \phi_3^0) = (0.7495, 0.2498, 0.00053)$. For this case, the first two modes $N = 1$ and $N = 2$ are driven unstable, a prediction that is consistent with the numerical results.

This point $U1$ has been marked on the phase diagram displayed in Figure 6.1. The point is in the unstable regime, and so I expect the numerical results for the PDE model to show that an initial perturbation from uniform initial conditions grows over time. Referring back to the linearization analysis given in Section 6.2.4, the

eigenvalues for mode N are given here by

$$\lambda_N^+(N) = 0.0040465N^2 + 0.760693 + \sqrt{5.849322 + 1.126049 \times 10^{-4}N^4 + 5.179485 \times 10^{-2}N^2},$$

$$\lambda_N^-(N) = 0.0040465N^2 + 0.760693 - \sqrt{5.849322 + 1.126049 \times 10^{-4}N^4 + 5.179485 \times 10^{-2}N^2}.$$

It is immediately obvious that $\lambda_N^+(N) > 0$ for all N , and so these values cannot give rise to unstable modes. In Figure 6.5, I plot λ_N^- as a function of N , and it is clear from this figure that $\lambda_N^-(N) < 0$ for $N = 1, 2$. Hence, the first two modes are unstable here. This is not surprising since the initial composition was chosen in the unstable regime under the spinodal curve. In Figure 6.4, it is clear that the initial perturbation to the initial values grows in time in a manner that is consistent with the first two modes being unstable.

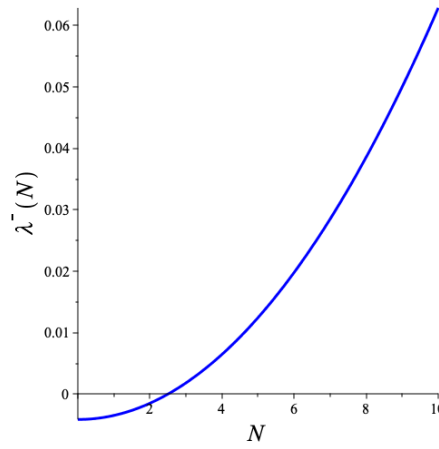


Figure 6.5: Plots of the eigenvalues λ_N^- for the unstable case $U1 : (\phi_1^0, \phi_2^0, \phi_3^0) = (0.7495, 0.2489, 0.00053)$. Notice that $\lambda_N^- < 0$ for $N = 1, 2$ here, indicating unstable behaviour.

A Second Unstable Case ($U2$: Four Modes Driven Unstable)

In Figure 6.6, I display some numerical results for the PDE model for the choice of initial conditions

$$U2 : (\phi_1^0, \phi_2^0, \phi_3^0) = (0.718, 0.2805, 0.0006).$$

For this case, the first four modes $N = 1, 2, 3, 4$ are driven unstable, and this is consistent with the numerical results shown.

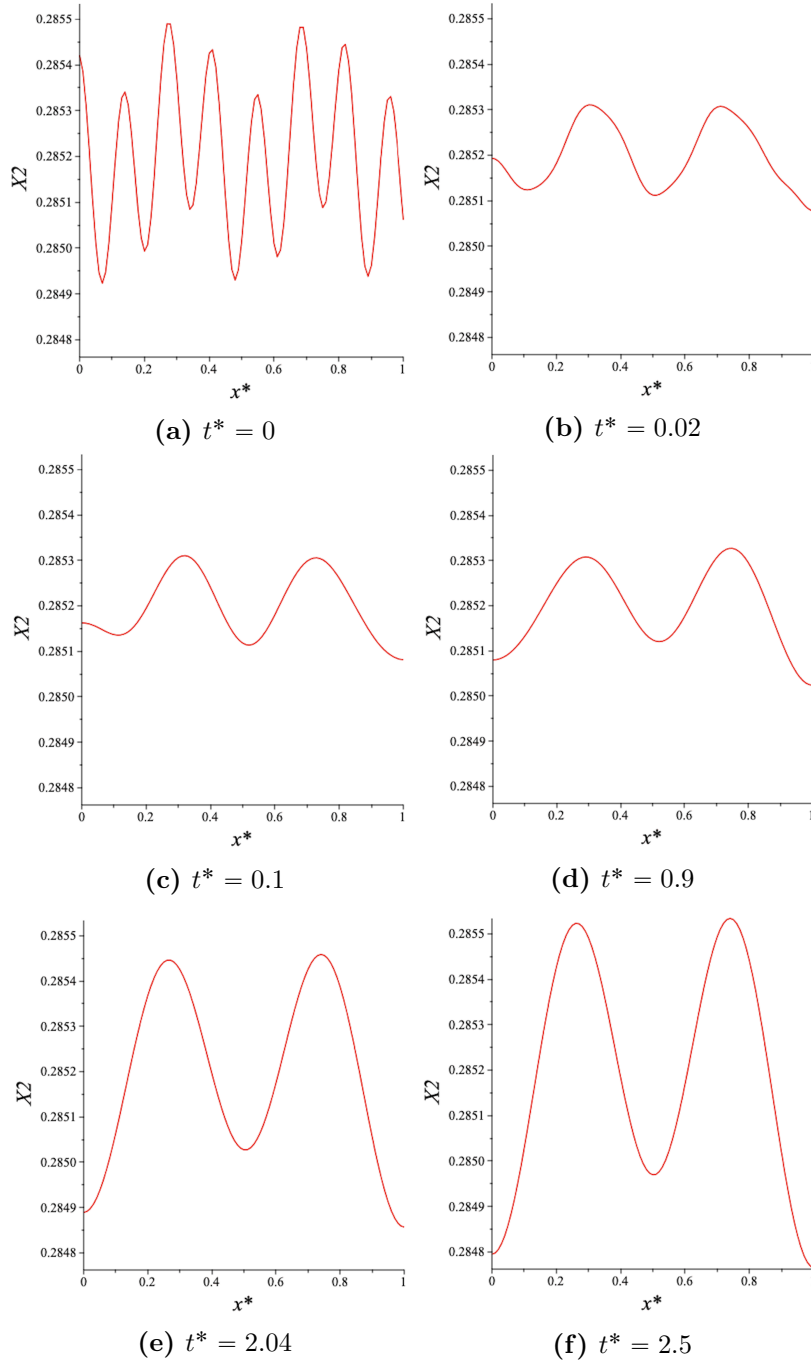


Figure 6.6: Plots of the concentration $X_2(x^*, t^*)$ for successive times for the unstable case $U1 : (\phi_1^0, \phi_2^0, \phi_3^0) = (0.718, 0.2805, 0.0006)$. For this case, the first four modes $N = 1, 2, 3, 4$ are driven unstable, a prediction that is consistent with the numerical results.

Chapter 7

Conclusions

7.1 Key Findings

The novel contributions of this thesis may be summarized as follows.

- In Chapter 3, I derive the Flory-Huggins model from first principles for ternary solid dispersions; the derivations in the standard text books are for binary systems.
- In Chapter 3, I also develop and describe `MATLAB` programs for calculating the binodal curves of a ternary phase diagram. The solution method was based on minimizing an objective function using the `fmincon` routine of `MATLAB`. I also developed `Maple` programs to calculate spinodal curves and plait points for a ternary phase diagram.
- In Chapter 4, I analyze the stability properties of polymer-polymer-drug ternary systems. There are quite a number of detailed results in this chapter, but in broad terms, the key findings may be parsed as follows. If the two polymers are incompatible, then the system generally has unfavourable stability properties - most initial compositions lead to phase separation. If the two polymers are compatible, then the system can have favourable stability properties. However, the behaviour can then be finely dependent on an asymmetry in how the two polymers interact with the drug.
- In Chapter 5, I analyze the stability properties of polymer-surfactant-drug systems. An extensive numerical investigation of the system was performed. The results of the analysis suggest that system stability is enhanced by such factors as reducing the molecular weight of the surfactant, improving the compatibility of the surfactant and the drug, and improving the compatibility of the polymer and the drug.
- In Chapter 6, I describe a partial differential equation model for the temporal and spatial evolution of a ternary solid dispersions. The model is based on earlier work by Meere, Pontrelli & McGinty [58]. The model is formulated as

a multi-component diffusion system, and the diffusion coefficients are written as functions of the system volume fractions. The equations are linearized and their stability properties are investigated for a particular set of boundary conditions. Some preliminary numerical investigations are performed using a **Maple** solver, and produce results that are consistent with the linearization analysis.

7.2 Limitations Of This Work And Some Proposals For Future Work

I now briefly indicate some limitations of the current work, and outline some ideas for future work.

7.2.1 Shortcomings Of Flory-Huggins Theory

One of the principal limitations of the current work is the use of Flory-Huggins theory as the thermodynamic model to describe the ternary mixture. The model is derived from first principles in Chapter 3 for a ternary system. From Chapter 3, it can be seen that the model is premised on a number of simplifying assumptions, and many of these are of questionable validity when dealing with solid dispersions. Among these assumptions are the following.

- (i) The total volume of the constituent components is assumed to not change when they are mixed together. However, this is a dubious assumption when dealing with real systems; see, for example, Chapter 4 of the book by Rubinstein & Colby [72].
- (ii) Only nearest neighbouring interactions are taken account of when calculating energies, and this is clearly an approximation. Weaker interactions from more distant molecules can also contribute obviously.
- (iii) The model is based on lattice theory. Specifically, the mixture is imagined to be divided into a set of cells of *equal volume* within which molecules can be *randomly* placed; again, see Chapter 4 of Rubinstein & Colby [72] for a critique of these assumptions.

PC-SAFT (Perturbed Chain Statistical Associating Fluid Theory) is another thermodynamic model that has been used to describe solid dispersions. PC-SAFT was initially developed by Gabriele Sadowski and Joachim Gross, as described in their paper Gross & Sadowski [30]. The authors Prudic *et al.* [68] and Lehmkemper *et al.* [52] have discussed the use of PC-SAFT in the context of modelling solid dispersions. Unlike Flory-Huggins theory, PC-SAFT is capable of describing specific molecular interactions - for example, hydrogen bonding or dipole-dipole interactions. PC-SAFT is founded on SAFT (Statistical Associating Fluid Theory), a theory in

which molecules are envisaged as chains of segments with specific association sites. The segments can interact via various forces, including dispersion forces, association effects, or attractive and repulsive interactions. Using this theory to calculate phase diagrams for ternary dispersions is a natural extension of the current work.

7.2.2 Further Numerical Simulations Of The Diffusion Model

In Chapter 6, I introduce a diffusion model to describe both the spatial and temporal evolution of a ternary solid dispersions. Some numerical results for a one-dimensional (in space) version of the model are also presented. The numerical solutions were calculated using a `Maple` partial differential equations solver. However, the results obtained were quite preliminary. The work may be extended in a number of ways as follows.

- Even within the context of the one-dimensional problems that were solved in Chapter 6, the `Maple` routine only succeeded in reliably solving the governing equations for a limited set of parameter values. For many parameter regimes (particularly for unstable cases), the routine quickly crashed, and would not integrate to a steady-state. There are a number of ways to approach this issue. One is to develop a finite difference code from scratch *by hand* to numerically integrate the equations. This would give the user more control over, and insight into, how the equations are solved. Another approach is to use a solver from another mathematical package, such as `MATLAB`.
- Another limitation of the current numerical calculations is that they only take account of one spatial dimension. However, the most interesting behaviour (the emergence of patterns, for example) often only manifests itself in two or three spatial dimensions. Higher dimensional solutions may be calculated using a finite element package (`COMSOL`, for example), or by writing code by hand for a finite difference scheme.

Appendix A

Maple and MATLAB Codes

A.1 Using Maple to Calculate the Plait Points

The following Maple program was used to calculate the plait points in this thesis.

```
1 # This{\color{red}{ Maple program }}calculates the plait points
2
3 restart:
4
5 # The values of the ratios of the molar volumes.
6 m[1] := 1000.0:
7 m[2] := 500.0:
8 m[3] := 1.0:
9
10 # Values for the Flory–Huggins interaction parameters.
11 chi[12] := 0.004857:
12 chi[13] := 0.303:
13 chi[23] := 0.300:
14 chi[1] := 0.5 * (chi[12] + chi[13] - chi[23]):
15 chi[2] := 0.5 * (chi[23] + chi[12] - chi[13]):
16 chi[3] := 0.5 * (chi[13] + chi[23] - chi[12]):
17
18 # Solving the following three equations simultaneously gives the plait
19 # points.
20 eq1 := phi[1] + phi[2] + phi[3] = 1:
21 eq2 := m[1]^2 * phi[1] / (-2 * chi[1] * m[1] * phi[1] + 1)^3 +
22 m[2]^2 * phi[2] / (-2 * chi[2] * m[2] * phi[2] + 1)^3 +
23 m[3]^2 * phi[3] / (-2 * chi[3] * m[3] * phi[3] + 1)^3 = 0:
24
25 eq3 := m[1] * phi[1] / (-2 * chi[1] * m[1] * phi[1] + 1) +
26 m[2] * phi[2] / (-2 * chi[2] * m[2] * phi[2] + 1) +
27 m[3] * phi[3] / (-2 * chi[3] * m[3] * phi[3] + 1) = 0:
28
29 # Solve the equations
30 p := solve(eq1, eq2, eq3, phi[1], phi[2], phi[3]):
31 p;
```

```
1 phi[1] = -0.04848387258, phi[2] = 0.06165768324, phi[3] =
0.9868261893,
```

```

2   phi[1] = 0.002217330870, phi[2] = -0.009669556768, phi[3] =
   1.007452226,
3   phi[1] = 0.1055152261, phi[2] = -0.7845498872, phi[3] =
   1.679034661,
4   phi[1] = -0.9915471917, phi[2] = 0.2840839453, phi[3] =
   1.707463246,
5   phi[1] = 0.06779239934 - 0.01731123736*I, phi[2] = -0.7209897280 +
6       0.002894581982*I, phi[3] = 1.653197329 + 0.01441665538*I
7
8 # Selecting a real-valued solution
9 rhs(p[1][3]);    0.4004754154
10 rhs(p[1][1]);   0.2487724873
11 rhs(p[1][2]);   0.3507520973}

```

A.2 Using Maple to Calculate the Spinodal Curves

The following Maple program was used to calculate the spinodal curves in this thesis.

```

1 # This Maple program calculates the spinodal curves
2 # The text is colour-coded as follows:
3 # comments are in blue, executable statements are in red,
4 # and output is in purple.
5 restart:
6
7 # The values of the ratios of the molar volumes.
8 m[1] := 1000.0: m[2] := 500.0: m[3] := 1.0:
9
10 # Values for the Flory-Huggins interaction parameters.
11 chi[12] := 0.004857: chi[13] := 0.303: chi[23] := 0.300:
12 chi[1] := (chi[12] + chi[13] - chi[23])/2:
13 chi[2] := (chi[12] + chi[23] - chi[13])/2:
14 chi[3] := (chi[13] + chi[23] - chi[12])/2:
15
16 # The approach taken here is as follows. First a fixed value
17 # for phi[3] is chosen. Then we set phi[2] := 1 - phi[1] - phi[3].
18 # We then solve equation (3.45) for phi[1] this has
19 # two solutions, and so a pair of points on the spinodal is
20 # determined. Then the value for phi[3] is changed and the
21 # process repeated to obtain another pair of points on
22 # the spinodal. Repeat until the spinodal curve is generated.
23 # Begin by fixing a value for phi[3].
24 phi[3] := -0.05:
25 for i from 1 to 20 do:
26   phi[3] := phi[3] + 0.05:
27   eq := m[1]*phi[1]/(-2*chi[1]*m[1]*phi[1] + 1) +
28         m[2]*(1-phi[1]-phi[3])/(1 - 2*chi[2]*m[2]*(1-phi[1]-phi[3])) +
29         m[3]*phi[3]/(-2*chi[3]*m[3]*phi[3] + 1) = 0:
30   phi[1] := solve(eq, phi[1]):
31   PL[i] := [phi[3], phi[1][1], 1 - phi[1][1] - phi[3]]:
32   PR[i] := [phi[3], phi[1][2], 1 - phi[1][2] - phi[3]]:
33 end do:
34
35

```

```

36 base:="c:/Data/":
37 datafile1 := cat(base, "dataL.xls");
38 datafile2 := cat(base, "dataR.xls");
39 qL := [seq([PL[n]], n = 1 .. 6)]:
40 qR := [seq([PR[19-n]], n = 13 .. 18)];
41 qL;
42 qR;

```

```

1 qL:
2 [[0., 0.1365106432, 0.8648963568],
3 [0.05, 0.1973073779, 0.8120926621],
4 [0.10, 0.1412840232, 0.7587179768],
5 [0.15, 0.1544413593, 0.7055586407],
6 [0.20, 0.107407467, 0.649259253],
7 [0.25, 0.489634875, 0.260365128],
8 [0.30, 0.465008432, 0.292341215],
9 [0.35, 0.548763202, 0.252109434],
10 [0.40, 0.554321222, 0.239053112]]:
11
12 qR:
13 [[0., 0.489634875, 0.510365125],
14 [0.05, 0.468653908, 0.479901092],
15 [0.10, 0.54923498, 0.420832894],
16 [0.15, 0.478634008, 0.426651992],
17 [0.20, 0.608312112, 0.379121903],
18 [0.25, 0.523831191, 0.371234128],
19 [0.30, 0.672834092, 0.300132919],
20 [0.35, 0.689054298, 0.26523211]]:

```

A.3 Using MATLAB to Calculate the Binodal Curve

The following MATLAB program was used to calculate the binodal curves in this thesis.

```

1 % This MATLAB program is saved in a file called minit.m
2 % The program calls fmincon to solve the minimization problem.
3 % The objective function being minimized is given by (3.63).
4 % The nonlinear constraint is given by (3.64),(3.65).
5 % The program is described in detail in section 3.4.3 of the thesis.
6 % Here 1 = polymer1, 2 = polymer2, 3 = solvent.
7 % The aim is to calculate the binodal curve. This is achieved by
8 % minimizing the sum of the squared differences of the
9 % potentials calculated at the left tie point and the right tie point.
10 % Denote the left tie point by (phi1L,phi2L,phi3L).
11 % and the right tie point by (phi1R,phi2R,phi3R).
12 % So that makes 6 unknowns, but phi1L= 1-phi2L-phi3R,
13 % phi1R= 1-phi2R-phi3R, so there are 4 unknowns really.
14 % These are given by - phi2L,phi3L,phi2R,phi3R.
15 % Then FIX a value for phi3L-say-phi3L=K
16 % for some given K. That leaves us with 3 unknowns,namely,
17 % phi2L = X(1), phi2R = X(2), phi3R = X(3),
18 % Then the left tie point is (phi1L,phi2L,phi3L) = (1-K-X(1), X(1),K)

```

```

19 % and the right tie point is (phi1R,phi2R,phi3R) = (1-X(2)-X(3), X(2),X
    (3))
20
21 lb = [0,0,0,0]; % Lower bounds for the solution vector.
22 ub = [1,1,1,1]; % Upper bounds for the solution vector.
23 X0 = [0.6,0.7,0.25]; % Initial guess for the solution vector.
24 A = []; b = []; % No linear inequality constraint.
25 Aeq = []; beq = []; % No linear equality constraint.
26 K = 0.25; % This fixes the value for phi3L.
27 %
28 % optimoptions sets the options for all call to fmincon.
29 % fmincon solves the optimization problem.
30 %
31 options = optimoptions('fmincon','Algorithm','sqp',...
32     'OptimalityTolerance',1.0e-9,'ConstraintTolerance',1.0e-8, ...
33     'MaxFunctionEvaluations',300000,'StepTolerance',1.0e-8, ...
34     'MaxIterations',4000,'Display','iter','FunctionTolerance',1.0e
    -11);
35
36 % Now call fmincon to solve the problem. In the below
37 % objective (X) is the function being minimized and
38 % nonloc(X) defines the nonlinear constraint.
39 Y = fmincon(@(x) objective(X),X0,A,b,Aeq,beq,lb,ub,@(X),@nonlcon,
    options);
40 % Now display some results.
41 disp(' ');
42 disp(['The solution is X = [num2str(Y(1)),Y(2),Y(3),']']);
43 disp(' ');
44 disp(['The final value of the objective function is: ', num2str(
    objective([Y(1),Y(2),Y(3)]))]);
45 disp(' ');
46 disp(['The right tie point is (', num2str([1-K-Y(1)],Y(1),K] '),')'],
47 disp(' ');
48 disp(['The right tie point is (', num2str([1-Y(2)-Y(3)],Y(2),Y(3)] '),')'],
    ,
49 % End of program.

```

The following MATLAB code defines the objective function to be minimized.

```

1 % This MATLAB program is saved in a file called objective.m
2 function cost = objective(X) % This is what we are minimizing.
3 m1 = 1000.0; % m1 = V1/V3
4 m2 = 1000.0; % m2 = V2/V3
5 m3 = 1.0; % m3 = V3/V3
6 % T = 298.0 K, temperature in Kelvin.
7 chi12=0.004; chi13=0.4; chi23=0.44; % FH interaction parameters.
8 chi1 = 0.5*(chi12 + chi13 - chi23);
9 chi2 = 0.5*(chi12 + chi23 - chi13);
10 chi3 = 0.5*(chi13 + chi23 - chi12);
11 K = 0.25; % The value for phi3L.
12
13 % Change in chemical potential for species one at left tie point.
14 deltamu-1L-divm1 = log(1-X(1)-K)/m1 + (1/m1-1/m2)*X(1) + ...
15 (1/m1-1/m3)*K + chi1*(X(1)+K)**2 + chi2*X(1)**2 + chi3*K**2;
16
17 % Species one right tie point.
18 deltamu-1R-divm1 = log(1-X(2)-X(3))/m1 + (1/m1-1/m2)*X(2) + ...
19 (1/m1-1/m3)*X(3) + chi1*(X(2)+X(3))**2 + chi2*(X(2))**2 + chi3*(X(3))

```

```

**2;
20
21 % Species two left tie point.
22 deltamu-2L-divm2 = log(X(1))/m2 + (1/m2-1/m1)*(1-X(1)-K) + ...
23 (1/m2-1/m3)*K + chi2*(1-X(1))**2 + chi1*(1-X(1)-K)**2 + chi3*K**2;
24
25 % Species two right tie point.
26 deltamu-2R-divm2 = log(X(2))/m2 + (1/m2-1/m1)*(1-X(2)-X(3)) + ...
27 (1/m2-1/m3)*X(3) + chi2*(1-X(2)-X(3))**2+chi1*(1-X(2)-X(3))**2+chi3*(X
    (3))**2;
28
29 % Species three left tie point.
30 deltamu-3L-divm3 = log(K)/m3 + (1/m3-1/m1)*(1-X(1)-K) + ...
31 (1/m3-1/m2)*X(1) + chi3*(1-K)**2 + +chi1*(1-X(1)-K)**2+chi2*X(1)**2;
32
33 % Species three right tie point.
34 deltamu-3R-divm3 = log(X(3))/m3 + (1/m3-1/m1)*(1-X(2)-X(3)) + ...
35 (1/m3-1/m2)*X(2)+chi3*(1-X(3))**2+chi1*(1-X(2)-X(3))**2+chi2*X(2)**2;
36
37 % Define the objective function to be minimized.
38 cost = (deltamu-1L-divm1 - deltamu-1R-divm1)**2 + ...
39 (deltamu-2L-divm2 - deltamu-2R-divm2)**2 + ...
40 (deltamu-3L-divm3 - deltamu-3R-divm3)**2;
41 % End of function.

```

The following MATLAB code defines the nonlinear constraint objective function.

```

1 % This MATLAB program is saved in a file called nonlcon.m
2 % It contains the nonlinear constraint on the objective function.
3 % The constraint prevents the trivial solution of the left tie
4 % point being the same as the right tie point.
5 % This is done by making the distance between the left
6 % tie point and the right tie point positive. Pick some
7 % value that this distance must be greater than.
8
9 function [c, ceq] = nonlcon(X)
10 K = 0.25; % This is phi3L, the third coord of left tie point.
11 lambda = 0.4; % Minimum distance**2 between left and right tie points.
12 c = lambda - (X(3) - K)**2 - (X(2) - X(1))**2 - (X(2) + X(3) - K - X(1)
    )**2;
13 ceq = []; % There is no nonlinear equality constraint.
14 % End of function.

```

We now display some output from running `minit.m`

```

1
2 The solution is X = [0.041676 0.71788 0.24168]
3 The final value of the objective function is: 3.0916e-15
4
5 The right tie point is (0.70832 0.041676 0.25)
6 The left tie point is (0.040441 0.71788 0.24168)

```

A.4 Using Maple to Solve ternary system in Chapter 6

The following Maple program was used to solve the 1D ternary system described in Chapter 6 in this thesis.

```

1 # Program to solve the 1D ternary system described in Chapter 6.
2 # In this program 1 = polymer , 2 = polymer , 3 = drug .
3
4 restart : with(PDEtools) :
5
6 # Parameters values .
7 m[1] := 1000.0 : m[2] := 1000.0 : m[3] := 1.0 : # Molar volume ratios .
8 chi[12] := 0.004 : chi[13] := 0.4 : chi[23] := 0.46 : # Flory-Huggins
   interaction parameters .
9 chi[1] := 0.5*(chi[12] + chi[13] - chi[23]) :
10 chi[2] := 0.5*(chi[23] + chi[12] - chi[13]) :
11 chi[3] := 0.5*(chi[13] + chi[23] - chi[12]) :
12 DD[2] := 0.1 : DD[3] := 1.0 : # Self-diffusion coefficients for the
   second polymer and drug .
13 delta[2] := sqrt(0.001) : delta[3] := sqrt(0.001) : # Parameters that
   determine thickness of transition regions between phase .
14
15 # phi[1], phi[2], phi[3] are the volume fractions .
16 # X1, X2, X3 are the molar fractions .
17
18 # Because of the constraint X1 + X2 + X3 = 1
19 # we can remove the X1 dependency by writing X1 = 1 - X2 - X3 .
20 phi[1] := (1.0 - X2(x,t) - X3(x,t)) / (1.0 - X2(x,t) - X3(x,t)) + (m[2]/m
   [1]) X2(x,t) + (m[3]/m[1]) X3(x,t) :
21 phi[2] := (m[2]/m[1]) X2(x,t) / (1.0 - X2(x,t) - X3(x,t)) + (m[2]/m[1])
   X2(x,t) + (m[3]/m[1]) X3(x,t) :
22 phi[3] := (m[3]/m[1]) X3(x,t) / (1.0 - X2(x,t) - X3(x,t)) + (m[2]/m[1])
   X2(x,t) + (m[3]/m[1]) X3(x,t) :
23
24 # Composition-dependent diffusion coefficients .
25 # See Chapter 6 of the thesis for more details .
26 DD[21] := DD[2] * phi[2] * [(m[1]/m[2])]^2 * (1 - m[2]/m[1]) * (phi[2] + phi[3])
   - (1 - m[2]/m[3]) * phi[3] - 1 + 2*m[2] * (chi[2] * phi[2] * (1 - phi[2]) + chi[1] *
   phi[1] * (1 - phi[1]) - chi[3] * [phi[3]**2]) :
27 DD[22] := DD[2] * (1 - phi[2] * (1 + ((1 - m[2]/m[1]) * phi[1] + ((1 - m[2]/m
   [3]) * phi[3]) +
28 2*m[2] * (chi[2] * (phi[1] + phi[3])^2 + chi[1] * phi[1]**2 + chi[3] * phi[3]**2)) :
29 DD[23] := DD[2] * phi[2] * [(m[3]/m[2])]**2 * (1 - m[2]/m[3]) * (phi[1] + phi[2])
   - (1 - m[2]/m[1]) * phi[1] - 1 + 2*m[2] * (chi[2] * phi[2] * (1 - phi[2]) + chi[3] *
   phi[3] * (1 - phi[3]) - chi[1] * [phi[1]**2]) :
30 DD[31] := DD[3] * phi[3] * [(m[1]/m[3])]^2 * (1 - m[3]/m[1]) * (phi[2] + phi[3])
   - (1 - m[3]/m[2]) * phi[2] - 1 + 2*m[3] * (chi[3] * phi[3] * (1 - phi[3]) + chi[1] * phi
   [1] * (1 - phi[1]) - chi[2] * [phi[2]**2]) :
31 DD[32] := DD[3] * phi[3] * [(m[2]/m[3])]^2 * (1 - m[3]/m[2]) * (phi[1] + phi[3])
   - (1 - m[3]/m[1]) * phi[1] - 1 + 2*m[3] * (chi[3] * phi[3] * (1 - phi[3]) + chi[2] * phi
   [2] * (1 - phi[2]) - chi[1] * [phi[1]**2]) :
32 DD[33] := DD[3] * (1 - phi[3] * (1 + ((1 - m[3]/m[1]) * phi[1] + ((1 - m[3]/m[2]) * phi
   [2] + 2*m[3] * (chi[3] * (phi[1] + phi[2])**2 + chi[1] * phi[1]^2 + chi[2] * phi
   [2]**2))) :

```

```

33
34
35 # The fluxes of the polymer X2 and the drug X3.
36 j2 := -(DD[22]-(m[2]/m[1])*DD[21])*diff(X2(x,t),x)-((m[2]/m[3])*DD
      [23]-(m[2]/m[1])*DD[21])*diff(x3(x,t),x)+DD[2]*delta[2]^2*X2(x,y)*
      diff(X2(x,t),x):
37 j3 := -(m[3]/m[2])*DD[32]-(m[3]/m[1])*DD[31])*diff(x2(x,t),x)-(DD
      [33]-(m[3]/m[1])*DD[31])*diff(X3(x,t),x)+DD[3]*delta[3]^2*X3(x,y)*
      diff(X3(x,t),x):
38 # The governing partial differential equations.
39 # They're written conservation form here.
40 PDEsys := {diff(x2(x,t),x)+diff(j2,x)=0,diff(x3(x,t),x)+diff(j3,x)=0}:
41 # Define the boundary conditions and the initial conditions.
42 # The boundary conditions are of no-flux and zero slope type.
43 # The initial conditions are noisy perturbations about constant values.
44 D[1,1,1](X2)(1,t)=0, X2(x,0)=0.5+0.001*(-3*sin(11*x)+log(1.4*cos(17*x)
      D[1,1,1](X3)(1,t)=0, X3(x,0)=0.10+0.001*(2*cos(17.0*x)-log(0.4*cos
      )) (11*x)**2+0.0024)):
45 # Solve the initial boundary value problem using Maple's pdsolve
      routine.
46 pds:=pdsolve(PDEsys,IBCSsys,spacestep=1/80,numeric);
47 pds:=module() ... end module
48 # Animate the solution. To see the animation, right click on the image
49 # and press "Animation" followed by "play".
50 pds:-animate(t=0.5,frames+100,labels=[x,X2],title="Time=%f");

```

Bibliography

- [1] Elias Abboud. On viviani’s theorem and its extensions. *College Mathematics Journal*, 3(43):203–211, 2011. (Cited on page 16.)
- [2] A. Ainurofiq, D.S. Putro, D.A. Ramadhani, G.M. Putra, and L.D.C. Do Espirito Santo. A review on solubility enhancement methods for poorly water-soluble drugs. *Journal of Reports in Pharmaceutical Sciences*, 10:137–147, 2021. (Cited on page 3.)
- [3] Hisham Al-Obaidi and Graham Buckton. Evaluation of griseofulvin binary and ternary solid dispersions with hpmcas. *AAPS PharmSciTech*, 10:1172–1177, 2009. (Cited on page 51.)
- [4] Hisham Al-Obaidi, Peng Ke, Steve Brocchini, and Graham Buckton. Characterization and stability of ternary solid dispersions with pvp and phpma. *International journal of pharmaceuticals*, 419(1-2):20–27, 2011. (Cited on page 51.)
- [5] Ahmad B Albadarin, Catherine B Potter, Mark T Davis, Javed Iqbal, Sachin Korde, Sudhir Pagire, Anant Paradkar, and Gavin Walker. Development of stability-enhanced ternary solid dispersions via combinations of hpmcp and soluplus® processed by hot melt extrusion. *International journal of pharmaceuticals*, 532(1):603–611, 2017. (Cited on page 51.)
- [6] GL Amidon, H Lennernas, VP Shah, and JR Crison. A theoretical basis for a biopharmaceutics drug classification: the correlation of in vitro drug product dissolution and in vivobioavailability. *Pharmaceutical Research*, 12(3):413–420, 1995. (Cited on page 2.)
- [7] B.D. Anderson. Predicting solubility/miscibility in amorphous dispersions: It is time to move beyond regular solution theories. *Journal of Pharmaceutical Sciences*, 107(1):24–33, 2018. (Cited on page 47.)
- [8] P. Atkins, J. de Paula, and J. Keeler. *Physical Chemistry*. Oxford University Press, 10th edition, 2014. (Cited on pages 10, 14, 18, and 26.)
- [9] K. Bansal, U.S. Baghel, and S. Thakral. Construction and validation of binary phase diagram for amorphous solid dispersion using flory–huggins theory. *AAPS PharmSciTech*, 17(2):318–327, 2016. (Cited on page 54.)
- [10] L.Z. Benet. The role of bcs (biopharmaceutics classification system) and bddcs (biopharmaceutics drug disposition classification system) in drug development. *Journal of pharmaceutical sciences*, 102(1):34–42, 2013. (Cited on page 2.)

- [11] H. Bleya, B. Fussnegger, and R. Bodmeier. Characterization and stability of solid dispersions based on peg/polymer blends. *International Journal of Pharmaceutics*, 390:165–173, 2010. (Cited on page 6.)
- [12] Ludwig Boltzmann. *Lectures on gas theory*. Dover Publications, New York, 1995. (Cited on page 24.)
- [13] S. Borde, S.K. Paul, and H. Chauhan. Ternary solid dispersions: classification and formulation considerations. *Drug Development and Industrial Pharmacy*, 47(7):1011–1028, 2021. (Cited on pages 8 and 50.)
- [14] R.A. Brualdi. *Introductory combinatorics*. Pearson Education, fifth edition, 2009. (Cited on page 25.)
- [15] T.R. Buggins, P.A. Dickinson, and G. Taylor. The effects of pharmaceutical excipients on drug disposition. *Advanced Drug Delivery Reviews*, 59:1482–1503, 2007. (Cited on page 4.)
- [16] J. W. Cahn and J. E. Hilliard. Free energy of a nonuniform system. i. interfacial free energy. *The Journal of Chemical Physics*, 28:258–267, 1958. (Cited on page 83.)
- [17] W.L. Chiou and S. Riegelman. Preparation and dissolution characteristics of several fast-release solid dispersions of griseofulvin. *Journal of Pharmaceutical Sciences*, 58(12):1505–1510, 1969. (Cited on page 6.)
- [18] F. Damian, N. Blaton, L. Naesens, J. Balzarini, R. Kinget, P. Augustijns, and G. Van den Mooter. Physicochemical characterization of solid dispersions of the antiviral agent uc-781 with polyethylene glycol 6000 and gelucire 44/14. *European Journal of Pharmaceutical Sciences*, 10:311–322, 2000. (Cited on page 7.)
- [19] Mark T Davis, Catherine B Potter, Maryam Mohammadpour, Ahmad B Albadarin, and Gavin M Walker. Design of spray dried ternary solid dispersions comprising itraconazole, soluplus and hpmcp: Effect of constituent compositions. *International Journal of Pharmaceutics*, 519(1-2):365–372, 2017. (Cited on page 51.)
- [20] Mark T Davis, Catherine B Potter, and Gavin M Walker. Downstream processing of a ternary amorphous solid dispersion: The impacts of spray drying and hot melt extrusion on powder flow, compression and dissolution. *International journal of pharmaceutics*, 544(1):242–253, 2018. (Cited on page 51.)
- [21] S.R. de Groot and P. Mazur. *Non-equilibrium Thermodynamics*. Dover Publications, 2nd edition, 2011. (Cited on page 10.)
- [22] G. Van den Mooter, I. Weuts, T. De Ridder, and N. Blaton. Evaluation of inutec sp1 as a new carrier in the formulation of solid dispersions for poorly soluble drugs. *International Journal of Pharmaceutics*, 316:1–6, 2006. (Cited on page 7.)
- [23] M. Doi. *Introduction To Polymer Physics*. Clarendon Press, 1st edition, 1996. (Cited on pages 48 and 50.)

- [24] W.J. Egan and G. Lauri. Prediction of intestinal permeability. *Advanced Drug Delivery Reviews*, 54:273–289, 2002. (Cited on page 2.)
- [25] N. Provatas & K. Elder. *Phase-field methods in material science and engineering*. John Wiley & Sons, Weinheim, Germany, first edition, 2010. (Cited on page 83.)
- [26] C.M. Elliott and Z. Songmu. On the cahn-hilliard equation. *Archive for Rational Mechanics and Analysis*, 96(4):349–357, 1986. (Cited on page 89.)
- [27] J. Fischer and M. Wendland. On the history of key empirical intermolecular potentials. *Fluid Phase Equilibria*, 573:1–10, 2023. (Cited on page 48.)
- [28] A.H. Goldberg, M. Gibaldi, J.L. Kanig, and M. Mayersohn. Increasing dissolution rates and gastrointestinal absorption of drugs via solid solutions and eutectic mixtures iv: Chloramphenicol—urea system. *Journal of Pharmaceutical Sciences*, 55(6):581–583, 1966. (Cited on page 6.)
- [29] D.J. Griffiths. *Introduction to electrodynamics*. Prentice Hall, 3rd edition, 1999. (Cited on page 48.)
- [30] J. Gross and G. Sadowski. Perturbed-chain saft: An equation of state based on a perturbation theory for chain molecules. *Industrial & engineering chemistry research*, 40(4):1244–60, 2001. (Cited on pages 47 and 101.)
- [31] F. Hallouarda, L. Mehennic, M. Lahiani-Skibaa, Y. Anouard, and M. Skibaa. Solid dispersions for oral administration: An overview of the methods for their preparation. *Current Pharmaceutical Design*, 22(00):1–17, 2016. (Cited on page 5.)
- [32] Naho Hanada, Kenjiro Higashi, Zhijing Zhao, Keisuke Ueda, and Kunikazu Moribe. Preparation of a ternary amorphous solid dispersion using hot-melt extrusion for obtaining a stable colloidal dispersion of amorphous probucol nanoparticles. *International Journal of Pharmaceutics*, 640:122959, 2023. (Cited on page 72.)
- [33] P.C. Hiemenz and T.P. Lodge. *Polymer Chemistry*. CRC Press, 2nd edition, 2007. (Cited on pages 16, 23, 30, 33, 48, 50, and 61.)
- [34] J.H. Hildebrand and R.L. Scott. *The Solubility of Nonelectrolytes*. Reinhold Publishing Corporation, 3rd edition, 1950. (Cited on page 50.)
- [35] Terrell L. Hill. *An introduction to statistical thermodynamics*. Dover Publications, New York, second edition, 1986. (Cited on pages 23 and 33.)
- [36] Mats Hillert. *Phase equilibria, phase diagrams and phase transformations: their thermodynamic basis*. Cambridge university press, 2007. (Cited on page 16.)
- [37] N. Hirasawa, S. Ishise, H. Miyata, and K. Danjo. An attempt to stabilize nilvadipine solid dispersion by the use of ternary systems. *Drug Development and Industrial Pharmacy*, 29(9):997–1004, 2003. (Cited on page 51.)

- [38] B.K. Hong, J.Y. Kim, W.H. Jo, and S.C. Lee. A closed-loop phase behaviour of ternary homopolymer blend composed of three miscible binaries. *Polymer*, 38(17):4373–4375, 1997. (Cited on page 68.)
- [39] C.C Hsu and J.M. Prausnitz. Thermodynamics of polymer compatibility in ternary systems. *Macromolecules*, 7(3):320, 1974. (Cited on pages 41, 44, 45, and 65.)
- [40] Y. Huang and W. Dai. Fundamental aspects of solid dispersion technology for poorly soluble drugs. *Acta Pharmaceutica Sinica B*, 4(1):18–25, 2014. (Cited on page 6.)
- [41] The MathWorks Inc. Matlab version: 9.13.0 (r2022b), 2022. (Cited on pages 41 and 44.)
- [42] The MathWorks Inc. Optimization toolbox version: 9.4 (r2022b), 2022. (Cited on page 42.)
- [43] S. Janssens and G. Van den Mooter. Review: physical chemistry of solid dispersions. *Journal of Pharmacy and Pharmacology*, 61(61):1571–1586, 2009. (Cited on page 6.)
- [44] Sandrien Janssens, Clive Roberts, Emily F Smith, and Guy Van den Mooter. Physical stability of ternary solid dispersions of itraconazole in polyethyleneglycol 6000/hydroxypropylmethylcellulose 2910 e5 blends. *International journal of pharmaceutics*, 355(1-2):100–107, 2008. (Cited on page 51.)
- [45] Mitali Kakran, Nanda Gopal Sahoo, Yong Wah Tan, and Lin Li. Ternary dispersions to enhance solubility of poorly water soluble antioxidants. *Elsevier*, 433:111–121, 2013. (Cited on page 72.)
- [46] Young Hun Kim, Dong Wuk Kim, Min Seok Kwon, Kwan Hyung Cho, Jong Oh Kim, Chul Soon Yong, and Han-Gon Choi. Clopidogrel napadisilate monohydrate loaded surface-modified solid dispersion: physicochemical characterization and in vivo evaluation. *The Pharmaceutical Society of Japan*, 38(7):1033–1040, 2015. (Cited on page 72.)
- [47] Justyna Knapik-Kowalczyk, Krzysztof Chmiel, Karolina Jurkiewicz, Natália T Correia, Wiesław Sawicki, and Marian Paluch. Physical stability and viscoelastic properties of co-amorphous ezetimibe/simvastatin system. *Pharmaceutics*, 12(1):40, 2019. (Cited on page 51.)
- [48] PT Koh, JN Chuah, Meghna Talekar, A Gorajana, and S Garg. Formulation development and dissolution rate enhancement of efavirenz by solid dispersion systems. *Wolters Kluwer–Medknow Publications*, 75(3):291, 2013. (Cited on page 72.)
- [49] G. M. Kontogeorgis and G. K. Folas. *Thermodynamic models for industrial applications*. John Wiley & Sons, Chichester, West Sussex, UK, first edition, 2010. (Cited on page 85.)

- [50] A. Kumar, S.K. Sahoo, K. Padhee, P.P.S. Kochar, A. Satapathy, and N. Pathak. Review on solubility enhancement techniques for hydrophobic drugs. *Pharmacie Globale*, 3(3):1–7, 2011. (Cited on pages 3 and 4.)
- [51] Jae-Young Lee, Wie-Soo Kang, Jingpei Piao, In-Soo Yoon, Dae-Duk Kim, and Hyun-Jong Cho. Soluplus®/tpgs-based solid dispersions prepared by hot-melt extrusion equipped with twin-screw systems for enhancing oral bioavailability of valsartan. *Taylor & Francis*, pages 2745–2756, 2015. (Cited on page 72.)
- [52] K. Lehmkemper, S.O. Kyeremateng, O. Heinzerling, M. Degenhardt, and G. Sadowski. Long-term physical stability of pvp- and pvpva-amorphous solid dispersions. *Molecular Pharmaceutics*, 14:157–171, 2017. (Cited on page 101.)
- [53] J. Li, Y. Wang, and D. Yu. Effects of additives on the physical stability and dissolution of polymeric amorphous solid dispersions: a review. *AAPS PharmSciTech*, 24(175), 2023. (Cited on page 72.)
- [54] H.A. Lieberman and L. Lachman. *The theory and practice of industrial pharmacy*. CBS Publishers & Distributors, 4th edition, 2017. (Cited on pages 1 and 2.)
- [55] H. Lima, P. Balakrishnana, D.H. Oha, K.H. Joea, Y.R. Kima, D.H. Hwanga, Y. Lee, C.S. Yonga, and H. Choi. Development of novel sibutramine base-loaded solid dispersion with gelatin and hpmc: Physicochemical characterization and pharmacokinetics in beagle dogs. *International Journal of Pharmaceutics*, 397(1–2):225–230, 2010. (Cited on page 6.)
- [56] S. Liu, M. Li, L. Jia, M. Chen, S. Du, and J. Gong. Investigation of drug-polymer miscibility, molecular interaction, and their effects on the physical stabilities and dissolution behaviors of norfloxacin amorphous solid dispersions. *Crystal Growth & Design*, 20:2952–2964, 2020. (Cited on page 53.)
- [57] Maplesoft, a division of Waterloo Maple Inc.. Maple, 2022. (Cited on page 41.)
- [58] Martin Meere, Giuseppe Pontrelli, and Sean McGinty. Modelling phase separation in amorphous solid dispersions. *Acta Biomaterialia*, 94:410–424, 2019. (Cited on pages 7, 83, and 100.)
- [59] Joke Meeus, David J Scurr, Xinyong Chen, Katie Amssoms, Martyn C Davies, Clive J Roberts, and Guy Van den Mooter. Combination of (m) dsc and surface analysis to study the phase behaviour and drug distribution of ternary solid dispersions. *Pharmaceutical research*, 32:1407–1416, 2015. (Cited on page 51.)
- [60] Laura I Mosquera-Giraldo, Niraj S Trasi, and Lynne S Taylor. Impact of surfactants on the crystal growth of amorphous celecoxib. *International journal of pharmaceutics*, 461(1-2):251–257, 2014. (Cited on page 72.)
- [61] A.R. Nair, Y.D. Lakshman, V.S. Anand, K. S. Sree, K. Bhat, and S.J. Den-gale. Overview of extensively employed polymeric carriers in solid dispersion technology. *AAPS PharmSciTech*, 21(309):1–20, 2020. (Cited on page 50.)

- [62] Stavroula Nanaki, Rodanthi Maria Eleftheriou, Panagiotis Barmpalexis, Margaritis Kostoglou, Evangelos Karavas, and Dimitrios Bikiaris. Evaluation of dissolution enhancement of aprepitant drug in ternary pharmaceutical solid dispersions with soluplus® and poloxamer 188 prepared by melt mixing. *Sci*, 1(2):48, 2019. (Cited on page 72.)
- [63] P.C. Painter, Y. Park, and M.M. Coleman. Hydrogen bonding in polymer blends. 2. theory. *Macromolecules*, 21(1):66–72, 1988. (Cited on page 47.)
- [64] L. Zeman & D. Patterson. Effects of the solvent on polymer incompatibility in solution. *Macromolecules*, 5(4):513–516, 1972. (Cited on page 65.)
- [65] Pelton. *Phase Diagrams and Thermodynamic Modeling of Solutions*. Elsevier, 1st edition, 2018. (Cited on page 17.)
- [66] R. Pirie, H.A. Stanway-Gordon, H.L. Stewart, K.L. Wilson, S. Patton, J. Tyrerman, D.J. Cole, K. Fowler, and M.J. Waring. An analysis of the physicochemical properties of oral drugs from 2000 to 2022. *The Royal Society of Chemistry*, 15:3125–3132, 2024. (Cited on page 50.)
- [67] J. M. Prausnitz, R. N. Lichtenthaler, and E. G. de Azevedo. *Molecular thermodynamics of fluid-phase equilibria*. Prentice Hall, New Jersey, third edition, 1999. (Cited on page 85.)
- [68] A. Prudic, Y. Ji, and G. Sadowski. Thermodynamic phase behavior of api/polymer solid dispersions. *Molecular Pharmaceutics*, 11:2294–2304, 2014. (Cited on page 101.)
- [69] M. Rabeony, D.B. Siano, D.G. Peiffer, E. Siakali-Kioulafa, and N. Hadjichristidis. Closed-loop immiscibility in a ternary mixture of homopolymers. *Polymer*, 35(5):1033–1037, 1994. (Cited on page 68.)
- [70] C.O. Rangel-Yagui, A. Pessoa-Jr, and L.C. Tavares. Micellar solubilization of drugs. *J Pharm Pharmaceut Sci*, 8(2):147–163, 2005. (Cited on page 4.)
- [71] Singiresu S. Rao. *Engineering Optimization Theory and Practice*. Wiley, 4th edition, 2009. (Cited on page 20.)
- [72] M. Rubinstein and R.H. Colby. *Polymer Physics*. Oxford University Press, 1st edition, 2003. (Cited on pages 28, 50, 51, 61, and 101.)
- [73] K.T. Savjani, A.K. Gajjar, and J.K. Savjani. Drug solubility: importance and enhancement techniques. *ISRN Pharmaceutics*, 2012:1–9, 2012. (Cited on pages 1, 3, and 4.)
- [74] Emilia Sawicki, Jos H Beijnen, Jan HM Schellens, and Bastiaan Nuijen. Pharmaceutical development of an oral tablet formulation containing a spray dried amorphous solid dispersion of docetaxel or paclitaxel. *Elsevier*, 511(2):765–773, 2016. (Cited on page 72.)
- [75] D. M. Saylor, J. E. Guyer, D. Wheeler, and J. A. Warren. Predicting microstructure development during casting of drug-eluting coatings. *Acta Biomaterialia*, 7:604–613, 2011. (Cited on page 83.)

- [76] D. M. Saylor, C. Kim, D. V. Patwardhan, and J. A. Warren. Diffuse-interface theory for structure formation and release behavior in controlled drug release systems. *Acta Biomaterialia*, 3:851–864, 2007. (Cited on page 83.)
- [77] L. Schreiber and J. Schönherr. *Water and solute permeability of plant cuticles*. Springer-Verlag, 1st edition, 2009. (Cited on page 2.)
- [78] R.L. Scott. The thermodynamics of high polymer solutions. v. phase equilibria in the ternary system: Polymer 1-polymer 2-solvent. *The Journal Of Chemical Physics*, 17(3):279–284, 1949. (Cited on page 65.)
- [79] K. Sekiguchi and N. Obi. Studies on absorption of eutectic mixtures. i. a comparison of the behavior of eutectic mixtures of sulphathiazole and that of ordinary sulphathiazole in man. *Chemical & Pharmaceutical Bulletin*, 9:866–872, 1961. (Cited on page 6.)
- [80] Xiangjun Shi, Tiantian Xu, Wan Huang, Baibai Fan, and Xiaoxia Sheng. Stability and bioavailability enhancement of telmisartan ternary solid dispersions: the synergistic effect of polymers and drug-polymer (s) interactions. *AAPS PharmSciTech*, 20:1–13, 2019. (Cited on page 51.)
- [81] A.P. Simonelli, S.C. Mehta, and W.I. Higuchi. Dissolution rates of high energy polyvinylpyrrolidone (pvp) sulfathiazole coprecipitates. *Journal of Pharmaceutical Sciences*, 58(5):538–549, 1969. (Cited on page 6.)
- [82] E. B. Smith. *Basic chemical thermodynamics*. Imperial College Press, London, UK, sixth edition, 2014. (Cited on page 83.)
- [83] A. Srivastava, T. Yadav, S. Sharma, A. Nayak, A. Kumari, and N. Mishra. Polymers in drug delivery. *Journal of Biosciences and Medicines*, 4:69–84, 2016. (Cited on page 8.)
- [84] L.S. Taylor and G. Zografi. Spectroscopic characterization of interactions between pvp and indomethacin in amorphous molecular dispersions. *Pharmaceutical Research*, 14:1691–1698, 1997. (Cited on page 6.)
- [85] S. Thakral and N. K. Thakral. Prediction of drug–polymer miscibility through the use of solubility parameter based flory–huggins interaction parameter and the experimental validation: Peg as model polymer. *Journal of Pharmaceutical Sciences*, 102(7):2254–2263, 2013. (Cited on pages 51 and 52.)
- [86] G.B. Thomas, M.D. Weir, and C. Heil. *Thomas’ Calculus*. Pearson, 13th edition, 2006. (Cited on pages 11 and 12.)
- [87] Bin Tian, Xingke Ju, Dan Yang, Yang Kong, and Xing Tang. Effect of the third component on the aging and crystallization of cinnarizine-soluplus® binary solid dispersion. *International Journal of Pharmaceutics*, 580:119240, 2020. (Cited on page 51.)
- [88] Yiwei Tian, Jonathan Booth, Elizabeth Meehan, David S Jones, Shu Li, and Gavin P Andrews. Construction of drug–polymer thermodynamic phase diagrams using flory–huggins interaction theory: identifying the relevance of

- temperature and drug weight fraction to phase separation within solid dispersions. *Molecular pharmaceuticals*, 10(1):236–248, 2013. (Cited on page 53.)
- [89] Yiwei Tian, Kaijie Qian, Esther Jacobs, Esther Amstad, David S. Jones, Lorenzo Stella, and Gavin P. Andrews. The investigation of flory–huggins interaction parameters for amorphous solid dispersion across the entire temperature and composition range. *Pharmaceutics*, 11(8), 2019. (Cited on pages 41, 52, and 53.)
- [90] H. Tompa. *Polymer Solutions*. Academic Press, 1st edition, 1956. (Cited on pages 10, 13, 14, 15, 18, 19, 22, and 34.)
- [91] K. Uekama. Design and evaluation of cyclodextrin-based drug formulation. *Chem Pharm Bull*, 52(8):900–915, 2004. (Cited on page 5.)
- [92] L.A. Utracki and C.A. Wilkie (Editors). *Polymer Blends Handbook*. Springer, 2nd edition, 2014. (Cited on pages 54 and 55.)
- [93] S.R. Vippagunta, Z. Wang, S. Hornung, and S.L. Krill. Factors affecting the formation of eutectic solid dispersions and their dissolution behavior. *Journal of Pharmaceutical Sciences*, 96(2):294–304, 2007. (Cited on page 6.)
- [94] C. L. Vo, C. Park, and B. Lee. Current trends and future perspectives of solid dispersions containing poorly water-soluble drugs. *European Journal of Pharmaceutics and Biopharmaceutics*, 85:799–813, 2013. (Cited on pages 6 and 7.)
- [95] Xin Wang, Armand Michoel, and Guy Van den Mooter. Solid state characteristics of ternary solid dispersions composed of pvp va64, myrj 52 and itraconazole. *Elsevier*, 303(1-2):54–61, 2005. (Cited on page 72.)
- [96] West and Saunders. *Ternary Phase Diagrams in Materials Science*. CRC Press, 3rd edition, 2002. (Cited on page 17.)
- [97] H.D. Williams, N.L. Trevaskis, S.A. Charman, R.M. Shanker, W.N. Charman, C.W. Pouton, and C.J.H. Porter. Strategies to address low drug solubility in discovery and development. *Pharmacological Reviews*, 65:315–499, 2013. (Cited on pages 3 and 4.)
- [98] Y. Zhao, P. Inbar, H.P. Chokshi, and A.W. Malick and D.S. Choi. Prediction of the thermal phase diagram of amorphous solid dispersions by flory–huggins theory. *Journal Of Pharmaceutical Sciences*, 100(8):3196–3207, 2011. (Cited on page 52.)
- [99] J. Zhu, R. Balieu, X. Lu, and N. Kringos. Numerical investigation on phase separation in polymer-modified bitumen: effect of thermal condition. *Journal of Materials Science*, 52(11):6525–6541, 2017. (Cited on page 83.)
- [100] J. Zhu, X. Lu, R. Balieu, and N. Kringos. Modelling and numerical simulation of phase separation in polymer modified bitumen by phase-field method. *Materials and Design*, 107:322–332, 2016. (Cited on page 83.)